DISSERTATION

De novo screening of new biomarker candidates in primary open-angle glaucoma (POAG)

Submitted in fulfillment of the requirements for the degree of

Doctorate of natural science

doctor rerum naturalium

at the faculty of Biology

Johannes Gutenberg-University Mainz

by

Carsten Schmelter

Born 18th June 1986

in Bad Dürkheim, Germany

Mainz, July 2019

„Die Neugier steht immer an erster Stelle eines Problems, das gelöst werden will."

Galileo Galilei

Declaration I

Parts of this dissertation have been published in international journals and presented at scientific conferences:

Published papers/manuscripts in revision

1) **Peptides of the variable IgG domain as potential biomarker candidates in primary open-angle glaucoma (POAG).**
   Schmelter C, Perumal N, Funke S, Bell K, Pfeiffer N, Grus FH
   Human Molecular Genetics, 2017, PMID: 29036575
2) **Comparison of Two Solid-Phase Extraction (SPE) Methods for the Identification and Quantification of Porcine Retinal Protein Markers by LC-MS/MS.**
   Schmelter C*, Funke S*, Treml J, Beschnitt A, Perumal N, Manicam C, Bell K, Pfeiffer N, Grus FH
   International Journal of Molecular Sciences, 2018, PMID: 30513899
3) **Synthetic polyclonal-derived CDR peptides as innovative strategy in glaucoma therapy.**
   Schmelter C, Nzogang Fomo K, Perumal N, Manicam C, Bell K, Pfeiffer N, Grus FH
   (Under revision in Journal of Clinical Medicine)
4) **An In-Depth View of the Porcine Trabecular Meshwork Proteome**
   Funke S, Beutgen VM, Bechter L, **Schmelter C**, Zurawski V, Perumal N, Pfeiffer N, Grus FH
   International Journal of Molecular Sciences, 2019, PMID: 31121981
5) **Sample Preparation for Mass-spectrometry-based Proteomics Analysis of Ocular Microvessels.**
   Perumal N, Straßburger L, **Schmelter C**, Gericke A, Pfeiffer N, Grus FH, Manicam C
   Journal of Visualized Experiments, 2019, PMID: 30855578
6) **Glaucoma related Proteomic Alterations in Human Retina Samples.**
   Funke S, Perumal N, Beck S, Gabel-Scheurich S, **Schmelter C**, Teister J, Gerbig C, Gramlich OW, Pfeiffer N, Grus FH
   Scientific Reports, 2016, PMID: 27425789
7) **In-depth proteomic analysis of the porcine retina by use of a four step differential extraction bottom up LC MS platform.**
   Funke S, Markowitsch S, **Schmelter C**, Perumal N, Kamau Mwirii FK, Gabel-Scheurich S, Pfeiffer N, Grus FH
   Molecular Neurobiology, 2016, PMID: 27796761

* = authors contributed equally

Oral presentations at scientific conferences:

1) **Synthetic polyclonal-derived CDR peptides as innovative strategy in glaucoma therapy.**
   Schmelter C, Perumal N, Funke S, Bell K, Pfeiffer N, Grus FH
   Optic Nerve Meeting 2018 in Obergurgl
2) **Discovery and Targeted MS-based strategies for the identification of glaucoma-related IgG V domain peptides.**
   Schmelter C, Perumal N, Funke S, Bell K, Pfeiffer N, Grus FH
   Optic Nerve Meeting 2017 in Obergurgl
3) **Peptides of the variable region of antibodies as potential biomarker candidates in primary open-angle glaucoma (POAG).**
   Schmelter C, Perumal N, Funke S, Bell K, Pfeiffer N, Grus FH
   Optic Nerve Meeting 2016 in Obergurgl
4) **Mass spectrometric analysis of human immunoglobulin peptides.**
   Schmelter C, Perumal N, Funke S, Bell K, Pfeiffer N, Grus FH
   Optic Nerve Meeting in 2015 Obergurgl

Poster presentations at scientific conferences:

1) **Comparison of two solid-phase extraction (SPE) methods for the identification and quantification of porcine retinal protein markers by LC MS/MS.**
   Schmelter C, Funke S, Treml J, Beschnitt A, Perumal N, Manicam C, Bell K, Pfeiffer N, Grus FH
   17th Human Proteome Organization (HUPO) World Congress 2018 in Orlando
2) **Discovery and Targeted MS-based strategies for the identification of glaucoma-related IgG V domain peptides.**
   Schmelter C, Perumal N, Funke S, Bell K, Pfeiffer N, Grus FH
   16th Human Proteome Organization (HUPO) World Congress 2017 in Dublin
3) **Characterization of specific antibody-peptide sequences in glaucoma sera using discovery proteomic strategies.**
   Schmelter C, Perumal N, Funke S, Bell K, Pfeiffer N, Grus FH
   15th Human Proteome Organization (HUPO) World Congress 2016 in Taipeh
4) **Mass spectrometric analysis of novel antibody-peptide sequences in glaucoma.**
   Schmelter C, Perumal N, Funke S, Bell K, Pfeiffer N, Grus FH
   The association for Research in Vision and Ophthalmology Congress 2016 in Seattle
5) **Identification and characterization of human tear film glycoproteins.**
   Schmelter C, Perumal N, Funke S, Pfeiffer N, Grus FH
   The association for Research in Vision and Ophthalmology Congress 2015 in Denver
6) **Mass spectrometric analysis of glycosylation sites of the human tear film proteome.**
   Schmelter C, Perumal N, Funke S, Pfeiffer N, Grus FH
   Deutsche Ophthalmologische Gesellschaft Kongress 2015 in Berlin

Declaration II

The present thesis was written under the supervision of Prof. Dr. Dr. Grus at the Department of Translational and Experimental Ophthalmology, University Medical Care Center, Johannes Gutenberg-University in Mainz. The following publications or submitted manuscripts were included in this thesis:

1) **Peptides of the variable IgG domain as potential biomarker candidates in primary open-angle glaucoma (POAG).**
   Schmelter C, Perumal N, Funke B, Bell K, Pfeiffer N, Grus FH
   Human Molecular Genetics, 2017
   PMID: 29036575, DOI: 10.1093/hmg/ddx332

2) **Synthetic polyclonal-derived CDR peptides as innovative strategy in glaucoma therapy.**
   Schmelter C, Nzogang Fomo K, Perumal N, Manicam C, Bell K, Pfeiffer N, Grus FH
   (Under revision in Journal of Clinical Medicine)

3) **Comparison of Two Solid-Phase Extraction (SPE) Methods for the Identification and Quantification of Porcine Retinal Protein Markers by LC-MS/MS.**
   Schmelter C*, Funke S*, Treml J, Beschnitt A, Perumal N, Manicam C, Bell K, Pfeiffer N, Grus FH
   International Journal of Molecular Sciences, 2018
   PMID: 30513899, DOI: 10.3390/ijms19123847

* = authors contributed equally

Table of contents

Abstract

Glaucoma is a neurodegenerative eye disease manifested by the slow progressive loss of retinal ganglion cells (RGC) and their axons, leading to optic nerve damages and visual field defects. Although glaucoma is clinically well known for many years by now, the elevated intraocular pressure (IOP) remains the major risk factor for the development of glaucoma and IOP-lowering medications still represent the gold standard in glaucoma therapy. However, rather than preventing or even curing the neurological damages the current therapeutic approaches can just delay and slow down the disease progression. These circumstances emphasize the urgent need for the development of new diagnostic or therapeutic strategies in order to provide a personalized medical management for each glaucoma patient.

The main objective of this doctoral thesis was to characterize the highly diverse antibody repertoire by liquid chromatography-mass spectrometry (LC-MS)-based quantitative proteomics and to identify new specific and sensitive biomarker candidates. As most important result, we identified 75 peptides of the variable IgG domain as potential biomarkers in primary-open angle glaucoma (POAG) patients. Moreover, we observed significant shifts in the variable heavy chain family distribution and disturbed κ/λ ratios in POAG patients strengthening the assumption of glaucoma-induced effects on the systemic humoral immune response. As second part of the project, we proved the neuroprotective potential of synthetic glaucoma-associated complementarity-determining regions (CDR) on RGCs *ex vivo*. Particularly, the treatment with CDR1 peptide *ASGYTFTNYGLSWVR* resulted in about 30 % significant higher RGC survival rates which can possibly be traced back to the active inhibition or modulation of the molecular function of mitochondrial protein serine protease *HTRA2*. This specific peptide-protein interaction led to significant lesser cellular stress responses and increased activation of antioxidative signaling pathways in the CDR-treated retinal explants. As final part of this doctoral thesis, we compared the analytical performance of two solid-phase extraction (SPE) methods for sample clean-up and peptide enrichment prior to LC-MS analysis. The retinal proteome of the house swine (*Sus scrofa domesticus*) provides excellent requirements for this qualitative as well as quantitative MS-based comparison and delivered convincing results in terms of ocular proteomics. Both SPE systems worked equally well regarding sensitivity, reproducibility and protein/peptide recovery. But in terms of analysis speed and semi-automation, the centrifugal-based SPE technology (SOLAμ™ HRP) clearly benefits compared to the pipette tip-based SPE method (ZIPTIP® C18).

In conclusion, the present doctoral thesis provided deep and detailed insights into the complex autoimmune processes in the pathophysiology of glaucoma and emphasized synthetic CDR peptides as innovative new strategy in future glaucoma therapy. Moreover, the faster and more standardized analytical procedure for the LC-MS analysis will facilitate the management as well as coordination of high-throughput study designs and will significantly increase the quality of large-scale research projects in future.

Zusammenfassung

Das Glaukom beschreibt eine neurodegenerative Erkrankung des Auges, charakterisiert durch den langsamen, progressiven Verlust der retinalen Ganglionzellen (RGZ) und deren Axone, gefolgt von Schäden am Sehnerv und irreversiblen Gesichtsfeldausfällen. Seit vielen Jahren ist ein erhöhter Augeninnendruck (IOD) als wichtiger Hauptrisikofaktor für die Entwicklung eines Glaukoms bekannt und IOD-senkende Medikamente bilden nach wie vor den Goldstandard in der Glaukom-Therapie. Nichtsdestotrotz führen die derzeitig verfügbaren Therapieansätze nur zu einer Verlangsamung des eigentlichen Krankheitsverlaufs, aber können ein Fortschreiten der neurologischen Schäden weder verhindern noch heilen. Aus diesen Gründen ist es von entscheidender Bedeutung neue diagnostische oder therapeutische Strategien zu entwickeln, um eine personalisierte und angemessene medizinische Behandlung der Glaukom-Patienten zu gewährleisten.

Das Hauptziel dieser Forschungsarbeit war es, dass hochdiverse Antikörperrepertoire mittels der Hochflüssigkeitschromatographie-massenspektrometrisch (LC-MS)-basierten Proteomik zu analysieren und neue spezifische sowie sensitive Immun-Peptidmarker zu detektieren. Als primäres Resultat konnten wir 75 Peptide der variablen IgG Domäne als potenzielle Biomarker des primären Offenwinkelglaukoms (POWG) identifizieren. Des Weiteren konnten wir signifikante Unterschiede innerhalb des variablen Gensegment-Expressionsprofils der schweren Kette sowie gestörte κ/λ-Verhältnisse in POWG-Patienten feststellen, die auf Glaukom-induzierte Effekte innerhalb der systemisch humoralen Immunantwort hindeuten. Im weiteren Rahmen dieser Arbeit wurde das neuroprotektive Potenzial von synthetischen Glaukom-assoziierten hypervariablen Regionen (HVR) auf RGZ *ex vivo* überprüft. Vor allem das HVR1-Sequenzmotiv *ASGYTFTNYGLSWVR* konnte eine um 30 % signifikant erhöhte RGZ-Überlebensrate induzieren, welche wahrscheinlich auf die aktive Inhibierung oder Modulierung der Proteinaktivität der mitochondrialen Serinprotease *HTRA2* zurückzuführen ist. Außerdem führte diese spezifische Peptid-Protein Interaktion zu einer signifikant verminderten zellulären Stressantwort und zu einer vermehrten Aktivierung von antioxidativen Signalwegen in den HVR-behandelten retinalen Explantaten. Zum Abschluss dieser Forschungsarbeit wurden zwei Festphasenextraktionsmethoden (FPE), welche hauptsächlich zur Probenaufreinigung bzw. Peptidanreicherung vor der LC-MS Analyse dienen, hinsichtlich ihrer analytischen Leistungsfähigkeit miteinander verglichen. Das retinale Proteom des Hausschweins (*Sus scrofa domesticus*) bietet exzellente Voraussetzungen für

diesen MS-basierten qualitativen als auch quantitativen Vergleich und sollte daher auch eine aussagekräftige Beurteilung beider Systeme hinsichtlich der Anwendung auf Augen-spezifische Proteinmarker erlauben. Beide FPE-Systeme zeigten vergleichbare Resultate bezüglich der Sensitivität, Reproduzierbarkeit und der spezifischen Protein/Peptid-Detektionsrate während der LC-MS Analyse. Allerdings in Anbetracht der Analysegeschwindigkeit und des halbautomatisierten Anwendungsprotokolls bietet die Zentrifugen-kompatible FPE-Technologie (SOLAμ™ HRP) deutlich mehr Vorteile als das Pipettenspitzen-basierte FPE-System (ZIPTIP® C18).

Die Ergebnisse dieser Forschungsarbeit konnten einen tiefen und detaillierten Einblick in die komplexen, autoimmun-assoziierten Prozesse der Glaukom-Erkrankung geben und belegen darüber hinaus das große, neuroprotektive Potenzial von synthetischen HRP-Peptiden in der zukünftigen Glaukom-Therapie. Darüber hinaus wird das schnellere als auch standardisierte FPE-basierte Probenvorbereitungsprotokoll für die LC-MS Analyse die Planung und Koordination von Hochdurchsatz-orientierten Studiendesigns deutlich erleichtern und die Qualität von zukünftigen Großforschungsprojekten erheblich steigern.

1 Introduction

1.1 Glaucoma - Pathology, diagnostics and treatment

Glaucoma is defined as a multifactorial neurodegenerative disease manifested by a slow progressive loss of retinal ganglion cells (RGC) and their axons, and optic nerve damages resulting in visual field defects and irreversible blindness (see Figure 1) [1]. It is one of the leading causes of blindness worldwide and at the age of 70 around 7 % of the population are suffering from glaucoma. From 2010 to 2020 it is expected that the prevalence for glaucoma will increase from 64.3 million to 76.0 million people in the whole world and will end up with 111.8 million people affected by glaucoma in 2040 [2]. One major risk factor for developing glaucoma is an elevated intraocular pressure (IOP), but besides this there are many other pathologic factors discussed such as advanced age [3], vascular blood flow [4], apoptosis [5], mitochondrial dysfunction [6] or genetic predisposition [7]. In the past recent years it was also extensively shown that autoimmunity plays an essential role in the pathogenesis of glaucoma [8,9], which will be discussed in detail in chapter 1.4.

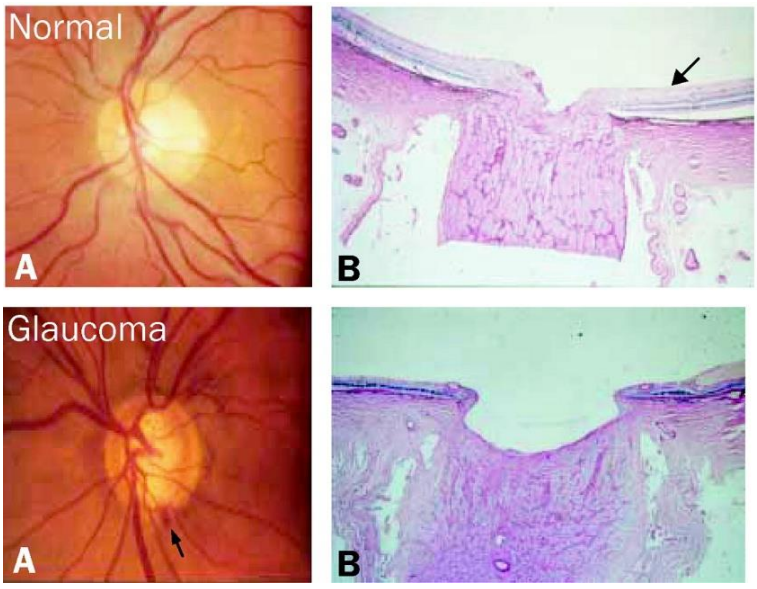

Figure 1: Condition of the optic nerve head in healthy and glaucomatous eyes. **(A)** Fundoscopy of a healthy and glaucomatous optic nerve head. Glaucomatous optic nerve disk is enlarged and deepened. Arrow indicates an optic disc haemorrhage in the glaucoma eye **(B)** Longitudinal cross-section of the optic nerve head of a glaucomatous eye and a healthy control eye. An excavation of the optic nerve disk and a loss of retinal nerve fiber layer (RNFL) can be observed in the glaucoma eye. Illustration was published by Weinreb *et al.* (2004) [10].

Approximately 70 % of the patients show an elevated IOP (> 21 mmHg) and are classified as primary open-angle glaucoma patients (POAG). A much more rare type of this eye disease represents the angle-closure glaucoma (ACG) or acute glaucoma, which is characterized by the mechanic blockade of the drainage canals in the angle of the anterior chamber resulting

in a tremendous increase of the IOP [11]. However, 30 % of all glaucoma patients never develop an elevated IOP (10 to 21 mmHg) and are termed as normal-tension glaucoma patients (NTG) [12]. Particularly this type of glaucoma is generally believed to occur because of the reduced blood flow to the optic nerve and vascular dysfunction accompanied by ischemia of the surrounding tissues [12]. Moreover, around 4-7 % of the people over the age of 40 show a prevalence for an ocular hypertension (OHT, IOP > 21 mmHg), but only around 1 % of this risk group develops glaucoma per year [13]. These findings indicate that an elevated IOP is not the sole reason for the development of glaucoma strengthening the assumption that the etiopathology of this eye disease is influenced by many other factors. Besides this, glaucoma can also occur as secondary disease as e.g. in pseudoexfoliation syndrome (PEXG) patients, who are developing this kind of eye disorder probably because of abnormal protein deposits in the trabecular meshwork followed by reduced aqueous humor outflow and IOP increase [14].

At present, the most promising therapeutic approaches (e.g. medications, laser treatment or surgery) aim for lowering the IOP, which slows down the disease progression but does not cure or prevent the disease [1,15]. In general, IOP-lowering drugs can be divided into 5 major classes comprising prostaglandin analogs, beta-blockers, diuretics, alpha agonists and cholinergic agonists [15]. As first-line treatment, prostaglandin analogs or beta-blockers are prescribed to the patients as monotherapy or in combination, since these medications already showed reliable IOP-lowering efficacy in long-term study designs [16,17]. Prostaglandin analogues lower the IOP by increasing the uveoscleral outflow of the aqueous humor, whereas beta blockers show this effect by decreasing aqueous humor production [1,15]. If the IOP-lowering effects are still missing, the patients will be treated additionally with second-line drugs with other mechanism of action in order to accomplish successful and continuous IOP reduction. Nevertheless, many of the current available medications have a multitude of local adverse effects such as stinging, burning, blurred vision, eye redness and discomfort through to serious systemic adverse effects such as bradycardia, irregular pulse, low blood pressure and asthma attacks [15,18]. In the absence of beneficial effects during medical management or because of pre-existing conditions of the patients, laser therapies or trabeculectomy represent currently the methods of choice for successful glaucoma therapy. Selective laser trabeculoplasty (SLE), for instance, represents the most widely used and accepted laser therapy for several forms of glaucoma (reviewed in [19]) and was shown to reduce the IOP

more than 20 % from baseline during the first 6 months of treatment [20]. However, it was also proved that SLE-induced IOP reduction decreased in 50 % of the patients after two years post-surgery [21] and serves nowadays mainly as additional treatment, especially if medical management alone does not lower the IOP adequately [19]. Altogether, there is no proper cure available for glaucoma so far, highlighting the importance of research going on in the ophthalmologic field in order to unravel the molecular mechanism and signaling pathways involved in the complex pathophysiology of glaucoma.

Besides the lack of proper treatment possibilities in glaucoma therapy, the diagnosis is also a very challenging task, since classical symptoms such as reduced reading ability or clinically detectable vision field defects for long time periods do not cause any symptoms. Due to that reason, they can only be detected at advanced stages of the disease using the routine clinical examinations. At early stages the visual field defects can be compensated by the brain and any sensation of pain is missing. Current routine investigations for the diagnosis of glaucoma are performed *via* repeated measurement of the IOP (tonometry), visual field tests (perimetry) as well as several imaging techniques such ophthalmoscopy and optical coherence tomography (OCT) to identify optic disc cupping. However, none of the present diagnosis techniques provides a reliable screening strategy for early stages of glaucoma or only identifies cases if neuronal damage already has developed. Although monitoring the individual patient's IOP may promote an earlier diagnosis and therapy prior to the initiation of neurodegenerative events, but it also neglects patient cohorts with IOP-independent forms of glaucoma. It is estimated that at least 25 to 35 % of RGC loss is associated with early abnormalities in automatic perimetric tests [22] and up to 41 % of RGC loss is accompanied by first observable glaucomatous damage [23]. Furthermore, around 50-90 % of true glaucoma subjects are still undiagnosed in the whole world, whereas nearly 50 % of positive diagnosed individuals are over-treated without any need [24]. All these findings indicate that there is an urgent need of new examination strategies for early glaucoma diagnosis in order to implement an appropriate and personalized diagnosis and medical management for each patient.

1.2 Immune system, autoimmunity and immune-privileged regions

Main ability of the immune system is to differentiate between endogenous and foreign substances, which is defined as immunotolerance. In general, the immune system is divided into the innate and the adaptive immunity. The innate immune system comprises the first line defense against many common bacteria or other pathogens, which is mainly triggered by

specialized immune cells such as macrophages, neutrophils or dendritic cells. These immune responses are elicited by the recognition of pathogen-associated molecular pattern (PAMPs), which are represented by highly conserved structural motives such as lipopolysaccharides, lipids or peptides [25]. Particularly, Toll-like receptors play an essential role in the recognition process of these conserved structures and are initial for the innate immune response [26]. The adaptive system, in contrast, consists of two major bulks of lymphocytes called B and T cells. T cells mature in the thymus and are involved in the cell-mediated immunity, whereas B cells mature in the bone marrow and build the foundation for the humoral immune response. The adaptive immune response is characterized by the secretion of highly specific antibodies by B cells and the activation of specific T cells several days after the initial encounter with the pathogen. In general, the adaptive immune system is hallmarked by the immunological specificity, the self-non-self-discrimination as well as the long-term memory and can be clearly differentiated from the innate immune system [25].

During maturation to B or T cells the precursor cells undergo positive and negative selection events in the primary lymphoid organs, also known as central tolerance. Positive selection triggers the survival rate of precursor cells with properly arranged antigen receptors (BCR or TCR), whereas negative selection promotes the elimination of autoreactive B or T cells with high affinity for self-antigens [27]. Since the number of presented autoantigens is limited in the generative lymphoid organs (thymus or bone marrow), the central tolerance mechanism cannot eliminate all autoreactive B and T lymphocytes. Peripheral tolerance mechanism include the anergy of autoreactive lymphocytes after activation without costimulation, clonal deletion after exposure to high antigen concentrations or suppression by regulatory T cells [27]. However, despite the large number of tolerance mechanisms, each individual person has a panel of autoreactive B and T cells as well as a natural repertoire of autoantibodies (AAB), also termed as natural autoimmunity [28]. In general, these naturally occurring AABs do not show any pathogenic or destructive properties and seem to be consistent along healthy individuals [29]. Nevertheless, any disruption of this equilibrium state may result in autoaggressive conditions and may promote the development or progression of autoimmune-related diseases. Several hypotheses to as how natural autoimmunity may become autoaggressive, exist. Besides genetic susceptibility [30], it is also believed that defective selection processes during lymphocyte maturation or specific environmental triggers (e.g. infections) may promote the increased development of autoreactive B and T cell

populations [31]. Ageing is also one important risk factor for autoimmunity, because of a disturbed immunocompetence and a decreased T lymphocyte generation in the elderly population [32]. Also, gender-specific differences such as pregnancy, sex hormones or epigenetics are suspected to influence autoreactive responses and to promote the formation of autoimmune-related diseases [33].

Regarding the prevention of autoimmune-induced tissue damage, several organs are able to suppress inflammatory immune responses, which is also known as the immune privilege. These regions include the central nerve system (CNS), testicles, placenta, fetus, brain and most importantly the eyes [34]. Since macrophage-mediated immune responses are characterized by neurotoxic effects followed by swelling of the tissue, the immune privilege aims to suppress inflammatory activities in favor of tissue preservation. On the one hand, this immune privilege will be achieved by physical separation of the compartments such as the blood-brain (BBB) or blood-retina barrier (BRB) in order to avoid an unregulated penetration of immunocompetent cells during immune responses [34]. On the other hand, these immune-privileged sites are possessed with specific immunosuppressive properties such as complement system inhibitors, immunosuppressive cytokines (e.g. TGF-β) or the increased occurrence of regulatory T cells [34]. Especially the aqueous humor of the eye contains several growth factors, cytokines and neuropeptides suppressing the proliferation and cytokine production of T cells after antigenic stimulation [35]. Furthermore, it is known that the retinal pigment epithelium (RPE), the iris and the ciliary body not only inhibit stimulated T cells, but also promote their conversion into regulatory T cells [36]. In summary, all these immunosuppressive mechanisms aim for the maintenance of the visual system and for the prevention of inflammatory-induced neurological damage.

1.3 Antibodies – Structure, classes and functions

Antibodies are mainly produced by B cells and are presented as membrane-bound protein receptors (B cell receptor, BCR) or can be secreted as protein molecules by antigen-stimulated B cell clones. In general, antibodies can be divided into five major classes (isotypes) termed as IgA, IgD, IgE, IgG and IgM [25]. Moreover, in human IgA and IgG isotypes can be further divided into closely related subtypes called IgA1 and IgA2 and IgG1, IgG2, IgG3 and IgG4. The C region of each isotype (or subtype) contains a unique amino acid sequence and triggers different kinds of effector functions. The basic structure of each antibody represents a large Y-shaped protein consisting of two identical heavy chains (HC) and two identical light chains (LC)

connected by disulfide bonds. In human, IgM and IgE antibodies contain four constant tandem Ig domains (CH1-CH4), whereas IgA, IgD and IgG molecules contain only three constant tandem Ig domains (CH1-CH3, see Figure 2). In addition, each heavy chain inherits a variable part (VH), which represents the antigen binding site of the antibody. The light chain, in contrast, is formed by one variable region (VL) and one constant Ig domain (CL). Each antibody molecule consists either two κ LCs or two λ LCs and is naturally expressed in the ratio 3:1 in human individuals [25]. Furthermore, the variable parts (VH and VL) with the first constant Ig domains (CH1 and CL) form the antigen-binding fragment (Fab) and the other two constant domains (CH2 and CH3) represent the crystallizable fragment (Fc) of the antibody molecule (see Fig. 2). Closer inspection of the variable region on the sequence level illustrates the classification of the V domain into complementarity-determining regions (CDR) and framework regions (FR) [37]. CDRs are hypervariable sequence motives resulted from somatic recombination and hypermutations events during B cell maturation or affinity maturation and determine the antigens specificity of the antibodies [38]. Each VH and VL fragment contains three different CDR sequence motives (CDR1, CDR2 and CDR3) and provides in total six CDRs per antibody molecule for antigen recognition and binding. In addition, each CDR sequence motive is surrounded by FR regions (FR1, FR2, FR3 and FR4), which represent moderately mutated sequence parts of the V domain and are primary not responsible for the antigen specificity of the antibody.

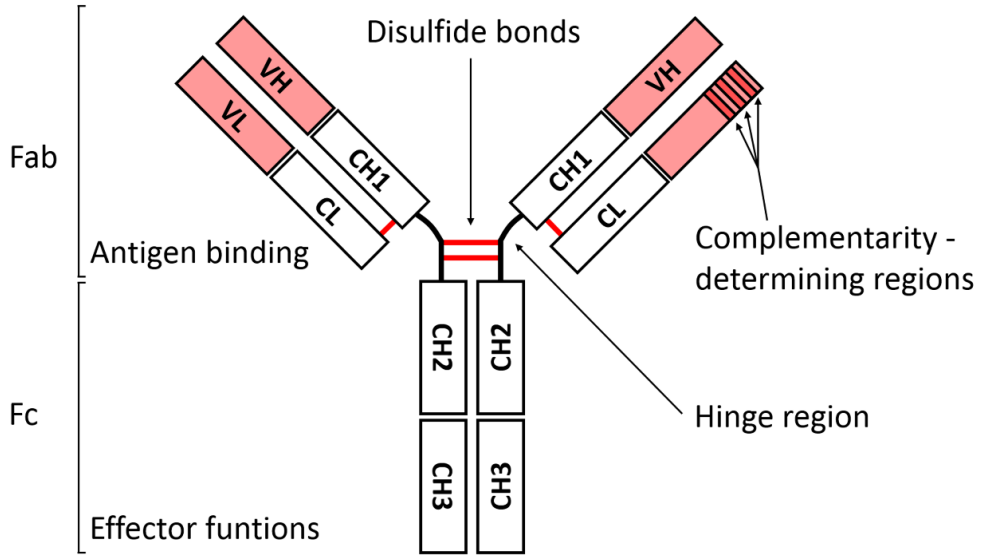

Figure 2: Structure of an IgG antibody molecule. Each IgG molecule consists of two identical heavy chains and two identical light chains connected by disulfide bonds. The variable part with the first constant domain (VH, VL and CL, CH1) forms the antigen-binding fragment (Fab), whereas the other two constant domains (CH2 and CH3) determine the crystallizable fragment (Fc) of the IgG antibody molecule.

The effector functions of the antibodies are mainly determined by the heavy chain constant region (Fc) of the Ig molecule and depends on the properties of the specific Ig isotype. Most of the effector functions require the binding to specific Fc receptors, which are expressed on various immunocompetent cells such as macrophages or neutrophils. The effector functions of antibodies compromise a multitude of activities such as neutralization of toxins, opsonization and phagocytosis of pathogens, activation of the complement system or antibody-dependent cellular cytotoxicity (ADCC) [25]. Particularly, conserved N-glycosylation sites of the Ig heavy chain mediate the binding affinity to the Fc receptors and greatly influence the efficiency of the respective effector functions [39].

1.4 Autoimmune processes in glaucoma disease

In recent years, it was extensively shown that the pathogenesis of glaucoma greatly influences the natural autoantibody (AAB) repertoire in human subjects and leads to significant changes in autoreactivities against several neuronal and ocular antigens. Wax and colleagues (1994) [40] were the first who provided evidence for increased AAB titers in sera of normal-tension glaucoma (NTG) patients against proteins such as Sjögren's syndrome A antigen or heat shock protein 60 (*HSP60*). During the last two decades, AAB profiling was performed for several other glaucoma phenotypes, not only focusing systemic occurring autoreactivities, but also local changes in the AAB profiles close to the site of damage (e.g. aqueous humor or tears) [41–43]. Within this scope, many of the studies performed immunoproteomic or mass spectrometry (MS)-based technologies for the detection and characterization of the targeted autoantigens. Besides the identification of ubiquitous proteins with chaperone properties such as *HSP27* [44], *HSP60* [45] or α-/β-crystallines [44], also neuronal or structural proteins such as myelin basic protein (*MBP*) [46], α-fodrin [47], glial fibrillary acidic protein (*GFAP*) [46], vimentin [46], and glycosaminoglycans [48] were discovered. Furthermore, many autoreactivities against functional proteins such as γ-enolase [49], neuron-specific enolase [50] or glutathione S-transferase (*GST*) [51] were observed, representing essential proteins for the maintenance of the cell homeostasis.

Interestingly, a high degree of congruence between systemic and local occurring autoreactivities (in sera and aqueous humor) were observed [8,41,42,52], strengthening the hypothesis that the pathogenesis of glaucoma goes along with significant changes in the humoral immune response. Besides that, it is also remarkable that POAG patients show preferential autoreactivities against retinal autoantigens, whereas the NTG patient cohort is

mainly characterized by increased autoreactivities against structures of the optic nerve head [53]. However, the exact role of these highly diverse AAB repertoires is still unknown and it is elusive if they are an epiphenomenon (e.g. develop as a consequence of the disease) or of causative nature. Probably some of the AAB titers, particularly which are increasing during disease progression, can be traced back to epiphenomenal conditions, nevertheless it remains unclear to what extend they are influencing the pathophysiology of glaucoma. Particularly, autoreactivities against the protein *MBP* are known to correlate with disease progression in multiple sclerosis (MS) patients and are currently under discussion as diagnostic and prognostic marker candidate [54,55]. With respect to glaucoma, many of the targeted autoantigens (e.g. several *HSPs* and *GST*) are associated with cellular stress responses and show high expression levels particularly in a pro-inflammatory environment. The protein *GST*, for instance, catalyzes the conjugation of glutathione and radical oxygen species (ROS) and prevents ROS-induced tissue damage during stress responses [56]. Yang *et al.* (2001) [51] assumed that increased AAB titers against *GST* in glaucoma patients may be considered as general immune response to glaucomatous tissue damage events and represent subsequently a secondary product. In contrast, Tezel *et al.* (2000) [57] observed that the treatment of retinal tissues with anti-*HSP27* antibody, also up-regulated in glaucoma patients, resulted in increased apoptosis rates of RGCs *in vitro* possibly by inactivating or attenuating the biological function of native *HSP27.* Beyond that, another study showed that systemic immunization of rats with different ocular antigens leads to continuous RGC loss *in vivo* accompanied by altered AAB profiles in the immunized animals [58]. In conclusion, it could be assumed that increased AAB titers automatically result in autoaggressive conditions and may be causative for the pathomechanism of the respective disease.

Nevertheless, many of the previous AAB profiling studies also confirmed decreased autoreactivities against a range of ocular antigens (e.g. *GFAP* or α-/γ-synuclein) in glaucoma patients in comparison to healthy controls [46]. Shoenfeld and colleagues (2005) [59] ascribed a protective role to these AABs in the cellular homeostasis and emphasized their clinical importance as well as therapeutic potential. Recent studies performed in our group agree with this hypothesis and provide evidence of AAB-induced effects in several *in vivo* / *ex vivo* glaucoma models. Amongst others, our group demonstrated neuroprotective activities of anti-*GFAP*, anti-14-3-3 anti-γ-synuclein on stressed RGCs in different *in-vitro* designed cell culture experiments and an *ex vivo* glaucoma model [60–63]. Consistent with that, our group

further verified decreased neurological damage and increased RGC survival rates in an IOP-dependent glaucoma animal model after intravitreal injection of anti-α-synuclein [64]. All study designs are accompanied with interesting retinal proteomic changes triggering the increased expression of neuroprotective and antiapoptotic proteins (e.g. cofillin-1 or glutamine synthetase).

However, despite the large numbers of studies focusing the humoral autoimmunity in glaucoma, it is still unclear how exactly these different AABs influencing the pathophysiology or the course of the disease. Nevertheless, it can be concluded that glaucoma does not present a 'classical' autoimmune disease due to increased as well as decreased AAB titers in various biological fluids of glaucoma patients. Furthermore, it still has to be determined if these abnormal autoreactivities in the humoral immune response are in accordance with other glaucoma-associated proteomic changes in the retina, which might promote or antagonize the neurodegenerative processes of RGCs *in vivo*.

1.5 Proteomics and biomarker discovery

The term proteomics was coined first by the Australian researcher Marc Wilkins in 1994 and originally combines the words 'protein' and 'genome'. Proteomics describes the entire composition of proteins in a cell, tissue or an organism during a specific set of conditions. It represents a large-scale study to investigate the structure, function and interaction of large protein networks and to evaluate their versatile role in complex biological systems [65]. In contrast to the genome, the proteome defines a highly dynamic platform, which is characterized by qualitative and quantitative proteomic changes at certain points in time mainly caused by external stimuli (e.g. environmental factors or therapeutic agents). However, in general proteins are composed of several amino acids, which are arranged to a single polypeptide chain or to multiple polypeptide subunits. Proteins provide many important biological activities for cell survival and homeostasis ranging from metabolic functions, cell signaling, energy supply, transport properties till molecules of the cytoskeleton and components of the immune response system [65]. Furthermore, many proteins are chemically modified by posttranslational modifications (PTMs) influencing the structure, folding, stability and biological activity of these macromolecules. Particularly, common PTMs such as glycosylation and phosphorylation are of great interest in basic research, because of their great importance in signaling cascades and pathway activation and also represent promising indicators for several kinds of diseases [66].

Mass spectrometry (MS) represents the instrument of choice for the qualitative and quantitative characterization of various proteomes in a single experiment providing high accuracy and sensitivity. Nevertheless, prior to MS analysis a prefractionation step is urgently needed due to the high complexity of various biological samples. This separation step is routinely performed by gel-based approaches (1D- or 2D-gel electrophoresis) and/or in combination with high-performance liquid-chromatography (HPLC) systems. Subsequently after separation, the purified protein species are either detected as intact protein molecules (top-down) or as enzymatically digested protein peptides (bottom-up) by high-resolution MS systems [67].

Bottom-up proteomic approaches, also termed as 'shotgun proteomics', are routinely used for the analysis of complex protein mixtures. Thus, the characterization of the respective protein species is based on the detection of unique and specific fragment peptides. Identification of the proteins/peptides is performed by fragmentation of the precursor ions (MS/MS) in the collision cell of the MS and by matching the experimental data with *in-silico* generated MS/MS spectra from public protein databases. Label-free quantification (LFQ) is based on the intensity of the precursor ions in the first MS scan and allows a statement about the relative frequency of the proteins/peptides between two or more groups. Particularly, clinical study designs apply the shotgun proteomics approach for biomarker discovery in various biological fluids of diseased and healthy control subjects. Abnormal protein expression levels may give essential insights into the involved protein signaling pathways and interaction networks and provide important information about the complex pathophysiology of the respective disease [68]. In contrast, top-down proteomics is more suitable for the structural analysis of highly purified protein species, which are injected directly as intact molecules into the MS [67]. Major advantage of this approach is the universal detection of all existing protein modifications (proteotypes) in one MS spectrum and provides much more structural information than conventional shotgun proteomic analyses.

1.6 Aims of the thesis

The pathophysiology of glaucoma is clearly associated with significant changes in the natural autoantibody (AAB) repertoire, but it is still unclear, if those are considered either as epiphenomenon or of causative nature. Conventional immunoproteomic profiling strategies such as microarray or western blot analysis require a predefined panel of proteins serving as potential epitope targets for the highly diverse AABs. Major disadvantage of these screening technologies is the lacking structural information about the active binding sites (paratopes) of the AAB molecules and their great potential as biomarker candidates in future.

Recent studies already proved the applicability of high-resolution mass spectrometry (MS) for the characterization of highly diverse AAB repertoires in various diseases and was applied in the present thesis to investigate disease-related IgG V domain peptides sequences, particularly CDRs, in POAG patients (manuscript I). Main objective of this project was to gain a fundamental understanding about the biological activity and function of AABs and acquire new knowledge how autoimmunity influences the pathogenesis and progression of glaucoma.

As second part of the thesis, we investigated the neuroprotective potential of two in glaucoma low abundant CDR peptides on RGCs *ex vivo* (manuscript II). State-of the-art MS-based affinity capture experiments were used for epitope target identification (interaction partner) of the CDR peptides in the pig retina. An adolescent retina organ culture of the house swine in combination with immunohistochemical staining techniques were used to evaluate CDR-induced effects on RGCs *ex vivo*. Accordingly, shotgun proteomic analyses of the retinal explants were performed to unravel the CDR-induced signaling pathways and interaction networks, which might also play important key functions in the course of glaucoma.

At the end of the project, two solid-phase extraction (SPE) methods for sample clean-up and peptide enrichment prior to MS analysis were compared with respect to analytical performance, reproducibility and analysis speed (manuscript III). The selection of proper SPE materials represents a crucial step for LC-MS-based proteomic study designs and greatly influences the quality and sensitivity of the acquired proteomic data. Due to that reason, we investigated the retinal proteome of the house swine for the technical performance of both SPE methods. The house swine represents a promising animal model for studying human eye diseases including glaucoma due to its anatomical similarities to human eyes and provides interesting biomarker candidates for the protein recovery analysis of both SPE methods.

2 Manuscripts

2.1 Publication I

Peptides of the variable IgG domain as potential biomarker candidates in primary open-angle glaucoma (POAG).

Schmelter C, Perumal N, Funke B, Bell K, Pfeiffer N, Grus FH

Human Molecular Genetics, 2017
PMID: 29036575, DOI: 10.1093/hmg/ddx332

Human Molecular Genetics, 2017, Vol. 26, No. 22 4451–4464

doi: 10.1093/hmg/ddx332
Advance Access Publication Date: 22 September 2017
Original Article

ORIGINAL ARTICLE

Peptides of the variable IgG domain as potential biomarker candidates in primary open-angle glaucoma (POAG)

Carsten Schmelter, Natarajan Perumal, Sebastian Funke, Katharina Bell, Norbert Pfeiffer and Franz H. Grus*

Department of Experimental and Translational Ophthalmology, University Medical Center, Johannes Gutenberg University, Mainz, Germany

*To whom correspondence should be addressed at: Department of Experimental and Translational Ophthalmology, Medical Center of the Johannes Gutenberg University Mainz, Langenbeckstr. 1, 55131 Mainz, Germany. Tel: +49 6131173328; Fax: +49 6131175509; Email: grus@eye-research.org

Abstract

Autoantibody profiling has gained increasing interest in the research field of glaucoma promising the detection of highly specific and sensitive marker candidates for future diagnostic purposes. Recent studies demonstrated that immune responses are characterized by the expression of congruent or similar complementarity determining regions (CDR) in different individuals and could be used as molecular targets in biomarker discovery. Main objective of this study was to characterize glaucoma-specific peptides from the variable region of sera-derived immunoglobulins using liquid chromatography-—mass spectrometry (LC-MS)—based quantitative proteomics. IgG was purified from sera of 13 primary open-angle glaucoma patients (POAG) and 15 controls (CTRL) and subsequently digested into Fab and Fc by papain. Fab was further purified, tryptic digested and measured by LC–MS/MS. Discovery proteomics revealed in total 75 peptides of the variable IgG domain showing significant glaucoma-related level changes ($P < 0.05$; log2 fold change ≥ 0.5): 6 peptides were high abundant in POAG sera, whereas 69 peptides were low abundant in comparison to CTRL group. Via accurate inclusion mass screening strategy 28 IgG V domain peptides were further validated showing significantly decreased expression levels in POAG sera. Amongst others 5 CDR1, 2 CDR2 and 1 CDR3 sequences. In addition, we observed significant shifts in the variable heavy chain family distribution and disturbed κ/λ ratios in POAG patients in contrast to CTRL. These findings strongly indicate that glaucoma is accompanied by systemic effects on antibody production and B cell maturation possibly offering new prospects for future diagnostic or therapy purposes.

Introduction

Glaucoma is a chronic neurodegenerative disease characterized by a progressive loss of retinal ganglion cells (RGC) and their axons, leading to optic nerve damage and gradual loss of the visual field (1). It is one of the primary causes of blindness worldwide and around 80 million people will be suffering from glaucoma by 2020 (2). Primary-open angle glaucoma (POAG), the most common form of glaucoma, is associated with an elevated intraocular pressure (IOP) which represents the major risk for developing this eye disease (1). Nevertheless, around 30% of the glaucoma patients never develop an elevated intraocular pressure, which then is defined as normal tension glaucoma (NTG) (3). Although the pathomechanism of glaucoma is still poorly understood, many other risk factors are involved such as advanced age (4), reduced ocular blood flow (5), apoptotic processes (6), genetic predisposition (7,8) and increased glutamate or nitric oxide levels (9). In the last decade a

Received: May 24, 2017. **Revised:** August 10, 2017. **Accepted:** August 15, 2017

multitude of studies demonstrated that autoimmunity plays an essential role in the pathogenesis of glaucoma and altered autoantibody profiles were observed in sera and aqueous humor of glaucoma patients (10,11). Many autoantibodies (AAB) against ocular and optic nerve antigens have been identified so far such as heat shock proteins (12), gluthathione S-transferase (13), alpha fodrin (14), glycosaminoglycans (15), gamma enolase (16) and myelin basic protein (17). However, the exact participation of AAB in the pathogenesis of glaucoma is not well understood and literature concerning the effects of autoimmunity is ambiguous. Tezel *et al*. (2000) (18) observed that anti-HSP27, up-regulated in glaucoma patients, promotes apoptotic cell death *in vitro* and may act as proinflammatory molecule. On the other hand, our group already showed that down-regulated AAB against gamma-synuclein, 14-3-3 and glial fibrillary acidic protein (GFAP) have an anti-apoptotic effect on stressed RGCs as well as retinal explants and are hypothesized to function as protective components of the immune system (19–22). In general, human immunoglobulins G (IgG) consist of two identical heavy chains and two identical light chains. Each light chain contains a variable (VL) and a constant domain (CL: κ or λ chain), whereas the heavy chain is composed of one variable domain (VH) and three different constant regions (CH1, CH2 and CH3). The variable part along with the first constant region forms the antigen-binding fragment (Fab) and the other three constant parts represent the crystallisable fragment (Fc) (23). Furthermore, the variable parts are subdivided into six hypervariable sequences called complementarity-determining regions (CDR) surrounded by relatively constant sequences termed framework regions (FR) (24). The CDR sequences determine the antigen specificity of the antibody and particular the highly diverse CDR3 of the VH domain plays a key role in the antigen recognition process (25). It is estimated that the diversity of antibodies is between 10^{11} and 10^{58} triggered by somatic recombination and hypermutations and makes it highly unlikely to find identically mutated CDR sequences among different individuals (23,26,27). Regardless to this widespread immunological concept, other research groups already demonstrated the successful identification of overlapping or similar CDR sequences in unrelated HIV as well as leukemia patients and disproved that B cell maturation (antibody production) is not a fully random process (28,29). VanDuijn *et al*. (2010) (30) provided further evidence that the immunization of individual rats with selected antigens leads to the expression of congruent CDR sequence phenotypes apparently driven by (auto-)antigenic pressures. Currently a research group introduced a novel proteomic approach for studying variable regions of immunoglobulins using liquid chromatography - mass spectrometry (LC-MS) without the requirement of previously known antigen panels (31,32). Employing this strategy they were able to identify disease-specific marker peptides of the variable IgG domain shared between lung cancer patients (33), multiple sclerosis patients (34) and paraneoplastic syndrome patients (35). All previous studies exploring the complex AAB profiles in glaucoma were based on conventional techniques such as microarray or western blot analysis, a targeted analysis of the antibody structures itself is still missing. For this reason, the main objective of this study was to identify peptides of the variable IgG domain, particular CDRs, shared between POAG patients in comparison to healthy subjects. Schematic Workflow of the sample preparation protocol is illustrated in Figure 1.

Results

Discovery proteomics of glaucoma-related IgG Fab peptides

Fab isolation of individual sera samples was confirmed by 1-D SDS PAGE for all CTRL and POAG subjects (Fig. 2 and Supplementary Material, Fig. S1A and B). The protein bands around 28 kDa show the Fab fragments, the protein bands around 49 kDa represent non-reduced F(ab')2 fragments and the protein bands around 62 kDa contain traces of albumin. Protein identifications were determined by MS and were in accordance with literature (31). Protein pattern of all subjects showed a high degree of congruency and densitometric analysis of Fab protein spots provided an average area of 57275 ± 7594 dpi (Supplementary Material, Fig. S2 and Table S1). As only very low contamination was detectable we decided to perform an In-solution trypsin digestion for further LC-MS analysis. In total 3752 peptides were identified in CTRL and POAG group with FDR < 1% (Supplementary file 1). The identified peptides were aligned to V-, J- and C- germline sequences derived from the IMGT database using NCBI IgBLAST algorithm. The best-matching IMGT database hit was selected for further analysis and an alignment match score of 70% was set as cutoff value. In that way, 3287 peptides were assigned to the V region, 183 peptides to the J region and 117 peptides to the C region of the IgG framework. Within the VH domain, 227 peptides were annotated as CDR1, 309 as CDR2 and 41 as CDR3. In contrast, within the VL domain it was possible to identify 425 peptides as CDR1, 489 as CDR2 and 59 as CDR3 (Supplementary Material, S1). Nevertheless, around 4% of the identified peptides showed to less similarity to IMGT germline sequences and were therefore excluded from the analysis.

Next, we were interested in peptides of the variable IgG domain, particular CDR sequences, which were significant differently distributed between POAG and CTRL group. In total 393 IgG V domain peptides were at least detectable in one of the study groups (15 CTRL or 13 POAG subjects) and selected for further analysis. As only 3% of the total data matrix was missing we decided to replace the values by their respective means assuming that these peptides were close to the limit of detection (36). Regarding label-free quantification (LFQ) statistics, 124 of the IgG V domain peptides showed a significant level change between both study groups using two-sided t-test ($P < 0.05$) (supplementary file 2). To determine the most meaningful changes and to avoid false-positive identifications a Volcano plot (Fig. 3) was performed. The data-set was filtered at a significance level of p value < 0.05 and $\log_2$ fold change ≥ 0.5 revealing 75 differently distributed IgG V domain peptides between both study groups: 6 of these peptides (filled squares) were high abundant in the POAG group in comparison to CTRL, whereas the abundances of 69 peptides (open triangles) were decreased (Supplementary Material, Table S2). Most peptides were annotated as framework regions (18 FR1, 10 FR2, 22 FR3 and 3 FR4) and the remaining peptides as complementarity determining regions (9 CDR1, 7 CDR2 and 6 CDR3). Exemplary box plots of differentially distributed IgG V domain peptides are shown in Figure 4. As further confirmation, we manually examined the raw LC-MS data files of a random set of CTRL subjects and POAG patients and found that the intensity of monoisotopic precursor ion 669.84 *m/z*, representing the peptide sequence NSLYLQMNSLR (FR3), was observably higher in the CTRL group in contrast to POAG (Fig. 5). Manual inspection was also performed for peptide sequence ASQSVSSYLAWYQQK (CDR1) as shown in Supplementary Material, Figure S3. Moreover, based on the abundances of the

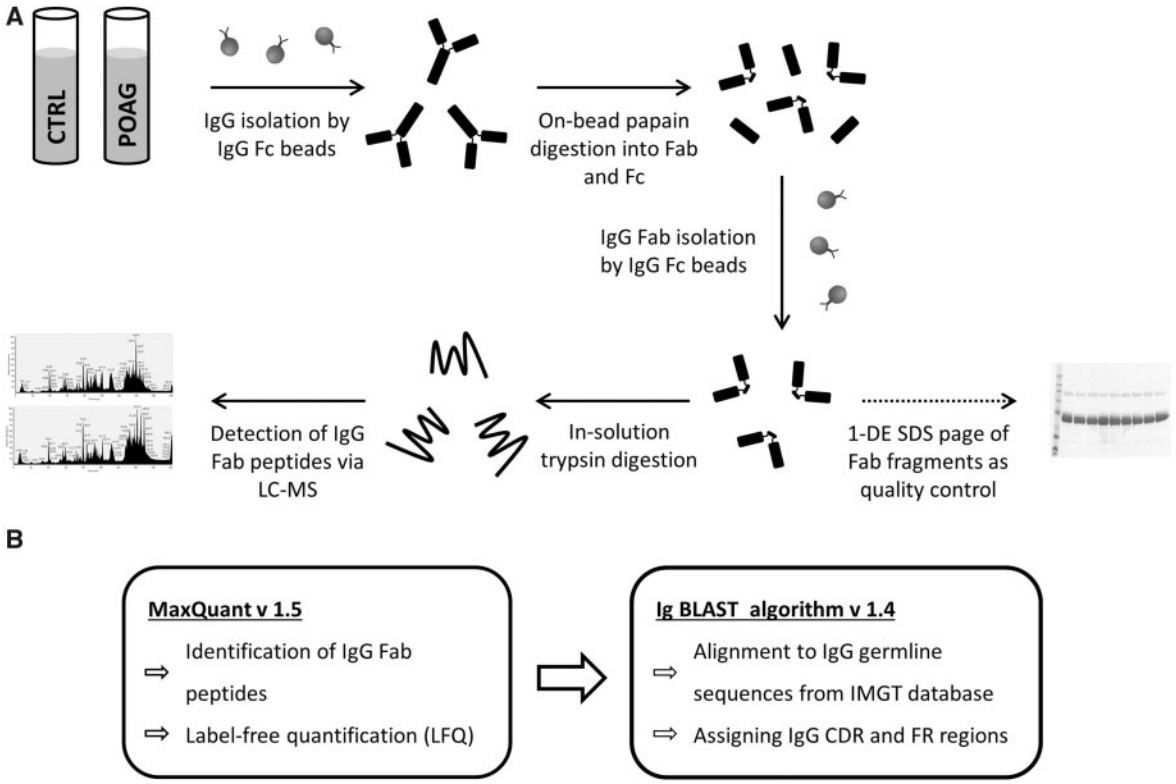

Figure 1. Schematic Workflow of Fab (antigen-binding fragment) purification steps, LC-MS/MS measurements and the data analysis. (**A**) IgG was purified from individual sera samples (100 µl) from 13 patients diagnosed with primary open-angle glaucoma (POAG) and 15 controls using Capture Select™ IgG-Fc (crystallisable fragment) resin beads. IgG were digested into Fab and Fc by immobilized papain resin beads followed by further purification of Fab via Capture Select™ IgG-Fc resin beads. 1-D SDS PAGE of flow-through fraction was performed to evaluate if the Fab purification steps were successful. In-solution trypsin digestion of Fab fragments (20 µg) was performed and measured on a HPLC-coupled LTQ Orbitrap XL mass spectrometry system. (**B**) Peptide identification and label-free quantification (LFQ) was performed employing bioinformatical tool MaxQuant v. 1.5 against human NCBI database (955.083 sequences). IgBLAST algorithm v. 1.4 was used to align identified peptides to V, J and C germline sequences derived from IMGT database (ImMunoGeneTics information system). Due to the identified peptides were assigned to the complementarity determining regions (CDR), framework regions (FR) or constant regions (C) of the IgG framework based on an alignment match score $\geq$ 70%. The sample preparation protocol was published first by de Costa *et al.* (31,33).

75 glaucoma-related IgG V domain peptides a principal component analysis (PCA) was performed. Figure 6 represents the score plot of the first two PCs explaining more than 55.5% of the total variance in the data. Healthy individuals are represented by open dots and POAG subjects are indicated by filled triangles. The first two PC allow effective separation of all individuals into CTRL and POAG group without any overlap. POAG subjects laid on average at positive scores at PC 1 (Ø PC1 score 4.43), whereas CTRL subjects were clustered on average at negative values on the same PC (Ø PC1 score -4.08).

Peptides derived from the constant region of the IgG heavy chain were equally distributed between CTRL and POAG group (data not shown). In addition, κ/λ ratios were calculated for both groups using representative peptides from the constant region (κ chain: $n = 17$; λ chain: $n = 12$) of the IgG light chain. The κ/λ ratios of each individual were calculated as percentage distributions based on the peptide abundances. POAG group showed a higher statistical dispersion of κ/λ ratios in comparison to CTRL group, but no significant difference ($P = 0.65$) was observed between both groups (Supplementary Material, Fig. S4).

VH, VK and VΛ family distribution in CTRL and POAG group

The variable genes of the heavy chain (VH) and the kappa chain (VK) are subdivided into seven families, while the variable genes of the lambda chain (VΛ) consist out of nine families. Family classification was based on sequence similarity according to previous publication (37). The family distributions of VH, VK and VΛ were calculated at the individual patient level and only peptide sequences validated by MS/MS identification were included in the analysis. Normalization of frequencies was performed using peptide counts of each family divided by the total number of identified peptides in a given chain family. The average family frequencies of VH, VK and VΛ were compared between both groups. Peptides used for Ig VH family distribution showed a mean alignment match score of 90 ± 6.9% and a mean average length of 14.3 ± 4.4 amino acids. Family VH3 (Fig. 7A) was significant increased in POAG patients compared to CTRL group (POAG: 65.3 ± 3.2% and CTRL: 62.1 ± 4.3%; $P = 0.04$). On the contrary, family VH2 (Fig. 7B) was slightly but significant decreased in the POAG group (POAG: 0.44 ± 0.26% and CTRL: 0.81 ± 0.43%; $P = 0.01$). The other five family members of VH did not show significant differences between both groups ($P > 0.05$) (Supplementary Material, Fig. S5A). Identified peptides used for Ig VK and VΛ family distribution showed mean alignment match scores of 91 ± 6.5%/91 ± 7.5% and mean average lengths of 15.3 ± 4.9/14.8 ± 5.2 amino acids. No significant differences in family distribution of VK and VΛ chains were observed between both groups ($P > 0.05$) (Supplementary Material, Fig. S5B and C).

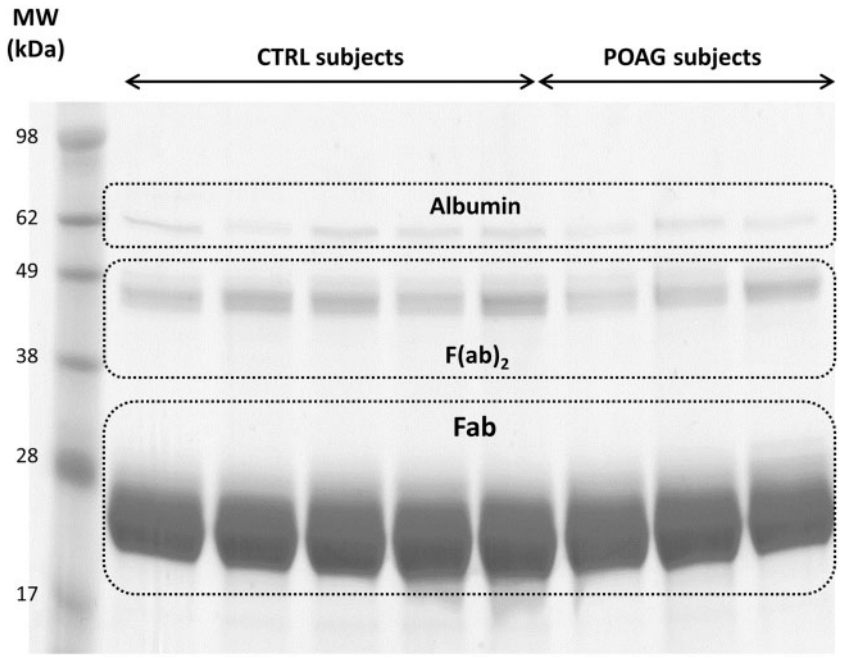

Figure 2. Exemplary 1-D SDS PAGE of the purified Fab fragments from 5 controls subjects and 4 POAG patients. The protein bands around 28 kDa represent the purified Fab fragments. Protein bands around 49 kDa show non-reduced $F(ab)_2$ fragments and protein bands around 62 kDa contain traces of albumin. Each sample lane contains a total protein amount of 20 µg.

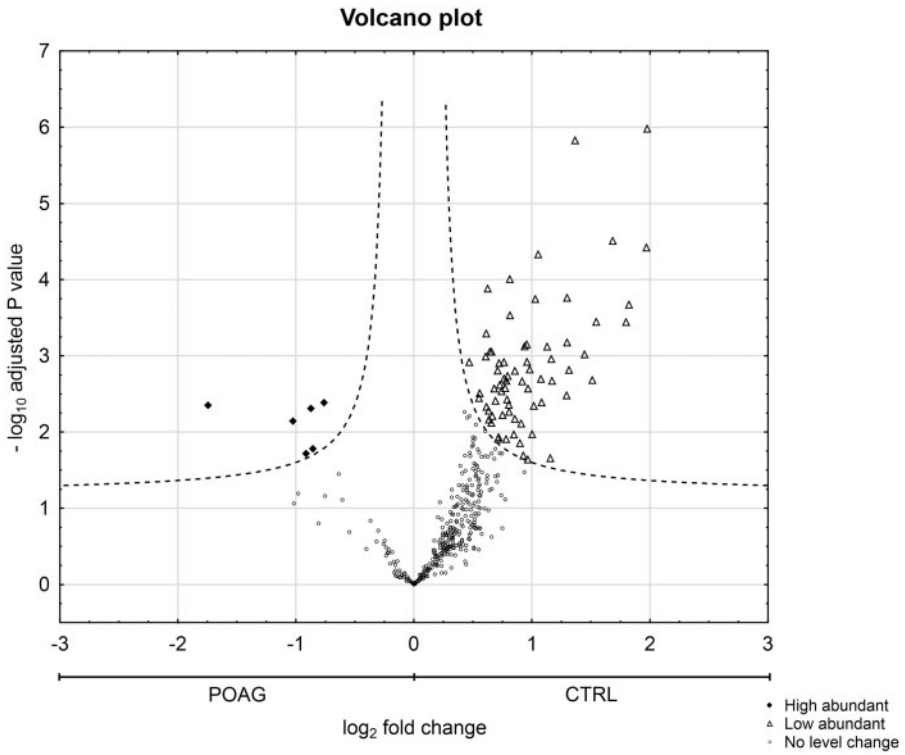

Figure 3. Statistical analysis of IgG V domain peptides between CTRL and POAG group detected in the discovery study. Volcano plot showing $\log_2$ fold change plotted against $-\log_{10}$ adjusted P value for samples from CTRL subjects versus samples from POAG patients. Filled squares represent 6 significant high abundant peptides and open triangles display 69 significant low abundant peptides in POAG patients in comparison to CTRL ($P < 0.05$, $\log_2$ fold change ≥ 0.5).

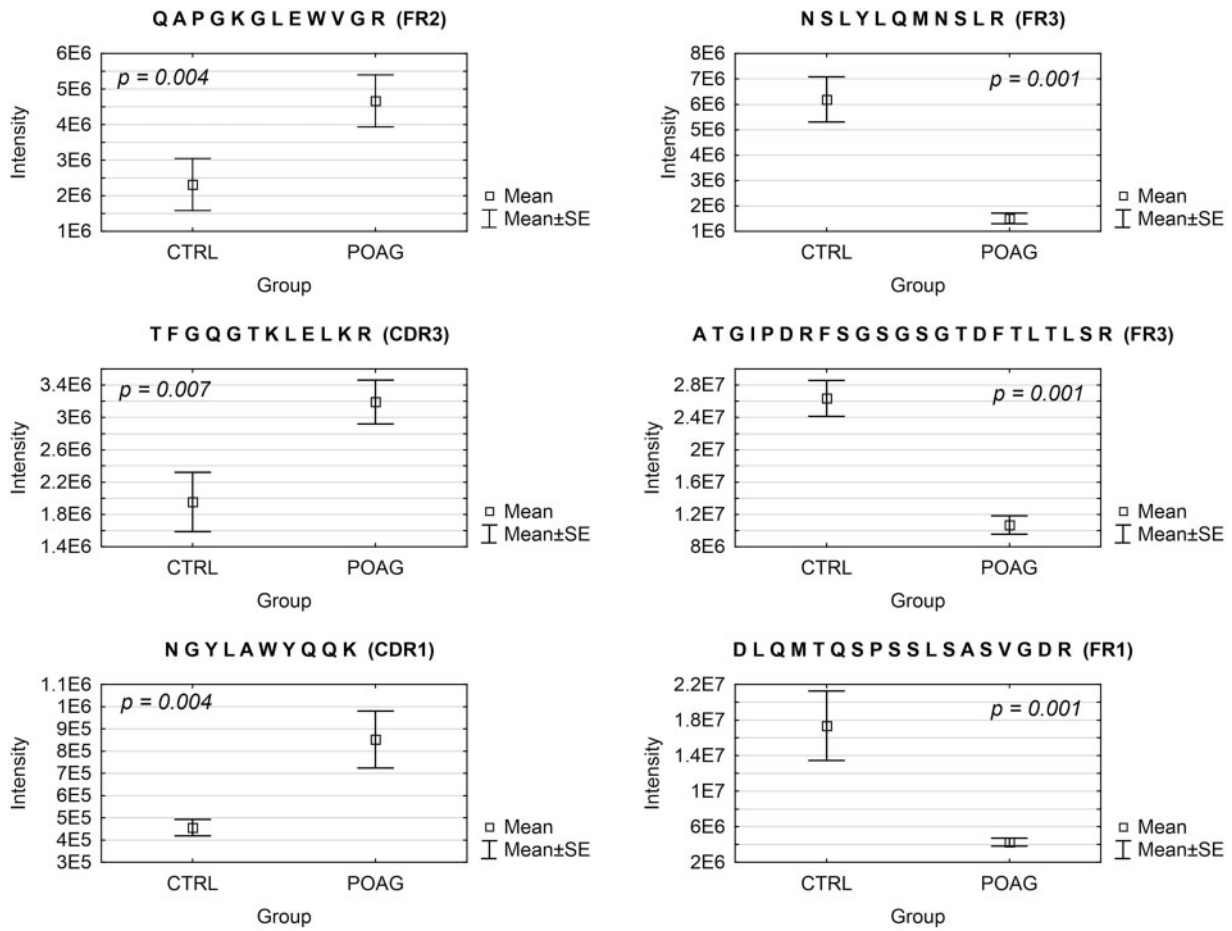

Figure 4. Exemplary IgG V domain peptides sequences showing significant differences in the expression level between POAG patients ($N = 13$) and CTRL group ($N = 15$). Peptides on the right were high abundant in the POAG group and peptides on the left were low abundant in POAG patients. Peptide abundances were revealed by LC-MS followed by label-free quantification and statistical analysis ($P < 0.05$; $\log_2$ fold change ≥ 0.5).

Targeted proteomics via accurate inclusion mass screening

In order to validate the glaucoma-related IgG V domain peptides revealed by discovery proteomics a targeted MS strategy was performed. Accurate inclusion mass screening (AIMS) analysis revealed in total 83 peptides (FDR < 1%) occurring at least in one of the study groups (14 CTRL or 13 POAG subjects). Around 3% of the total data matrix were missing and replaced by their respective means as described before (36). Exactly 64 of the detected peptides were in accordance with the targeted peptide sequences (in total 124 targeted peptides) providing a detection rate of 52%. Up to 25 of the targeted peptides fulfilled the previously defined Volcano plot criteria (p value < 0.05 and $\log_2$ fold change ≥ 0.5) and showed a significant decrease in the POAG group in contrast to CTRL (see Table 1). AIMS analysis provided 3 further IgG V domain peptides which were significant decreased in the POAG group but not on the targeted inclusion list (see Table 1). These identifications resulted from peptides which have overlapping precursor masses with included peptides and were therefore selected for MS/MS identification. A validation of in glaucoma high abundant IgG V domain peptides was not feasible. Supplementary Material, Figure S6 and File S2 show the statistical analysis of the targeted MS data-set.

Discussion

The main objective of this study was to identify peptides of the variable IgG domain, particular CDR sequences, which are differently distributed between patients diagnosed with primary open-angle glaucoma (POAG) and healthy controls (CTRL). Autoantibody profiling studies regarding glaucoma were mainly performed by techniques such as microarray or western blot analysis just focusing autoreactivities against a predefined panel of retinal or optic nerve antigens. Recently, many studies demonstrated that high-resolution LC-MS/MS represents a powerful instrument to identify and quantify structures of highly diverse antibodies without prior knowledge of the targeted (auto-) antigens (31,32). This new approach provided highly specific IgG V domain peptides as potential biomarker candidates in diseases such as lung cancer or multiple sclerosis (33,34) promising new insights into autoimmune processes in glaucoma. To reduce the complexity of the samples due to the high sequence variation of antibodies, only tryptic peptides of purified Fab fragments were analyzed by LC-MS as illustrated in Figure 1.

As shown in Figure 2, the Fab purification step showed a high degree of reproducibility between the individual study samples and was confirmed by the densitometric analysis of the Fab protein spots. Data analysis of the discovery proteomic

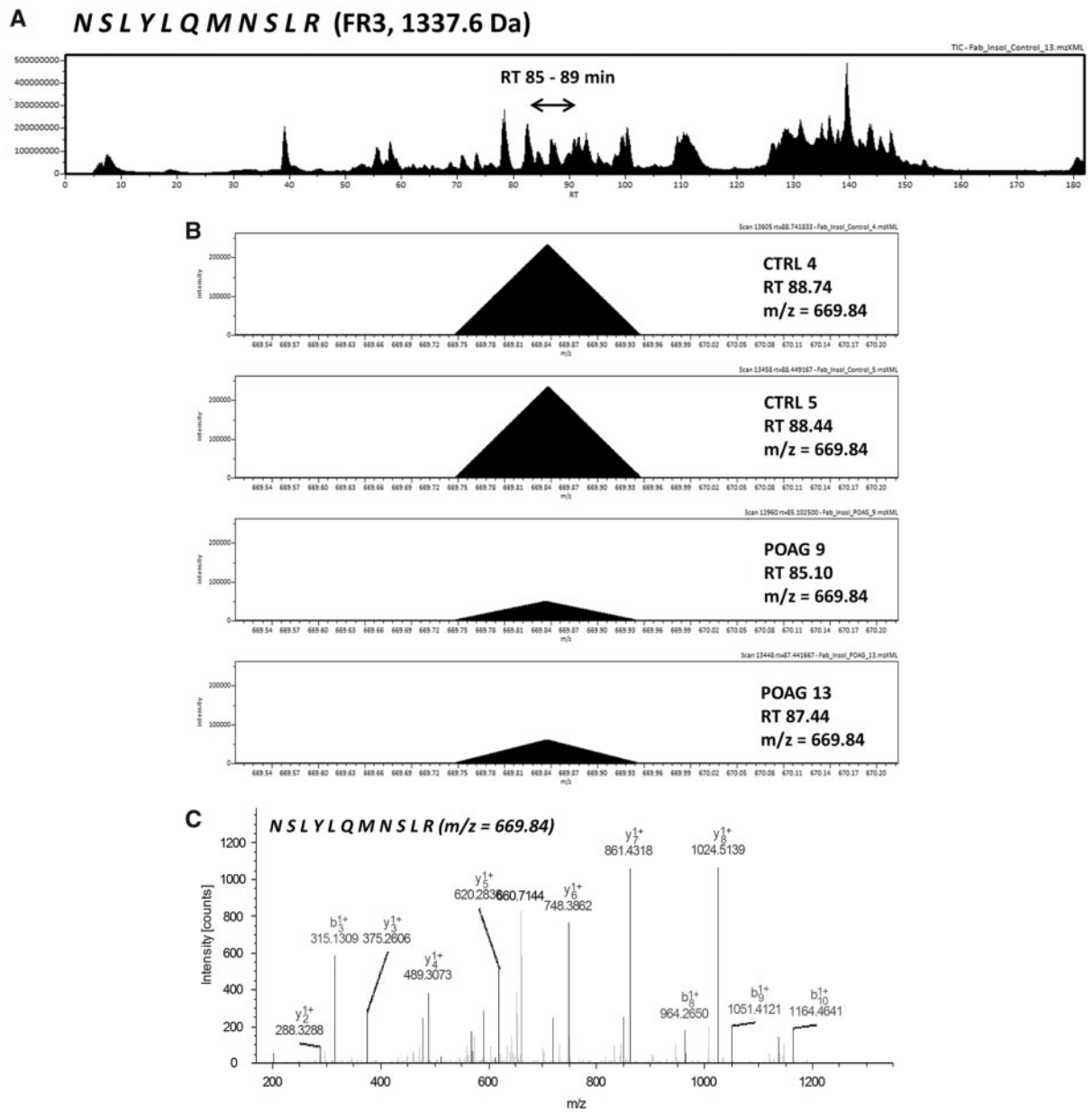

Figure 5. (**A**) Exemplary LC-MS total ion current chromatogram (TIC) displaying the exemplary identification of IgG V domain peptide sequence NSLYLQMNSLR annotated as framework region 3 (FR3). The peptide sequence eluted around RT 85-89 min within a 180 min HPLC gradient. (**B**) MS-spectra showing the monoisotopic precursor ion (m/z = 669.84) in a random set of CTRL subjects and POAG patients. Intensity of the precursor ion is observably larger in the CTRL group in contrast to POAG. (**C**) Tandem MS spectra of the precursor ion (m/z = 669.84) representing the peptide sequence NSLYLQMNSLR.

study revealed in total 3753 peptides in both study groups with a FDR < 1%. Around 3500 of these detected peptides were assigned to the variable IgG domain, whereas Singh *et al.* (2013) (34) identified only around 1600 IgG V domain peptides despite a larger study population of around 30 multiple sclerosis patients. Instead of purifying only the Fab fragments for the analysis, Singh *et al.* (2013) (34) sequenced the whole antibody structures (heavy and light chain) using gel-based MS analysis. This may results to the preferred detection of high abundant peptides from the constant region of the antibodies masking the identification of low abundant peptides from the variable region. Tryptic IgG V domain peptides determine the antigen specificity of the antibodies and are expected to show a higher variability in case-control studies in comparison to peptides of the constant IgG domain. Statistical analysis of the discovery data revealed in total 75 peptides of the variable IgG domain showing a significant level change ($P < 0.05$; $\log_2$ fold change ≥ 0.5) between both study groups and demonstrates for the first time that structures of the variable region of antibodies are associated to glaucoma (Figs 3–5). Most of these peptides derived from relatively constant FR regions of the IgG framework rather than from CDR regions. FR regions show much lesser mutations relative to hypervariable CDR sequences and are more likely to be shared between several B cell clones. This leads to higher abundances of FR peptides and favors the detection by mass spectrometry instead of highly mutated CDR sequences. Interestingly, around 90% of the IgG V domain peptides were low abundant in the POAG group in contrast to CTRL. These

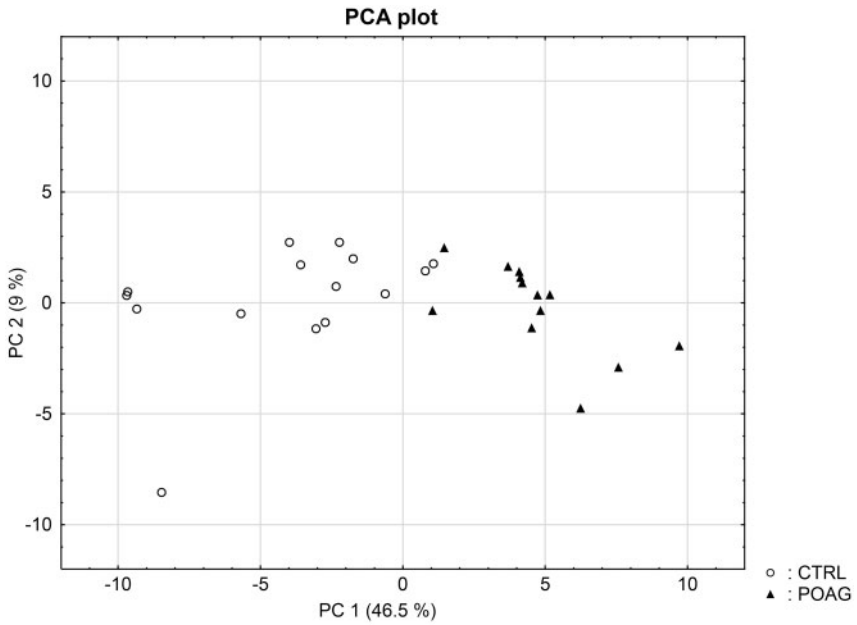

Figure 6. Principal component analysis (PCA) score plot for the 28 subjects. Clustering of the subjects was based on the abundances of the 75 significant differently expressed IgG V domain peptides. The cumulative proportions of PC1 and PC2 were 46.5% and 9%. The closer the data points in the figure the more similar are the individuals to each other. PCA plot provides a clear separation of CTRL (open dots) and POAG (filled triangles) group without any overlap.

findings would be in accordance with our hypothesis that some of these peptide sequences, incorporated in an antibody structure, may have a neuroprotective function in glaucoma and that there loss maybe promotes the degeneration process of RGCs *in vivo* (19–22). Recently, many studies demonstrated that short synthetic peptides of CDR regions can mimic the function of whole antibodies (mini-antibody) and exhibit antimicrobial and antitumor activities in a range of *in vitro/in vivo* experiments (38–40). Assuming that some of these low abundant IgG V domain peptides may promote neuroprotective activities *in vivo* would offer new treatment possibilities in glaucoma therapy. Interestingly Sohn *et al.* (2007) (41) and Britschgi *et al.* (2009) (42) received similar results and proved that the normal ageing process, also one main risk for glaucoma, leads to decreased sera levels of neuroprotective antibodies against amyloidogenic peptides favoring the formation of Alzheimer's disease in the elderly population. However, 28 of the IgG V domain peptides were further validated by targeted MS showing a significant lesser abundance in the POAG group in comparison to CTRL (Table 1). A validation of in glaucoma high abundant peptide sequences was not possible.

In consideration of the fact that the antigen specificities of the glaucoma-associated IgG V domain peptides are unknown, it is very interesting that some of these peptide sequences are already known in literature concerning with aberrant protein deposits and other neurodegenerative diseases. In glaucoma low abundant peptide sequences ASQSVSSYLAWYQQK (CDR1, homologous to IGKV3-11*01) and ASQSVSSSYLAWYQQKPGQA PR (CDR1, homologous to IGKV3-20*02), for instance, were identified by laser capture microdissection and LC-MS analysis as an immunoglobulin derived deposit in the central nerve system and are related to the disease pattern of light chain amyloidosis (AL) (43). AL amyloidosis is defined as a rare disease caused by proteinaceous deposits, particular immunoglobulin light chain proteins, which occur in different parts of the body like kidney, heart, brain or nerves (44). These abnormal protein aggregations can dramatically interfere with proper organ function and are also associated with plaque deposits in neurodegenerative diseases like Parkinson (PD) or Alzheimer's (AD) disease (45–47). Patients suffering from AL amyloidosis show increased concentrations of serum free light chains (FLC) and are used as biomarker in clinical diagnostics (44). POAG group showed a higher statistical dispersion of κ/λ ratios of intact antibodies in contrast to CTRL, but no significant difference ($P = 0.65$) was found between both groups (Supplementary Material, Fig. S4). The κ/λ ratio of intact antibodies is about 3: 1 in healthy individuals and was in agreement with our experimental data (24). This result leads to the assumption that some of the cases may show a dysregulation in the light chain expression pattern resulting from a disturbed B cell maturation. Moreover, representative peptides AAPSVTLFPPSSEELQANK (C region, homologous to IGLC3*01) and ADSSPVKAGVETTTPSK (C region, homologous to IGLC3*01) from the constant region of the IgG light chain were also detected in protein deposits of renal amyloidosis by MS (48). So far, only some cases are known that ocular amyloidosis leads to secondary glaucoma (49,50). However, our group proved increased IgG antibody accumulations in glaucomatous donor eyes accompanied by increased infiltration of $CD27^+/IgG^+$ plasma cells using immunohistochemical-staining techniques (51). Moreover, by using an Experimental Autoimmune Glaucoma (EAG) animal model we were able to demonstrate that antibody deposits in the retina are associated with the neurodegeneration process of retinal ganglion cells *in vivo* (52,53). If these disturbed light chain expression pattern may favor the formation of antibody deposits remains to be determined. Gonzalez-Iglesias *et al.* (2014) (54) observed increased concentrations of transthyretin and apolipoprotein A-1 in sera of POAG patients by LC-MS analysis, both favoring the formation of amyloid deposits (55). In addition, our group verified increased levels of transthyretin in aqueous humor of POAG patients, strengthening the probability of amyloid deposits close to the side of damage (56). Another peptide sequence DIVMTQSPDSLAVSLGER

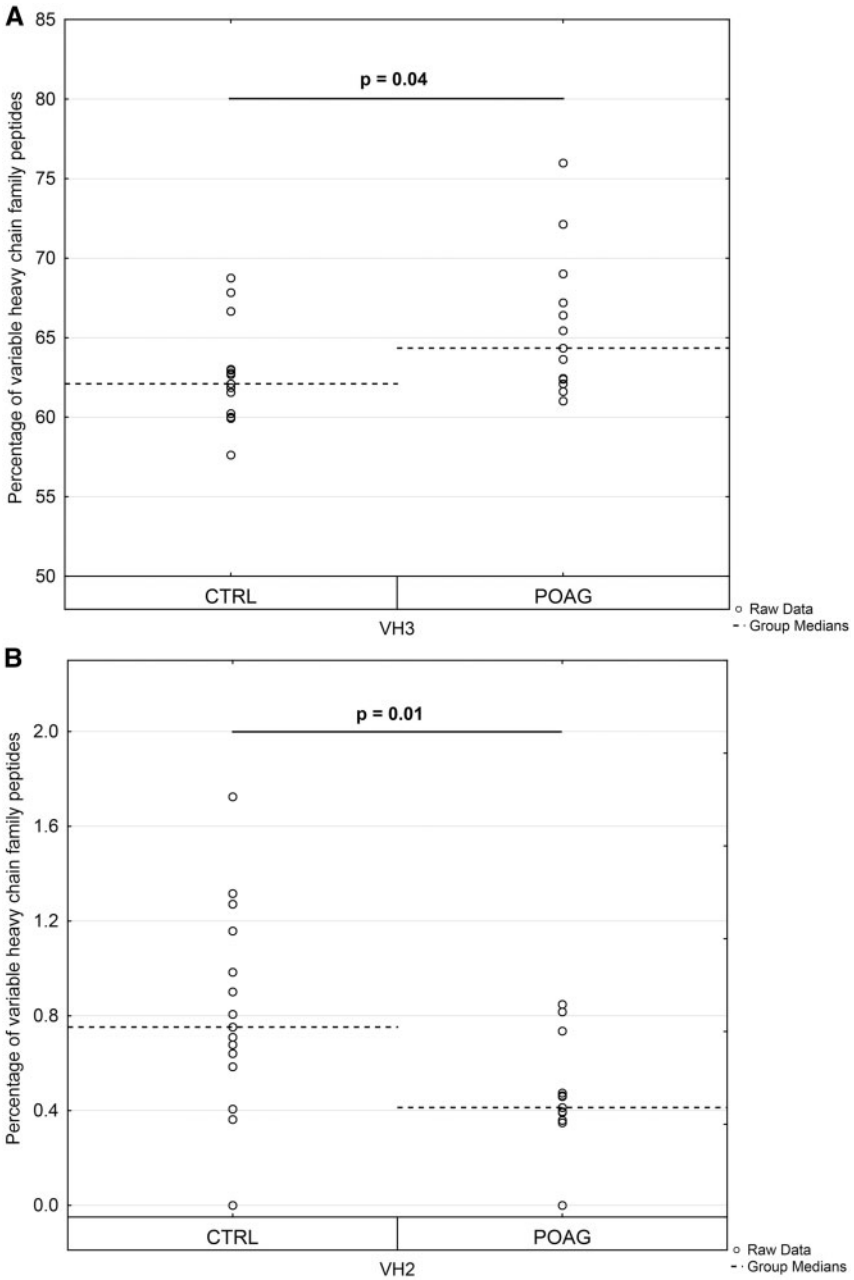

Figure 7. Expression profile of variable heavy chain (VH) family peptides in POAG patients in comparison to the CTRL group. Dashed horizontal lines represent median values. Peptide counts were normalized at the individual patient level and only peptide sequences validated by MS/MS identification were included in the analysis. Percentages of variable heavy chain family peptides are plotted along the y-axis. (**A**) Expression level of family VH3 was significantly increased in the POAG group ($P = 0.04$). (**B**) Family VH2 was significantly decreased in POAG patients relative to the CTRL group ($P = 0.01$).

(FR1, homologous to IGKV4-1*01), decreased in POAG patients, was mentioned to be highly abundant in patients with presymtomatic AD (57). Also another study revealed many other significant increased Ig kappa and lambda peptides in sera of AD patients using MS-based techniques (58). D'Andrea *et al.* (2003 and 2005) (59,60) provided evidence of increased Ig concentrations in AD brain tissues accompanied by increased neurodegenerative apoptotic effects and postulated to categorize Alzheimer's disease as a novel autoimmune disease. However, the exact role of this in glaucoma low abundant peptide sequence remains unclear, especially due to failed validation by targeted MS.

Apart from focusing on the expression levels of single IgG V domain peptides, we also investigated the preferred usage of specific VH, VK or VΛ family members. The family distributions were calculated at the individual patient level and compared between both study groups. VH3 was significantly higher expressed in the POAG group in contrast to CTRL ($P = 0.04$), whereas family VH2 was slightly but significant diminished in POAG patients ($P = 0.01$). No significant differences were found in the family distribution of VK and VΛ between CTRL and POAG group. Using LC-MS measurements Singh *et al.* (2013) (34) proved increased family usage of VH3 and VH4 in the CSF of multiple sclerosis patients and hypothesized that these changes

Table 1. Information about 28 IgG V domain peptides validated by targeted MS

CDR/FR	Sequence	Protein	m/z	Charge	Score	Length	Germline hit (gene name)	BLAST bit score	Homology (%)	Discovery study ($P < 0.05$; log2 fold change ≥ 0.5)	AIMS strategy ($P < 0.05$; log2 fold change ≥ 0.5)	P-value
CDR2	ALIYLASTLQSGVPSR	gi|18025706	838.5	2	165.89	16	IGKV1-27*01	30	93.3	–	√	0.012
CDR1	ASGYTFTNYGLSWVR	gi|304562650	861, 4	2	230.57	15	IGHV1-18*02	34.3	86.7	–	√	0.007
CDR1	ASQSVSSNLAWYQQKPGQAPR	gi|284521128	1152.1	2	210.43	21	IGKV3-15*01	47	100	–	√	0.011
CDR1	ASQSVSSSLAWYQQKPGQAPR	gi|323432554	1138.6	2	166.67	21	IGKV3-15*01	45.1	95.2	√	√	0.005
CDR1	ASQSVSSSYLAWYQQKPGQAPR	gi|149673891	1220.1	2	212.41	22	IGKV3-20*02	48.9	100	√	√	0.001
CDR1	ASQSVSSYLAWYQQK	gi|339272255	873.4	2	225.09	15	IGKV3-11*01	34.3	100	√	√	0.001
FR3	ATGIPDRFSGSGSGTDFTLTLSR	gi|70797863	1172.1	2	178.07	23	IGKV3-20*01	48.9	95.7	√	√	0.001
FR1	DLQMTQSPSSLSASVGDR	gi|327410291	939.9	2	293.13	18	IGKV1-27*01	37	94.4	√	√	0.001
FR1	ELVLTQSPATLSLSPGER	gi|339272255	949.5	2	401.46	18	IGKV3-20*02	37	94.4	√	√	0.001
FR1	ELVLTQSPGTLSLSPGER	gi|61970173	942.5	2	394.86	18	IGKV3-20*01	37.7	94.4	√	√	0.022
FR1	EVQLVESGGGLVK	gi|662565320	657.9	2	233.59	13	IGHV3-69-1*01	28.5	100	n.d.	√	0.001
FR1	EVQLVQSGAEVKKPGESLK	gi|761232722	1013.6	2	266.39	19	IGHV5-51*01	39.7	100	–	√	0.001
FR2	GLEWVSYLSR	gi|371446921	605.3	2	141.1	10	IGHV3-11*01	22.7	88.9	–	√	0.006
CDR2	LLIYDASDR	gi|630869089	533.2	2	147.4	9	IGKV3-11*01	19.6	88.9	–	√	0.011
FR1	LVESGGGLVKPGGSLR	gi|323433102	763.4	2	154.81	16	IGHV3-69-1*01	35.4	100	√	√	0.012
FR1	LVLTQSPGTLSLSPGER	gi|2599536	877.9	2	289.5	17	IGKV3-20*01	35.8	94.1	–	√	0.003
FR2	NDLGWYQQKPGK	gi|152149150	717.4	2	193.62	12	IGKV1-17*01	32.7	100	√	√	0.001
FR3	NQFSLK	gi|284521128	368.7	2	133.47	6	IGHV4-39*04	16.2	100	√	√	0.003
FR3	NSLYLQMNSLR	gi|209402818	669.8	2	303.71	11	IGHV3-13*01	25.4	100	√	√	0.001
FR1	QLVQSGAEVK	gi|323430773	529.8	2	119.22	10	IGHV1-69*03	22.3	100	–	√	0.002
FR1	QVQLVESGAEVKKPGESLK	gi|674841854	1013.6	2	185.96	19	IGHV5-51*01	37.4	89.5	n.d.	√	0.001
FR1	QVELVESGGGLVK	gi|371446908	657.9	2	255.08	13	IGHV3-11*01	27.3	92.3	√	√	0.001
FR1	QVELVESGGGLVKPGGSLR	gi|371446908	941.5	2	59.15	19	IGHV3-11*01	39.7	94.7	n.d.	√	0.004
FR3	SLSTAYLQWSSLK	gi|4097044	742.4	2	208.27	13	IGHV5-51*05	28.9	92.3	√	√	0.001
FR3	STSTAYLQWSSLK	gi|106897850	736.4	2	179.46	13	IGHV5-78*01	28.5	92.3	√	√	0.002
FR3	VTSVTAADTAVYYCAR	gi|219566321	874.4	2	241.42	16	IGHV4-34*13	33.1	87.5	–	√	0.004
CDR3	WFDPWGQGTLVTVSSASTK	gi|304563132	1034.0	2	219.99	19	IGHJ5*02	38.5	100	√	√	0.001
FR4	YFDLWGR	gi|304563378	478.7	2	128.57	7	IGHJ2*01	21.9	100	√	√	0.001

CDR, complementarity determining region (CDR1, CDR2 and CDR3); FR, framework region (FR1, FR2, FR3 and FR4). √, peptide sequence fulfilled criteria; -, peptide sequence failed to fulfill criteria; n.d., peptide sequence was not detectable in at least one study group (13 POAG or 14 CTRL).

are apparently driven by specific (auto-)antigenic pressures influencing the clonal selection and expansion process during B cell maturation. Also other studies validated the increased usage of VH4 gene segments in the CSF and brain of multiple sclerosis patients on the transcriptional level (61,62). This leads to the assumption that some of the glaucoma-related antigens (e.g. HSP27 or alpha fodrin), discovered by autoantibody profiling, may favor the selection of specific V gene segments during B cell maturation resulting in predefined antigen specificities of the circulating antibodies. Interestingly also another study showed that VH2 gene transcripts are significant overexpressed in ankylosing spondylitis patients (63). Ankylosing spondylitis is described as chronic inflammatory arthritis mainly located in the joints of the spine leading to increasing stiffness of the patients over time. To what extant the decreased family usage of VH2 is related to the pathomechanism of glaucoma remains unclear.

In conclusion, this proteomic study shows for the first time that peptides of the variable region of antibodies are related to glaucoma and can be used to discriminate POAG patients from healthy controls. Moreover, this study design combines unbiased proteomic profiling strategies for discovery with targeted MS for verification resulting in 28 IgG V domain peptides, which are confidently low abundant in POAG patients. If these quantitative differences are driven by autoantigens and to what extent those are related to pathogenesis of glaucoma remains to be determined. In future, it will be of great importance to perform the experimental set-up with a larger cohort of study participants in order to increase the robustness and reliability of the obtained results.

Materials and Methods

Study samples

28 subjects were included in this study compromising of 13 patients with primary open-angle glaucoma (POAG; mean age = 60 ± 7 years; ♂: 5 ♀: 8) and 15 age-matched control subjects (CTRL; mean age = 56 ± 5 years; ♂: 4 ♀: 11). All subjects were recruited for full ophthalmologic examination at the Department of Ophthalmology (Medical Center of the Johannes Gutenberg University Mainz, Germany). The investigation was conducted in accordance with the tenets of the Declaration of Helsinki. Inclusion criteria for POAG patients were IOP > 21 mm Hg, optic disc cupping and visual field defects according the guidelines of the European Glaucoma Society (64). Subjects with other types of glaucoma, any kind of retinal or corneal pathology or eye surgeries within the last year were excluded from the study. Based on verbal confirmation, none of the subjects had a history of Diabetes mellitus, Alzheimer's disease, Parkinson's disease, any kind of other autoimmune diseases or cancer to our best knowledge. The control group did not show any clinical signs of glaucoma or any other eye disorders. Ten milliliters of venous blood was taken from each subject after they gave their informed consent. Blood samples were allowed to clot for 30 min at room temperature and centrifuged at 3000 g for 10 min at 10° C. The supernatant containing the sera was distributed in 1.5 ml aliquots and stored at -80° C.

IgG Fab purification

IgG was isolated from sera samples using CaptureSelect™ IgG-Fc (Hu) Affinity Matrix (Thermo Fisher Scientific, Rockford, USA) according to manufacturer's introductions with slight modifications. All sera samples (100 µl per subject) were diluted at a ratio 1: 3 with PBS and subsequently added to the spin columns (Thermo Fisher Scientific, Rockford, USA) containing anti IgG-Fc Affinity Matrix. After 10 min of incubation, the spin columns were centrifuged at 5000 g for 2 min. The IgG remained attached to the beads and the flow-through fraction was discarded. The samples were washed three times with 400 µl PBS to avoid unspecific bindings to the matrix. Finally, the IgG fraction was eluted using 400 µl Pierce™ IgG Elution Buffer pH 2.0 (Thermo Fisher Scientific, Rockford, USA) and collected into tubes containing 1 M Tris HCl pH 8.5 to neutralize the elution liquid. This procedure was repeated two times and the eluate fractions were pooled. Protein amounts were estimated using BCA protein Assay Kit (Thermo Fisher Scientific, Rockford, USA) according to the supplier's protocol with the modification that bovine gamma globulin (BGG) was used as internal calibration standard. Triplicate measurements were performed using Multiscan Ascent photometer (Thermo Fisher Scientific, Rockford, USA) at a wavelength of 570 nm. Afterwards, 600 µl of the IgG eluate was exchanged in 500 µl papain digestion buffer (20 mM cysteine·HCl 20 mM sodium phosphate 10 mM EDTA pH 7.0) by using an Amicon 10k centrifugal filter device (Millipore, Billerica, USA). IgG were digested overnight at 37° C into Fab and Fc using papain immobilized on agarose resin beads (Thermo Fisher Scientific, Rockford, USA) according to the manufacturer's introduction. Next day, 750 µl 10 mM Tris · HCl pH 7.5 were added to the samples and centrifuged at 2000 g for 2 min. The supernatant containing the digested mixture was collected. After this, the digested mixture was exchanged in 300 µl PBS by using an Amicon 10k centrifugal filter device. To purify Fab from Fc and the undigested IgG the samples were loaded onto spin columns filled with CaptureSelect™ IgG-Fc (Hu) Affinity Matrix. The flow-through fraction containing the Fab was collected and protein measurement was performed as described above. To check the quality of the Fab isolation each sample was analyzed by 1-D SDS PAGE under reduced conditions. After separation, gels were fixed and stained using Novex Colloidal Blue Staining Kit (Invitrogen, Carlsbad, USA) according to the supplier's protocol. Gels were destained overnight with deionized water and scanned using a DCP-9042 CDN bench top scanner (Brother Industries Ltd., Nagoya, Japan) at 600 dpi. Protein bands were visually inspected to determine if Fab purification steps were successful. Open-source ImageJ software (http://imagej.nih.gov/ij/) was used to perform densitometric analysis of the protein spots (65).

In-solution digestion

Purified Fab (20 µg) were dried for 30 min in the SpeedVac (Eppendorf, Darmstadt, Germany) and subjected for further In-solution trypsin digestion using a method with slight adjustments described earlier (66). In brief, the samples were resolved in 30 µl 50 mM ammonium bicarbonate (NH4HCO3) and sonicated for 5 min. Afterwards disulfide bonds reduction of the samples was performed with 100 mM DTT in NH4HCO3 at 56 °C for 30 min following alkylation with 200 mM IAA in NH4HCO3 for 30 min in the dark. The reduced and alkylated Fab proteins were further digested with 0.2 mg/ml trypsin (Promega, Madison, USA) in 50 mM NH4HCO3 10% ACN at 37° C for 16 h. The reaction was quenched using 0.1% formic acid and evaporated in the Speedvac for 30 min until dryness. The dried samples were resolved in 20 µl 0.1% TFA and purified prior MS analysis using ZIPTIP® C18 solid phase extraction tips (Millipore, Billerica, USA) according to manufacturer's introductions.

LC–MS/MS analyses

LC-MS/MS measurements were carried out by a Rheos Allegro pump (Thermo Fisher Scientific, Rockford, USA) downscaled to a capillary HPLC system (flow rate: 6.7 ± 0.3 µl/min) online coupled to a hybrid linear ion trap - Orbitrap MS (LTQ Orbitrap XL; Thermo Fisher Scientific, Rockford, USA) (67,68). Six microliters of digested Fab peptides (1.5 mg/ml) were loaded onto a BioBasic® C18 column system (30 × 0.5 mm pre-column + 150 x 0.5 mm analytical column; Thermo Fisher Scientific, Rockford, USA). Solvent A consists of 2% ACN and 0.1% FA in water and solvent B consists of 80% ACN and 0.1% FA in water. Peptides were eluted within 180 min using following gradient: 5% solvent B (0–10 min), 5–50% solvent B (10–170 min), 50–90% solvent B (170–177 min) and 90–10% solvent B (177–180 min). For positive electrospray ionization a low flow metal needle (Thermo Fisher Scientific, Rockford, USA) was used, spray voltage was set to 2.15 kV and the heated capillary temperature adjusted to 220 °C. LTQ Orbitrap operated in a data-dependent acquisition method: High-resolution survey full scan (from m/z 300 to 2000) was detected in the Orbitrap with a resolution of 30.000 at 400 m/z and a target automatic gain control of 1 x 10^6 ions. Lock mass was set to 445.120025 m/z (polydimethylcyclosiloxane) and used for internal calibration. Based on the full scan the five most intense precursor ions were selected for collision-induced dissociation (CID) fragmentation in the ion trap applying normalized collision energy of 35%. Dynamic exclusion settings included a repeat count of 3, repeat duration of 30 s, exclusion list size of 100 and exclusion duration of 300 s. Inspection and evaluation of the raw data was performed using visualization tool Qual Browser v. 2.0.7 SP1 (Thermo Fisher Scientific, Rockford, USA) and open-source software Mass ++ (Shimadzu Corporation, Kyoto, Tokyo).

Peptide identification

Acquired LC-MS profiles were analyzed by MAXQuant computational proteomics platform version 1.5.2.8 (Max Planck Institute of Biochemistry, Martinsried) for peptide identification and label-free quantification (69,70). Tandem MS spectra were searched against NCBI human database (date: 05/01/16; sequences: 955.083 sequences) with following settings: peptide mass tolerance of ± 30 ppm, fragment mass tolerance of ± 0.5 Da, tryptic cleavage, a maximum of two missed cleavages, carbamidomethylation as fixed modification of cysteine, acetylation (N-terminal) and oxidation as variable modification of methionine. Peptides were identified with a false discovery rate < 1% (FDR) with ≥ 6 amino acid residues. All peptide sequences identified in cases and controls were subsequently aligned to variable (V), joining (J) and constant (C) germline sequences derived from the International ImMunoGeneTics Information System (IMGT) database (Montpellier, France) (71,72). According to previous studies IgBLASTp search algorithm (NCBI IgBLAST version 1.4) was used to arrange the identified peptide sequences to the IgG framework (73). Peptide alignments with a bitscore ≥ 12.5 and alignment match ≥ 70% were evaluated as true hits and selected for further analysis according to previous publications (30,34). Peptide sequences were assigned automatically to their corresponding CDR or FR regions according to the IMGT numbering system. Peptides were positioned in the IgG framework if a minimum of three amino acids was part of a CDR or FR region. Since IgBLASTp algorithm was not suitable to perform CDR3 identification automatically, sequence annotation was performed manually according to the unique IMGT numbering system (74).

Statistical analysis

Results of the IgBLASTp search were combined with MaxQuant generated output matrix containing protein hit, sequence, length, mass, charge, score, intensity and MS/MS fragmentation spectra of the detected peptides. The statistical analysis and graphical presentation was performed using Perseus version 1.5.5.0 (Max Planck Institute of Biochemistry, Martinsried). At first, the raw intensities of the detected peptides were $\log_2$ transformed for further analyses (75). Prior statistical analysis, the output data were filtered for contaminants, reversed hits and for a minimum number of valid values in at least one study group (15 CTRL or 13 POAG subjects). After this, missing values were replaced by their respective means assuming that these peptides were close to the limit of detection (36). Finally, two-sided *t*-test statistics with *P* values < 0.05 was applied to identify significant glaucoma-related level changes in peptide abundances. Further statistical analyses and graphical presentation of data were performed using Statistica version 12 (Statsoft, Tulsa, USA) and Excel 2010 function.

Targeted MS

In order to validate the glaucoma-associated IgG V domain peptides observed in the discovery study a targeted MS strategy via AIMS was performed (76). The Orbitrap MS system targets selected masses on the software inclusion list in each MS scan and requires only MS/MS spectra if a listed peptide is detected with the accurate mass and charge state. Selection of the peptides for the inclusion list was carried out manually using experimentally observable IgG V domain peptides which were significant differentially distributed in the POAG group in contrast to CTRL in the discovery study ($P < 0.05$). The selected proteolytic peptides were required to be fully tryptic with a maximum of two missed cleavages. Purified Fab fragments (20 µg) of 14 controls and 13 POAG patients were subjected for further In-solution trypsin digestion and analyzed individually by targeted MS strategy. One control sample was excluded from MS analysis because of sample material limitation. For targeted MS analysis the Orbitrap MS system was operated with the previously described settings with some slight modifications (68,77). The use of global parent list was enabled and the repeat duration was set to 300 instead of 30 s. Acquired Tandem MS spectra were searched against NCBI human database (date: 05/01/16; sequences: 955.083 sequences) with the previous settings. IgBLASTp search algorithm and IMGT database were used to assign the identified peptides to their corresponding CDR or FR regions as described above in detail.

A list of all identified peptides is provided in Supplementary File S1. Information about the statistical analysis of discovery and targeted MS data-set is listed in Supplementary File S2.

Supplementary Material

Supplementary Material is available at *HMG* online.

Conflict of Interest statement. None declared.

Funding

This research did not receive any specific grant from funding agencies in the public, commercial, or not-for-profit sectors.

References

1. Weinreb, R.N., Aung, T. and Medeiros, F.A. (2014) The pathophysiology and treatment of glaucoma: a review. *JAMA*, **311**, 1901–1911.
2. Quigley, H.A. and Broman, A.T. (2006) The number of people with glaucoma worldwide in 2010 and 2020. *Br. J. Ophthalmol.*, **90**, 262–267.
3. Gutteridge, I.F. (2000) Normal tension glaucoma: diagnostic features and comparisons with primary open angle glaucoma. *Clin. Exp. Optom.*, **83**, 161–172.
4. Guedes, G., Tsai, J.C. and Loewen, N.A. (2011) Glaucoma and aging. *Curr. Aging Sci.*, **4**, 110–117.
5. Flammer, J., Orgul, S., Costa, V.P., Orzalesi, N., Krieglstein, G.K., Serra, L.M., Renard, J.-P. and Stefansson, E. (2002) The impact of ocular blood flow in glaucoma. *Prog. Retin. Eye Res.*, **21**, 359–393.
6. Garcia-Valenzuela, E., Shareef, S., Walsh, J. and Sharma, S.C. (1995) Programmed cell death of retinal ganglion cells during experimental glaucoma. *Exp. Eye Res.*, **61**, 33–44.
7. Kumar, S., Malik, M.A., Goswami, S., Sihota, R. and Kaur, J. (2016) Candidate genes involved in the susceptibility of primary open angle glaucoma. *Gene*, **577**, 119–131.
8. Tikunova, E.V. and Churnosov, M.I. (2014) Genetic studies of primary open-angle glaucoma. *Vestn. Oftalmol.*, **130**, 96–99.
9. Harada, T., Harada, C., Nakamura, K., Quah, H.-M.A., Okumura, A., Namekata, K., Saeki, T., Aihara, M., Yoshida, H. and Mitani, A. (2007) The potential role of glutamate transporters in the pathogenesis of normal tension glaucoma. *J. Clin. Invest.*, **117**, 1763–1770.
10. Grus, F.H., Joachim, S.C., Hoffmann, E.M. and Pfeiffer, N. (2004) Complex autoantibody repertoires in patients with glaucoma. *Mol. Vis.*, **10**, 132–137.
11. Grus, F.H., Joachim, S.C. and Pfeiffer, N. (2003) Analysis of complex autoantibody repertoires by surface-enhanced laser desorption/ionization-time of flight mass spectrometry. *Proteomics*, **3**, 957–961.
12. Wax, M.B., Tezel, G., Kawase, K. and Kitazawa, Y. (2001) Serum autoantibodies to heat shock proteins in glaucoma patients from Japan and the United States. *Ophthalmology*, **108**, 296–302.
13. Yang, J., Tezel, G., Patil, R.V., Romano, C. and Wax, M.B. (2001) Serum autoantibody against glutathione S-transferase in patients with glaucoma. *Invest. Ophthalmol. Vis. Sci.*, **42**, 1273–1276.
14. Grus, F.H., Joachim, S.C., Bruns, K., Lackner, K.J., Pfeiffer, N. and Wax, M.B. (2006) Serum autoantibodies to alpha-fodrin are present in glaucoma patients from Germany and the United States. *Invest. Ophthalmol. Vis. Sci.*, **47**, 968–976.
15. Tezel, G., Edward, D.P. and Wax, M.B. (1999) Serum autoantibodies to optic nerve head glycosaminoglycans in patients with glaucoma. *Arch. Ophthalmol.*, **117**, 917–924.
16. Maruyama, I., Ohguro, H. and Ikeda, Y. (2000) Retinal ganglion cells recognized by serum autoantibody against gamma-enolase found in glaucoma patients. *Invest. Ophthalmol. Vis. Sci.*, **41**, 1657–1665.
17. Joachim, S.C., Reichelt, J., Berneiser, S., Pfeiffer, N. and Grus, F.H. (2008) Sera of glaucoma patients show autoantibodies against myelin basic protein and complex autoantibody profiles against human optic nerve antigens. *Graefes Arch. Clin. Exp. Ophthalmol.*, **246**, 573–580.
18. Tezel, G. and Wax, M.B. (2000) The mechanisms of hsp27 antibody-mediated apoptosis in retinal neuronal cells. *J. Neurosci.*, **20**, 3552–3562.
19. Wilding, C., Bell, K., Beck, S., Funke, S., Pfeiffer, N., Grus, F.H. and Vavvas, D. (2014) gamma-Synuclein antibodies have neuroprotective potential on neuroretinal cells via proteins of the mitochondrial apoptosis pathway. *PLoS ONE*, **9**, e90737.
20. Bell, K., Wilding, C., Funke, S., Pfeiffer, N. and Grus, F.H. (2015) Protective effect of 14-3-3 antibodies on stressed neuroretinal cells via the mitochondrial apoptosis pathway. *BMC Ophthalmol.*, **15**, 64.
21. Bell, K., Wilding, C., Funke, S., Perumal, N., Beck, S., Wolters, D., Holz-Muller, J., Pfeiffer, N. and Grus, F.H. (2016) Neuroprotective effects of antibodies on retinal ganglion cells in an adolescent retina organ culture. *J. Neurochem.*, **139**, 256–269.
22. Wilding, C., Bell, K., Funke, S., Beck, S., Pfeiffer, N. and Grus, F.H. (2015) GFAP antibodies show protective effect on oxidatively stressed neuroretinal cells via interaction with ERP57. *J. Pharmacol. Sci.*, **127**, 298–304.
23. Abbas, A.K., Lichtman, A.H. and Pillai, S. (2011) *Cellular and Molecular Immunology*. Saunders Elsevier, Philadelphia, PA.
24. Schroeder, H.W. Jr and Cavacini, L. (2010) Structure and function of immunoglobulins. *J. Allergy Clin. Immunol.*, **125**, 52.
25. Xu, J.L. and Davis, M.M. (2000) Diversity in the CDR3 region of V(H) is sufficient for most antibody specificities. *Immunity*, **13**, 37–45.
26. Saada, R., Weinberger, M., Shahaf, G. and Mehr, R. (2007) Models for antigen receptor gene rearrangement: CDR3 length. *Immunol. Cell Biol.*, **85**, 323–332.
27. Li, Z., Woo, C.J., Iglesias-Ussel, M.D., Ronai, D. and Scharff, M.D. (2004) The generation of antibody diversity through somatic hypermutation and class switch recombination. *Genes Dev.*, **18**, 1–11.
28. Hoogeboom, R., van Kessel, K.P.M., Hochstenbach, F., Wormhoudt, T.A., Reinten, R.J.A., Wagner, K., Kater, A.P., Guikema, J.E.J., Bende, R.J. and van Noesel, C.J.M. (2013) A mutated B cell chronic lymphocytic leukemia subset that recognizes and responds to fungi. *J. Exp. Med.*, **210**, 59–70.
29. Scheid, J.F., Mouquet, H., Ueberheide, B., Diskin, R., Klein, F., Oliveira, T.Y.K., Pietzsch, J., Fenyo, D., Abadir, A., Velinzon, K. *et al.* (2011) Sequence and structural convergence of broad and potent HIV antibodies that mimic CD4 binding. *Science*, **333**, 1633–1637.
30. VanDuijn, M.M., Dekker, L.J.M., Zeneyedpour, L., Smitt, P.A.E.S. and Luider, T.M. (2010) Immune responses are characterized by specific shared immunoglobulin peptides that can be detected by proteomic techniques. *J. Biol. Chem.*, **285**, 29247–29253.
31. de Costa, D., Broodman, I., VanDuijn, M.M., Stingl, C., Dekker, L.J.M., Burgers, P.C., Hoogsteden, H.C., Sillevis Smitt, P.A.E., van Klaveren, R.J. and Luider, T.M. (2010) Sequencing and quantifying IgG fragments and antigen-binding regions by mass spectrometry. *J. Proteome Res.*, **9**, 2937–2945.
32. Dekker, L.J.M., Zeneyedpour, L., Brouwer, E., Duijn, M.M., Sillevis Smitt, P.A.E. and Luider, T.M. (2011) An antibody-based biomarker discovery method by mass spectrometry sequencing of complementarity determining regions. *Anal. Bioanal. Chem.*, **399**, 1081–1091.
33. de Costa, D., Broodman, I., Calame, W., Stingl, C., Dekker, L.J.M., Vernhout, R.M., de Koning, H.J., Hoogsteden, H.C., Smitt, P.A.E.S., van Klaveren, R.J. *et al.* (2014) Peptides from the variable region of specific antibodies are shared among lung cancer patients. *PLoS ONE*, **9**, e96029.
34. Singh, V., Stoop, M.P., Stingl, C., Luitwieler, R.L., Dekker, L.J., van Duijn, M.M., Kreft, K.L., Luider, T.M. and Hintzen, R.Q.

(2013) Cerebrospinal-fluid-derived immunoglobulin G of different multiple sclerosis patients shares mutated sequences in complementarity determining regions. *Mol. Cell. Proteomics*, **12**, 3924–3934.
35. Maat, P., VanDuijn, M., Brouwer, E., Dekker, L., Zeneyedpour, L., Luider, T. and Smitt, P.S. (2012) Mass spectrometric detection of antigen-specific immunoglobulin peptides in paraneoplastic patient sera. *J. Autoimmun.*, **38**, 354–360.
36. Karpievitch, Y.V., Dabney, A.R. and Smith, R.D. (2012) Normalization and missing value imputation for label-free LC-MS analysis. *BMC Bioinformatics*, **13 Suppl 16**, S5.
37. Sitnikova, T. and Su, C. (1998) Coevolution of immunoglobulin heavy- and light-chain variable-region gene families. *Mol. Biol. Evol.*, **15**, 617–625.
38. Polonelli, L., Ponton, J., Elguezabal, N., Moragues, M.D., Casoli, C., Pilotti, E., Ronzi, P., Dobroff, A.S., Rodrigues, E.G. and Juliano, M.A. (2008) Antibody complementarity-determining regions (CDRs) can display differential antimicrobial, antiviral and antitumor activities. *PLoS ONE*, **3**, e2371.
39. Rabaca, A.N., Arruda, D.C., Figueiredo, C.R., Massaoka, M.H., Farias, C.F., Tada, D.B., Maia, V.C., Silva Junior, P.I., Girola, N., Real, F. *et al.* (2016) AC-1001 H3 CDR peptide induces apoptosis and signs of autophagy in vitro and exhibits antimetastatic activity in a syngeneic melanoma model. *FEBS Open Bio.*, **6**, 885–901.
40. Timmerman, P., Barderas, R., Desmet, J., Altschuh, D., Shochat, S., Hollestelle, M.J., Hoppener, J.W.M., Monasterio, A., Casal, J.I. and Meloen, R.H. (2009) A combinatorial approach for the design of complementarity-determining region-derived peptidomimetics with in vitro anti-tumoral activity. *J. Biol. Chem.*, **284**, 34126–34134.
41. Sohn, J.-H., So, J.O., Kim, H., Nam, E.J., Ha, H.J., Kim, Y.H. and Mook-Jung, I. (2007) Reduced serum level of antibodies against amyloid beta peptide is associated with aging in Tg2576 mice. *Biochem. Biophys. Res. Commun.*, **361**, 800–804.
42. Britschgi, M., Olin, C.E., Johns, H.T., Takeda-Uchimura, Y., LeMieux, M.C., Rufibach, K., Rajadas, J., Zhang, H., Tomooka, B., Robinson, W.H. *et al.* (2009) Neuroprotective natural antibodies to assemblies of amyloidogenic peptides decrease with normal aging and advancing Alzheimer's disease. *Proc. Natl. Acad. Sci. U S A*, **106**, 12145–12150.
43. Rodriguez, F.J., Gamez, J.D., Vrana, J.A., Theis, J.D., Giannini, C., Scheithauer, B.W., Parisi, J.E., Lucchinetti, C.F., Pendlebury, W.W., Bergen, H.R.3. *et al.* (2008) Immunoglobulin derived depositions in the nervous system: novel mass spectrometry application for protein characterization in formalin-fixed tissues. *Lab. Invest.*, **88**, 1024–1037.
44. Baker, K.R. and Rice, L. (2012) The amyloidoses: clinical features, diagnosis and treatment. *Methodist Debakey Cardiovasc. J.*, **8**, 3–7.
45. Vidal, R. and Ghetti, B. (2011) Characterization of amyloid deposits in neurodegenerative diseases. *Methods Mol. Biol.*, **793**, 241–258.
46. Koo, E.H., Lansbury, P.T., JR. and Kelly, J.W. (1999) Amyloid diseases: abnormal protein aggregation in neurodegeneration. *Proc. Natl. Acad. Sci. U S A*, **96**, 9989–9990.
47. Dugger, B.N., Serrano, G.E., Sue, L.I., Walker, D.G., Adler, C.H., Shill, H.A., Sabbagh, M.N., Caviness, J.N., Hidalgo, J., Saxon-Labelle, M. *et al.* (2012) Presence of Striatal Amyloid Plaques in Parkinson's Disease Dementia Predicts Concomitant Alzheimer's Disease: Usefulness for Amyloid Imaging. *J. Parkinsons Dis.*, **2**, 57–65.
48. Sethi, S., Vrana, J.A., Theis, J.D., Leung, N., Sethi, A., Nasr, S.H., Fervenza, F.C., Cornell, L.D., Fidler, M.E. and Dogan, A. (2012) Laser microdissection and mass spectrometry-based proteomics aids the diagnosis and typing of renal amyloidosis. *Kidney Int.*, **82**, 226–234.
49. Nelson, G.A., Edward, D.P. and Wilensky, J.T. (1999) Ocular amyloidosis and secondary glaucoma. *Ophthalmology*, **106**, 1363–1366.
50. Tsukahara, S. and Matsuo, T. (1977) Secondary glaucoma accompanied with primary familial amyloidosis. *Ophthalmologica*, **175**, 250–262.
51. Gramlich, O.W., Beck, S., von Thun und Hohenstein-Blaul, N., Boehm, N., Ziegler, A., Vetter, J.M., Pfeiffer, N., Grus, F.H. and Trounce, I.A. (2013) Enhanced insight into the autoimmune component of glaucoma: IgG autoantibody accumulation and pro-inflammatory conditions in human glaucomatous retina. *PLoS ONE*, **8**, e57557.
52. Joachim, S.C., Gramlich, O.W., Laspas, P., Schmid, H., Beck, S., von Pein, H.D., Dick, H.B., Pfeiffer, N., Grus, F.H. and Libby, R. (2012) Retinal ganglion cell loss is accompanied by antibody depositions and increased levels of microglia after immunization with retinal antigens. *PLoS ONE*, **7**, e40616.
53. Joachim, S.C., Mondon, C., Gramlich, O.W., Grus, F.H. and Dick, H.B. (2014) Apoptotic retinal ganglion cell death in an autoimmune glaucoma model is accompanied by antibody depositions. *J. Mol. Neurosci.*, **52**, 216–224.
54. Gonzalez-Iglesias, H., Alvarez, L., Garcia, M., Escribano, J., Rodriguez-Calvo, P.P., Fernandez-Vega, L. and Coca-Prados, M. (2014) Comparative proteomic study in serum of patients with primary open-angle glaucoma and pseudoexfoliation glaucoma. *J. Proteomics*, **98**, 65–78.
55. Gertz, M.A. (2004) The classification and typing of amyloid deposits. *Am. J. Clin. Pathol.*, **121**, 787–789.
56. Grus, F.H., Joachim, S.C., Sandmann, S., Thiel, U., Bruns, K., Lackner, K.J. and Pfeiffer, N. (2008) Transthyretin and complex protein pattern in aqueous humor of patients with primary open-angle glaucoma. *Mol. Vis.*, **14**, 1437–1445.
57. IJsselstijn, L., Dekker, L.J.M., Stingl, C., van der Weiden, M.M., Hofman, A., Kros, J.M., Koudstaal, P.J., Sillevis Smitt, P.A.E., Ikram, M.A., Breteler, M.M.B. and Luider, T.M. (2011) Serum levels of pregnancy zone protein are elevated in presymptomatic Alzheimer's disease. *J. Proteome Res.*, **10**, 4902–4910.
58. Hye, A., Lynham, S., Thambisetty, M., Causevic, M., Campbell, J., Byers, H.L., Hooper, C., Rijsdijk, F., Tabrizi, S.J., Banner, S. *et al.* (2006) Proteome-based plasma biomarkers for Alzheimer's disease. *Brain*, **129**, 3042–3050.
59. D'Andrea, M.R. (2003) Evidence linking neuronal cell death to autoimmunity in Alzheimer's disease. *Brain Res.*, **982**, 19–30.
60. D'Andrea, M.R. (2005) Add Alzheimer's disease to the list of autoimmune diseases. *Med. Hypotheses*, **64**, 458–463.
61. Owens, G.P., Kannus, H., Burgoon, M.P., Smith-Jensen, T., Devlin, M.E. and Gilden, D.H. (1998) Restricted use of VH4 germline segments in an acute multiple sclerosis brain. *Ann. Neurol.*, **43**, 236–243.
62. Owens, G.P., Winges, K.M., Ritchie, A.M., Edwards, S., Burgoon, M.P., Lehnhoff, L., Nielsen, K., Corboy, J., Gilden, D.H. and Bennett, J.L. (2007) VH4 gene segments dominate the intrathecal humoral immune response in multiple sclerosis. *J. Immunol.*, **179**, 6343–6351.
63. Kim, Y.J., Kim, N.Y., Lee, M.K., Choi, H.J., Baek, H.J. and Nam, C.H. (2010) Overexpression and unique rearrangement of VH2 transcripts in immunoglobulin variable heavy chain genes in ankylosing spondylitis patients. *Exp. Mol. Med.*, **42**, 319–326.
64. (2017) European Glaucoma Society Terminology and Guidelines for Glaucoma, 4th Edition - Chapter 2: Classification

and terminologySupported by the EGS Foundation: Part 1: Foreword; Introduction; Glossary; Chapter 2 Classification and Terminology. *Br. J. Ophthalmol.*, **101**, 73–127.
65. Schneider, C.A., Rasband, W.S. and Eliceiri, K.W. (2012) NIH Image to ImageJ: 25 years of image analysis. *Nat. Methods*, **9**, 671–675.
66. Leon, I.R., Schwammle, V., Jensen, O.N. and Sprenger, R.R. (2013) Quantitative assessment of in-solution digestion efficiency identifies optimal protocols for unbiased protein analysis. *Mol. Cell. Proteomics*, **12**, 2992–3005.
67. Funke, S., Markowitsch, S., Schmelter, C., Perumal, N., Mwiiri, F.K., Gabel-Scheurich, S., Pfeiffer, N. and Grus, F.H. (2016) In-depth proteomic analysis of the porcine retina by use of a four step differential extraction bottom up LC MS platform. *Mol. Neurobiol.*, DOI: 10.1007/s12035-016-0172-0
68. Perumal, N., Funke, S., Pfeiffer, N. and Grus, F.H. (2016) Proteomics analysis of human tears from aqueous-deficient and evaporative dry eye patients. *Sci. Rep.*, **6**, 29629.
69. Cox, J. and Mann, M. (2008) MaxQuant enables high peptide identification rates, individualized p.p.b.-range mass accuracies and proteome-wide protein quantification. *Nat. Biotechnol.*, **26**, 1367–1372.
70. Cox, J., Neuhauser, N., Michalski, A., Scheltema, R.A., Olsen, J.V. and Mann, M. (2011) Andromeda: a peptide search engine integrated into the MaxQuant environment. *J. Proteome Res.*, **10**, 1794–1805.
71. Lefranc, M.-P., Giudicelli, V., Duroux, P., Jabado-Michaloud, J., Folch, G., Aouinti, S., Carillon, E., Duvergey, H., Houles, A., Paysan-Lafosse, T. *et al.* (2015) IMGT(R), the international ImMunoGeneTics information system(R) 25 years on. *Nucleic Acids Res.*, **43**, D413–D422.
72. Lefranc, M.-P. (2014) Antibody Informatics: IMGT, the International ImMunoGeneTics Information System. *Microbiol. Spectr.*, **2**.
73. Ye, J., Ma, N., Madden, T.L. and Ostell, J.M. (2013) IgBLAST: an immunoglobulin variable domain sequence analysis tool. *Nucleic Acids Res.*, **41**, W34–W40.
74. Lefranc, M.-P., Pommie, C., Ruiz, M., Giudicelli, V., Foulquier, E., Truong, L., Thouvenin-Contet, V. and Lefranc, G. (2003) IMGT unique numbering for immunoglobulin and T cell receptor variable domains and Ig superfamily V-like domains. *Dev. Comp. Immunol.*, **27**, 55–77.
75. Cox, J. and Mann, M. (2012) 1D and 2D annotation enrichment: a statistical method integrating quantitative proteomics with complementary high-throughput data. *BMC Bioinformatics*, **13**, S12.
76. Jaffe, J.D., Keshishian, H., Chang, B., Addona, T.A., Gillette, M.A. and Carr, S.A. (2008) Accurate inclusion mass screening: a bridge from unbiased discovery to targeted assay development for biomarker verification. *Mol. Cell. Proteomics*, **7**, 1952–1962.
77. Perumal, N., Funke, S., Wolters, D., Pfeiffer, N. and Grus, F.H. (2015) Characterization of human reflex tear proteome reveals high expression of lacrimal proline-rich protein 4 (PRR4). *Proteomics*, **15**, 3370–3381.

2.2 Publication II

Synthetic polyclonal-derived CDR peptides as innovative strategy in glaucoma therapy.

Schmelter C, Nzogang Fomo K, Perumal N, Manicam C, Bell K, Pfeiffer N, Grus FH

(Under revision in Journal of Clinical Medicine)

Synthetic polyclonal-derived CDR peptides as innovative strategy in glaucoma therapy

Carsten Schmelter [1], Kristian Nzogang Fomo [1], Natarajan Perumal [1], Caroline Manicam [1], Katharina Bell, Norbert Pfeiffer [1], Franz H. Grus [1,*]

[1] Department of Experimental and Translational Ophthalmology, University Medical Center, Johannes Gutenberg University, Mainz, Germany
[*] Corresponding author

E-mail addresses of all authors:

Carsten Schmelter: cschmelter@eye-research.org

Kristian Nzogang Fomo: kristianfomo@yahoo.de

Dr. Natarajan Perumal: nperumal@eye-research.org

Dr. Caroline Manicam: caroline.manicam@unimedizin-mainz.de

Dr. Katharina Bell kbell@eye-research.org

Prof. Dr. Norbert Pfeiffer: norbert.pfeiffer@unimedizin-mainz.de

Prof. Dr. Dr. Franz H. Grus: grus@eye-research.org

Conflict of Interest:

None

Address of the corresponding author:

Prof. Dr. Dr. Franz H. Grus

Department of Experimental and Translational Ophthalmology, University Medical Care Center, Johannes Gutenberg University, Mainz, Germany

Tel: +49 6131 / 173328

Fax: +49 6131 / 175509;

E-mail: grus@eye-research.org

Abstract

The pathogenesis of glaucoma is strongly associated with the occurrence of autoimmune-mediated loss of retinal ganglion cells (RGCs) and recently it was proven that specific antibody-derived signature peptides are significantly differentially expressed in sera of primary-open angle glaucoma patients (POAG) compared to healthy controls. Synthetic antibody-derived peptides are known since several years to modulate various effector functions of the immune system and to act as antimicrobial or antiviral molecules. The present study shows for the first time that polyclonal-derived complementarity-determining regions (CDRs) significantly increased the survival rate of RGCs in an *ex vivo* glaucoma model (P=0.013) by using immunohistochemical staining techniques. Affinity capture experiments verified serine protease *HTRA2* (mitochondrial) as high-confident retinal epitope target of CDR1 sequence motive *ASGYTFTNYGLSWVR.* Quantitative proteomic analysis of the CDR-treated retinal explants revealed increased expression of various anti-apoptotic and anti-oxidative proteins (e.g. *VDAC2* and *TXN*) compared to untreated controls (P<0.05) and decreased expression levels of cellular stress response markers (e.g. *HSPE1* and *HSP90AA1*) were observed. Mitochondrial dysfunction, protein ubiquitination pathway and oxidative phosphorylation were annotated as the most significantly affected signaling pathways and can possibly be traced back to the CDR-induced inhibition or modulation of the master regulator *HTRA2*. These findings emphasize the great potential of synthetic polyclonal-derived CDR peptides as therapeutic agents in future glaucoma therapy and provide an excellent basis for affinity-based biomarker discovery purposes.

Key words: Glaucoma; Autoimmunity; Synthetic CDR peptides; Neuroprotection; HTRA2; Sus scrofa domesticus

1 Introduction

Glaucoma is defined as a neurodegenerative ocular disease characterized by the progressive loss of retinal ganglion cells (RGCs) and their axons, resulting in an optic nerve damage und visual field defects [1]. Elevated intraocular pressure (IOP) is one of the most common risk factors for the development of glaucoma and can be detected in approximately 70 % of all patients, which is termed as the primary open-angle glaucoma (POAG) [1]. However, in recent years the participation of an autoimmune component, including autoantibodies (AAB), has become a focus of attention in glaucoma research providing new attractive targets for future diagnostic or therapeutic purposes [2–7]. A multitude of AABs against different kinds of retinal or optic nerve antigens were identified such as several heat shock proteins (*HSP27*, *HSP60* and *HSP70*) [8,9], various crystallins (α- and β-crystallin) [10,8], vimentin [10], glycosaminoglycans [11] or α-fodrin [12]. Interestingly, many of these autoreactivities showed a high degree of congruence in sera as well as aqueous humor of glaucoma patients [13,14] and also remain remarkably stable between different study populations [12]. Besides the great potential of these immune-related biomarker candidates for diagnostic applications [14], several recent studies of our group have also provided important evidence of neuroprotective effects of various AAB molecules (e.g. against *GFAP*, 14-3-3, α- and γ-synuclein) on RGCs in a range of *in vivo* and *ex vivo* glaucoma models [15–19]. These findings underline the important therapeutic potential of AABs found in low abundant titers in glaucoma patients and could also serve as an additional treatment option in glaucoma therapy in combination with IOP-lowering medications. However, many of these therapeutic macromolecules such as antibodies have several disadvantages such as immunogenic properties, poor tissue penetration and high manufacturing costs, thus limiting their application spectrum in daily clinical routine [20].

Recently it was shown that liquid-chromatography mass spectrometry (LC-MS) represents a powerful instrument for the reproducible identification and quantification of peptides from the variable domain of highly diverse antibodies without any prior knowledge about the targeted (auto-)antigens [21–24]. By implementation of the MS-based analytical approach we were able to identify several polyclonal IgG V domain peptides, particularly complementarity-determining regions (CDR), which were significantly differentially expressed in the protein backbone of sera-derived IgG between POAG patients and healthy controls [25]. In addition, this procedure facilitates the direct sequencing of Ig-derived peptide motives which are

shared between several B cell clones and is independent of predefined protein panels providing the basis for AAB profiling *via* microarray or Western Blot analysis. However, CDRs are hypervariable sequence motives (paratope) of the variable Ig domain and determine the active bindings sites of the antibodies which are primary responsible for the antigen specificity [26]. Many previous studies already highlighted the versatile biological functions of synthetic CDR-derived peptides ranging from immunomodulatory or immunoregulatory effects [27,28] to antiviral, antibacterial or antitumor activities [29–31], which are independent of the antigen specificity of the native antibodies. On the one hand, Rabaça *et al.* (2016) [32] demonstrated that a synthetic CDR-related peptide, encoding the VH CDR3 of murine monoclonal antibody AC 1001, displayed cytotoxic effects on murine and human melanoma cells *ex vivo* by inducing reactive oxygen species (ROS) and apoptotic signaling pathways. On the other hand, another synthetic tolerogenic CDR peptide showed ameliorating effects in different animal models for Systemic Lupus Erythematosus (SLE) by triggering immunomodulatory and immunosuppressive activities [33–35], favoring the general application of synthetic CDR peptides as therapeutic agents in other autoimmune-related neurodegenerative diseases.

Based on these previous observations, the main objective of the present study was to evaluate if selected synthetic glaucoma-associated CDR1 peptides (comprising *ASGYTFTNYGLSWVR* and *ASQSVSSYLAWYQQK*) may trigger any neuroprotective or even neurodamaging events on RGCs in an *ex vivo* glaucoma model. Furthermore, both CDR1 sequence motives were screened for potential interaction partners (epitope targets) in the retinal porcine proteome by using state-of-the-art affinity capture LC-MS technologies. Due to this reason, the present work provides important information about the applicability and effectiveness of synthetic CDR peptides in future glaucoma therapy and aims to unravel the complex biological function of these highly specific immune-related biomarker candidates.

2 Methods & Materials

2.1 Retina isolation and homogenization

Retina tissues were prepared from freshly removed eye bulbs (N = 20) from house swine *Sus scrofa domestica* Linnaeus, 1758 individuals (sacrificed at 3-6 month, female: male = 3:2) provided by local slaughterhouses (Landmetzgerei Harth, Stadecken-Elsheim, Germany; Hofgut Acker, Bodenheim, Germany). Preparation of the eye bulbs was performed under sterile conditions not later than 3 h after slaughtering. First, eye bulbs were disinfected with 70 % ethanol (EtOH) and subsequently radially opened with a scalpel to remove lens, vitreous body, iris and ciliary body. Next, retina tissues were carefully separated from the retinal pigment epithelium (RPE) with a paintbrush and cut off from the optic nerve head with pair of scissor. Samples were transferred into 2 ml screw cap microtubes, snap-frozen in liquid nitrogen and stored at -80° C. Prior to homogenization, 1.4/2.8 mm ceramic balls (VWR International GmbH, Darmstadt, Germany) were added to frozen retinal tissues and filled with 1 ml Tissue Protein Extraction Reagent (T-PER, Thermo Fisher Scientific, Rockford, USA). Retina samples were subjected for homogenization with Precellys® 24 homogenizer (VWR International GmbH, Darmstadt, Germany) for 45 s three times at 5000 rpm. Retinal homogenates were centrifuged at 10,000x *g* for 12 min at 4° C and the supernatant was collected into new 2 ml reaction tubes. To avoid sample contamination by insoluble cell components the centrifugation step was repeated once again and the supernatant containing soluble retinal proteins was exchanged in 300 µl phosphate-buffered saline (PBS) using an Amicon 3 kDa centrifugal filter device (Millipore, Billerica, USA). The concentrated protein lysates were pooled and protein measurements were performed using Pierce BCA Protein Assay Kit (Thermo Fisher Scientific, Rockford, USA) according to the manufacturer's protocol. Protein lysate pool was diluted in the ratio of 1:20, 1:30 and 1:40 in PBS (v/v) and measured three times using a Multiscan Ascent photometer (Thermo Fisher Scientific, Rockford, USA) at a wavelength of 570nm.

2.2 CDRs and scrambled as control peptides

Two complementarity-determining regions (CDRs), which were associated with glaucoma [25], were synthesized in cooperation with the Translational Oncology Mainz of the Johannes Gutenberg University (TRON, Mainz, Germany) and PEPSCAN (Lelystad, Netherlands). CDR peptide sequences were synthesized as followed: *ASGYTFTNYGLSWVR*

(CDR1) and *ASQSVSSYLAWYQQK* (CDR1). In the first stage, both CDR peptides were synthesized with an N-terminal Biotin-[TTDS] linker for epitope identification experiments (see section 2.3). CDR peptides (*ASGYTFTNYGLSWVR*) with successful identified interaction partners were further synthesized without modification and their respective scrambled peptide analogs as proper controls (*YVWAGSTLSRTGNFY*; without modification and N-terminal Biotin-[TTDS] linker)

2.3 Identification of CDR-specific epitope targets

The synthetic CDR peptides with N-terminal Biotin-[TTDS] linker were immobilized on Pierce™ Streptavidin Magnetic Beads (Thermo Fisher Scientific, Rockford, USA) according to the supplier's protocol (N=3). In brief, 50 µl of the magnetic beads were washed two times with 200 µl PBS using a magnetic stand and labeled for 1 h at room temperature (RT) with 80 µg of the N-terminal biotin-labeled synthetic peptides. As control group (N=3), biotin-labeled (0.5 mg/ml) magnetic beads were included in the experiment to distinguish unspecific from CDR-specific binders. After peptide immobilization, magnetic bead fractions (N=3) were washed twice with PBS followed by incubation and gentle mixing with 5 mg homogenized pig retina (see section 2.1) at 4° C overnight. Next day, the unbound protein fraction was discarded and the labeled magnetic beads were extensively washed with 300 µl PBS for three times to diminish unspecific bindings. The remained attached proteins were eluted with 100 µl Pierce™ IgG Elution Buffer pH 2.0 (Thermo Fisher Scientific, Rockford, USA) and transferred into reaction tubes containing 10 µl 1M Tris · HCl pH 8.5. The eluate fractions were evaporated in the SpeedVac (Eppendorf, Darmstadt, Germany) for 30 min at 30° C until dryness and stored at -20° C prior to further in-solution trypsin digestion. As spike-in experiment for the verification of the interaction partner, recombinant *HTRA2/Omi* (Human Serine Protease, cat. no. C760) was purchased from Novoprotein (Summit, USA). Spike-in experiment also included a scrambled peptide analog as proper control to confirm sequence specificity for the CDR peptide-protein interaction.

2.4 Retinal explants and immunohistology

The adolescent retina organ culture (*Sus scrofa*) represents an excellent *ex vivo* glaucoma model and was already used to study the neuroprotective effects of specific AABs on RGCs [17]. The optic nerve cut (ONC) during slaughtering initiated the neurodegeneration process and lead to a significant decrease of RGCs after 24 h of incubation. Preparation of the retina-

RPE complexes (5x5 mm) was performed in accordance to previous publication [17] and were cut in the dorsal periphery above the visual streak to ensure homogeneous distribution of RGCs in each experiment. Afterwards, the retinal explants were cultured in neurobasal A medium supplemented with 2% B27, 1% N2, 0.8 mM L-alanyl-L-glutamine and 1% penicillin/streptomycin in an incubator at 37°C and 5% CO2 for 24 h. Control explants were cultured for 24 h without any synthetic peptides (N=4). In addition, further retinal explants were treated with 25 µg/ml synthetic CDR peptide (*AS<u>GYTFTNYG</u>LSWVR*) or 25 µg/ml scrambled peptide analog (*YVWAGSTLSRTGNFY*) as proper control (N=4 for each group). After cultivation, control and treated retinal section were carefully removed from the RPE, washed twice with PBS and fixed in 4 % paraformaldehyde (PFA) for 30 min. Retinal flatmounts were washed twice with PBS and subsequently blocked and permeabilised for 2 h with 200 µl 0.3% Triton-X-100 (Sigma-Aldrich, St. Louis, USA) and 10% fetal calf serum (Merck Millipore, Darmstadt, Germany) in PBS. Afterwards, the blocking buffer was discarded and the flatmounts were stained with 1: 250 goat anti-Brn3a (Santa Cruz Biotechnology, Dallas, USA) overnight at 4° C. Next day, the retinal flatmounts were washed twice with PBS and incubated with 1:400 Alexa Flour 568 donkey anti-goat (H+L; Thermo Fisher Scientific, Rockford, USA) for 2 h in the dark. Subsequently, after the staining a TUNEL assay via In Situ Cell Death Detection Kit, Fluorescein (Roche, Basel, Switzerland) was performed according to the supplier's protocol at 37° C for 1 h. Retinal flatmounts were washed three times with PBS and stained with 1:2500 4',6-Diamidin-2-phenylindol (DAPI; Thermo Fisher Scientific, Rockford, USA) in PBS for 5 min at RT. After washing, the retinal flatmounts were mounted with vector shield mounting medium (Vector Laboratories, Burlingame, USA) on Superfrost Plus™ slides (Thermo Fisher Scientific, Rockford, USA). Fluorescence microscopy was performed with a Nikon Eclipse TS100 microscope (Nikon Instruments, Tokyo, Japan) combined with a DS-Fi1-U2 digital camera and NIS elements software. Eleven high-resolution pictures (20-fold magnification) were taken from each the retinal flatmount at different positions, resulting in 44 pictures per experimental group (TRITC, FITC and DAPI channel). High-resolution fluorescent images were analyzed randomized *via* open-source ImageJ software package (http://imagej.nih.gov/ij/) by experienced laboratory workers. Brightness and contrast of the high-resolution fluorescent images was adjusted to facilitate the manual counting of the $Brn3a^+$ and $TUNEL^+$ cells. The number of RGCs ($Brn3a^+$) was extrapolated to RGC/mm^2 and the percentage distribution of $Brn3a^+$ and $TUNEL^+$ was calculated.

2.5 In-gel and in-solution trypsin digestion

For the identification of the CDR-specific interaction partners the eluate fractions (see section 2.3) were subjected for further in-solution trypsin digestion as described elsewhere [25,36,37]. In brief, the eluate fractions were dissolved in 30 µl of 50mM ammonium bicarbonate (ABC) and sonicated for 5 min on ice. Subsequently, 6 µl of 100mM dithiothreitol (DTT) in 50 mM ABC were added and incubated for 30 min at 56° C. Next, 6 µl of 200mM iodoacetamide (IAA) in 50 mM ABC were added and incubated for 30 min at RT in the dark. The reduced and alkylated proteins were digested overnight with 0.2 mg/ml trypsin (Promega, Madison, USA) in 50 mM ABC 10 % acetonitrile (ACN) at 37° C. Next day, the digestion was quenched with 10 µl of 0.1 % formic acid (FA), evaporated in the SpeedVac for 30 min at 30° C to dryness and stored at -20° C. To unravel the CDR-induced proteomic changes in the retinal explants (see section 2.4), in-gel trypsin digestion for mass spectrometry (MS)-based proteomics was performed. CDR-treated and untreated retinal explants (N=3 per group) were transferred into 2 ml screw cap microtubes and subsequently frozen in liquid nitrogen. Frozen explants were filled with 400 µl T-PER buffer and 1.4/2.8 mm ceramic balls were added. Protein extraction was performed using the Precellys® 24 homogenizer and homogenates were exchanged in 200 µl PBS by using an Amicon 3 kDa centrifugal filter device (as described in detail in section 2.1). Total protein amounts of the retinal explants were determined by Pierce BCA Protein Assay Kit and Multiscan Ascent photometer. Up to 40 µg of protein lysate per explant were separated under reduced conditions on 10-well NuPAGE 12 % Bis-Tris minigels (Thermo Fisher Scientific, Rockford, USA) by using NuPAGE™ MOPS SDS Running Buffer 20X (Thermo Fisher Scientific, Rockford, USA) in accordance to the supplier's protocol. 1-DE SDS PAGE was run at 150 V for 1.5 h at 4 °C and subsequently stained by using Novex Colloidal Blue Staining Kit (Thermo Fisher Scientific, Rockford, USA) according to the manufacturer's introduction. Gels were destained overnight and scanned using an Epson Perfection V600 Photo Scanner (Seiko Epson Corporation, Suma, Nagano, Japan) at 700 dpi. Each lane was subdivided into 17 slices and subjected to further in-gel trypsin digestion as described in previous publications [38,39,36,40]. Prior to LC-MS/MS analysis the tryptic peptides of the in-solution or in-gel digest were purified by SOLAµ™ HRP SPE spin plates (Thermo Fisher Scientific, Rockford, USA) according to the manufacturer's protocol [41].

2.6 LC-MS/MS analysis

LC-MS/MS measurements were performed with the hybrid linear ion trap - Orbitrap MS system (LTQ Orbitrap XL; Thermo Fisher Scientific, Rockford, USA) as described in detail elsewhere [36,38,40–42]. Solvent A consisted of 0.1 % formic acid (FA) in water and solvent B consisted of 0.1 % FA in ACN. Peptides of the in-solution tryptic digest were eluted within 120 min using following gradient program: 10–20 % B (0-5 min), 15–20 % B (5–15 min), 20–35 % B (15–85 min), 35–90 % B (85–105 min) and 10 % B (105–120 min). In contrary, peptides of the in-gel tryptic digest were eluted within 60 min using following gradient program: 15–40 % B (0-30 min), 40–60 % B (30–35 min), 60–90 % B (35–45 min) and 10 % B (45–60 min). LTQ Orbitrap operated with a resolution of 30.000 in the positive ion mode and the target automatic gain control (AGC) was set to 1×10^6 ions. The lock mass for internal calibration was set to 445.120025 m/z (polydimethylcyclosiloxane). Dynamic exclusion (DE) mode was enabled with the following settings for the in-solution digest: repeat count = 2, repeat duration = 30 s, exclusion list size = 250, exclusion duration = 300 s and exclusion mass width= ± 10 ppm. For the in-gel digest the DE setting exclusion duration was set to 90 s. High-resolution MS scan of the Orbitrap-FTMS analyzer provided the selection of the 5 most intense peptide ions for collision induced dissociation (CID) fragmentation in the ion trap employing a normalized collision energy of 35 %. Quality control of the total ion current (TIC) chromatogram was performed by using Qual Browser v. 2.0.7 SP1 (Thermo Fisher Scientific, Rockford, USA).

2.7 Protein identification and quantification

For protein identification and quantification the acquired tandem MS spectra were analyzed with the computational proteomics platform MaxQuant version 1.6.1.0 (Max Planck Institute of Biochemistry, Martinsried, Germany). Output data were searched against SwissProt databases with the taxonomies *Homo sapiens* (Date: 07/18/2018, 20.385 sequences) and *Sus scrofa* (Date: 07/18/2018, 1424 sequences) with following settings: peptide mass tolerance of ± 30 ppm, fragment mass tolerance of ± 0.5 Da, tryptic cleavage, a maximum of two missed cleavages, carbamidomethylation as fixed modification, acetylation (Protein N-terminal) and oxidation as variable modifications. In addition, proteins were filtered with a false discovery rate (FDR) of < 1 % and MaxQuant specific feature “match between run” was enabled.

2.8 Data analysis and bioinformatics

Statistical analysis of the MaxQuant generated output data ("proteins.txt") was performed by using software program Perseus version 1.5.5.0 (Max Planck Institute of Biochemistry, Martinsried). At first, intensities of the detected proteins were log2 transformed prior to further analysis. Data matrix was filtered for contaminants, reversed hits, "only identified by site" and for a minimum number of 3 valid values in at least in one study group. Missing intensity values were imputed by random numbers received from the normal distribution (width: 0.3, down shift: 1.8). For the identification of CDR-specific interaction partners (see section 2.3) only missing values of the control bead group were imputed in accordance to previous publication [43]. Afterwards, two-sided t-test statistics with P values < 0.05 was applied in order to identify significant changed protein species. For the illustration of the heat map the log2 transformed protein abundances were standardized by z-score. Further statistical analyses and graphical presentation of data were performed by using Statistica version 13 (Statsoft, Tulsa, USA) or excel 2013 functions. Functional annotation and pathway analyses were performed with web-based biological database STRING version 10.5 (Search Tool for the Retrieval of Interacting Genes/Proteins) and Ingenuity Pathway Analysis software version 1-04 (IPA, Ingenuity QIAGEN Redwood City, USA; www.qiagen.com/ingenuity), as described in detail in previous publications [44,37].

3 Results

3.1 Identification of CDR-specific epitope targets

To proof the concept and the feasibility of the MS-based epitope identification workflow (see Fig. 1 and method section 2.3), we choose two in glaucoma low abundant CDR1 peptide sequences (see Fig. 2) for the affinity capture experiment. Both CDR1 sequence motives (*AS<u>GYTFTNYG</u>LSWVR* homologous to IGHV1-18*02 and *AS<u>QSVSSY</u>LAWYQQK* homologous to IGKV3-11*01) were significantly lesser expressed in the protein backbone of polyclonal, sera-derived IgG molecules in glaucoma patients in contrast to healthy controls and provide attractive targets for the MS-based epitope identification [25]. Binding efficiency of both synthetic N-terminal biotinylated CDR1 peptides to magnetic streptavidin beads was confirmed by LC-MS (see supplementary Fig. 1).

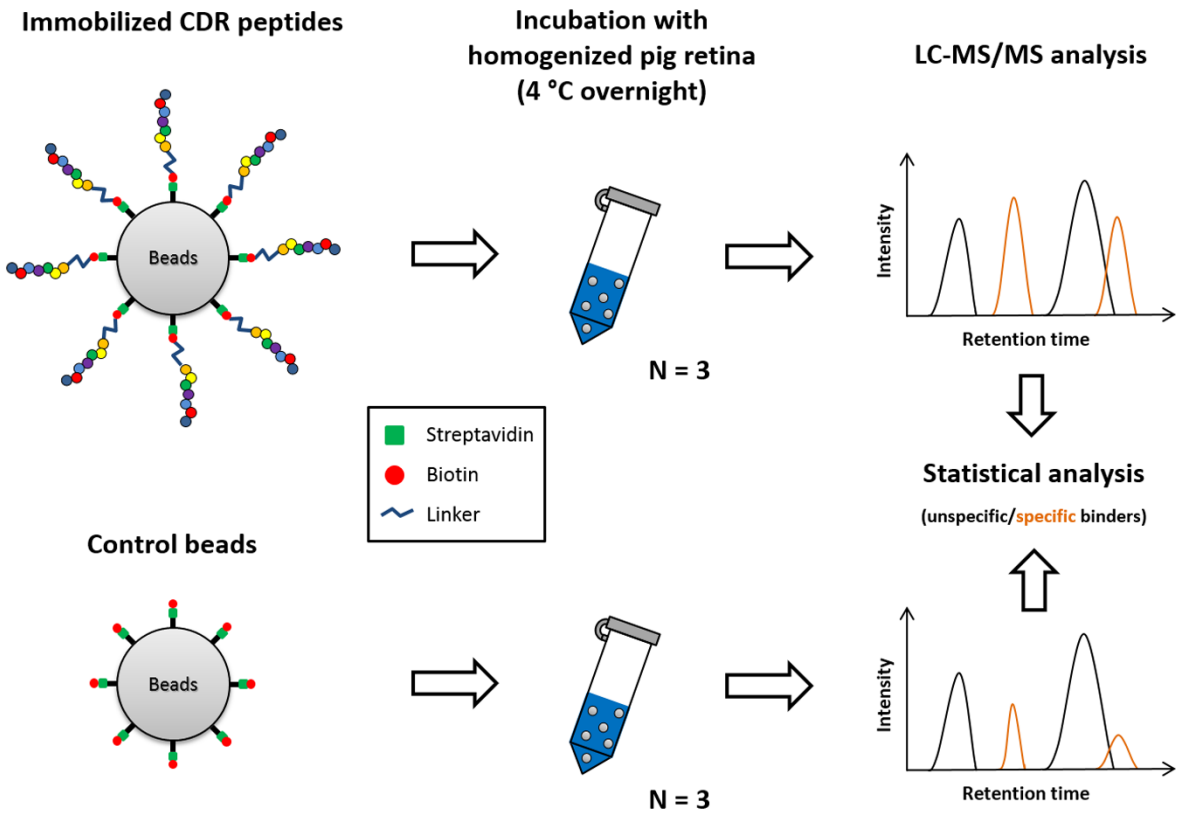

Fig. 1: Schematic illustration showing affinity capture experiments of potential epitope targets by synthetic CDR-derived peptides. CDR peptides were synthesized with an N-terminal [TTDS]-biotin modification by a specialist manufacturer. For epitope identification the modified synthetic peptides (80 µg) were attached to commercial available streptavidin beads and incubated with 5 mg homogenized pig retina. To distinguish unspecific from specific protein binders a biotin-labeled control group was included in the analysis. After incubation, all bead fractions were extensively washed and the remaining attached proteins were eluted by pH shift. Eluate fractions were subjected for further in-solution trypsin digestion and analyzed by LC-MS/MS. Statistical analysis revealed high-confident epitope targets (interaction partners) of the synthetic CDR peptides.

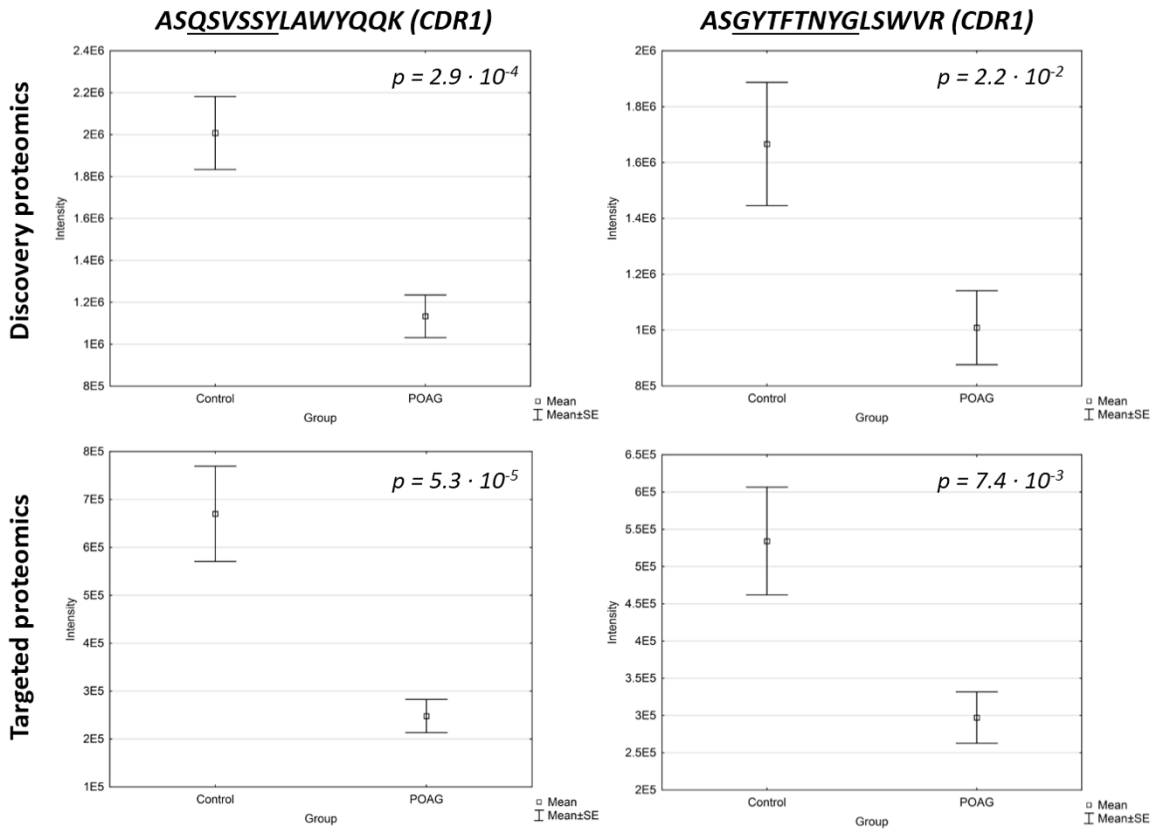

Fig. 2: Bar plot showing the expression levels of two CDR1 sequences (*ASQSVSSYLAWYQQK* and *ASGYTFTNYGLSWVR*) in sera of primary open-angle glaucoma patients (N=13) in comparison to healthy controls (N=15). Both sera-derived CDR1 sequences were significantly low abundant in POAG patients ($P < 0.05$) in contrast to healthy controls and were also validated by targeted MS via accurate inclusion mass screening (AIMS) strategy. Results were published previously by Schmelter *et al.* (2017) [25].

Affinity capture experiments revealed that serine protease *HTRA2*, mitochondrial represents a high-confident interaction partner for the CDR1 sequence motive *ASGYTFTNYGLSWVR* (see Fig. 3A and supplementary file 1, P<0.001 and log2 fold change >3). In addition, epitope target *HTRA2* shows an overall low protein abundance (cumulative intensity) in the entire retinal porcine proteome (Fig. 3B) and confirms the specific interaction behavior to the glaucoma-associated CDR1 peptide. Furthermore, specific affinity of the CDR1 peptide to *HTRA2* was verified by the spike-in experiment (see Fig. 3C and method section 2.3) and proved the unique sequence specificity of the peptide-protein interaction by use of a scrambled peptide analog as proper control. However, no significant interaction partner for CDR1 sequence motive *ASQSVSSYLAWYQQK* was identified by affinity capture experiments (see supplementary Fig. 2 and file 1, P<0.001 and log2 fold change >3). Due to that reason, only CDR1 peptide sequence *ASGYTFTNYGLSWVR* was used for further experimental analyses.

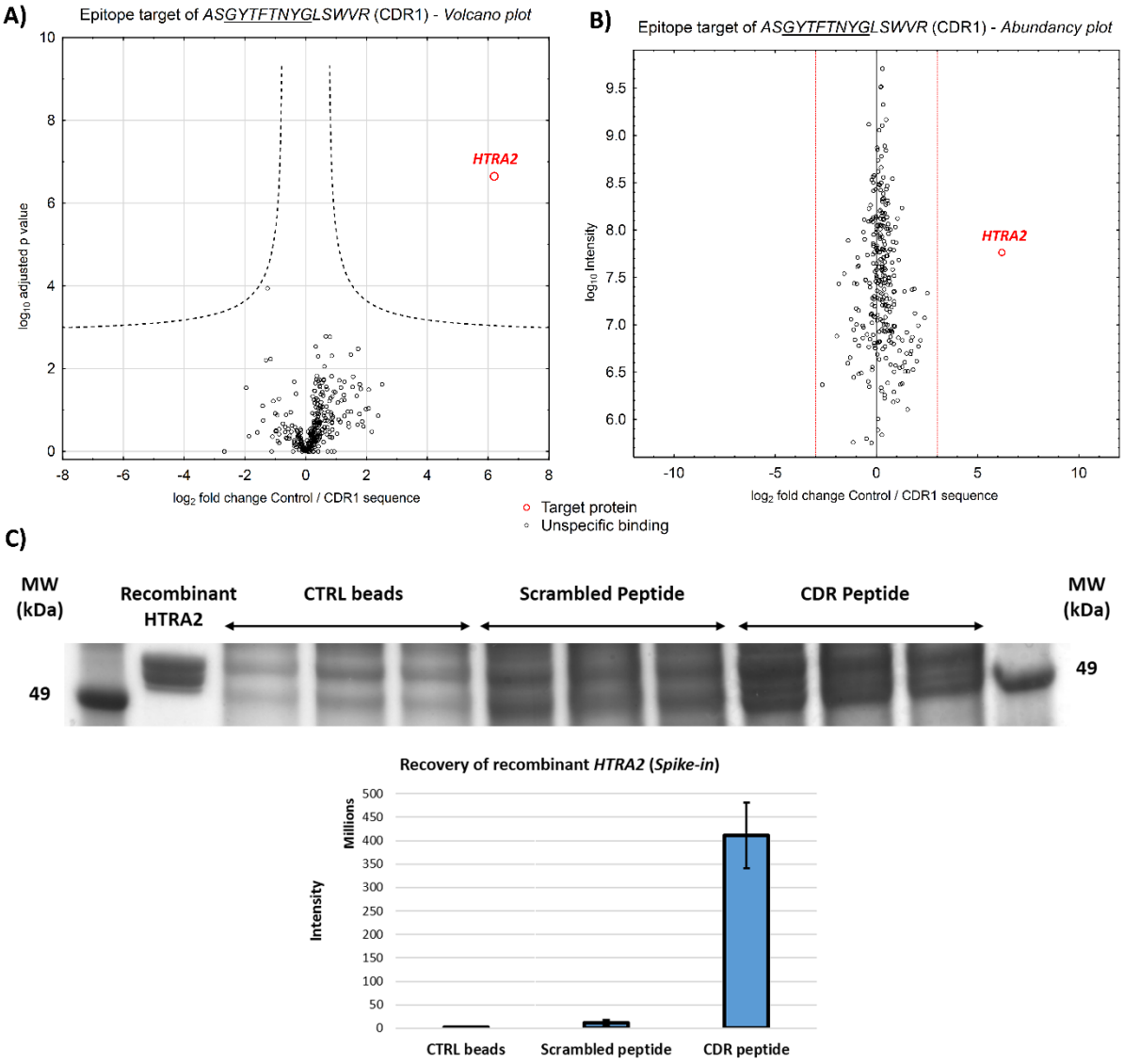

Fig. 3: Identification of potential epitope targets of the CDR peptides by affinity based proteomic strategy with 5 mg homogenized pig retina. **(A)** Volcano plot showing log2 fold change plotted against -log10 adjusted P value for samples from CDR-labeled bead group (N=3) versus samples from control bead group (N=3) (P<0.001; log2 fold change >3). Protein serine protease *HTRA2* (mitochondrial) was identified as high-confident interaction partner for synthetic CDR1 peptide *ASGYTFTNYGLSWVR*. **(B)** Abundancy plot showing log2 fold change plotted against -log10 adjusted cumulative intensity. *HTRA2* represents a low abundant protein in the porcine retina and confirms the specific interaction with the synthetic CDR1 peptide. **(C)** Spike-in experiment of 2 µg recombinant *HTRA2* in 5 mg homogenized pig retina followed by affinity-based proteomics. In-gel trypsin digestion revealed that control (CTRL) beads and scrambled peptide analog recovered much lesser quantities of recombinant *HTRA2* in contrast to the original CDR peptide and confirms the sequence specificity of the interaction to *HTRA2*.

3.2 CDR-induced effects in an *ex vivo* glaucoma model

To address the question, if the synthetic CDR1 sequence motive *ASGYTFTNYGLSWVR* may trigger any neuroprotective or even neurodamaging activities in glaucoma, we used an established *ex vivo* glaucoma model for evaluation. The adolescent porcine retina organ culture [17] provides excellent requirements to study CDR-induced effects on RGCs after optic nerve cut (ONC) and is suitable to assess the effectiveness of synthetic CDR peptides as

potential drug candidates in future glaucoma therapy. And indeed, quantitative analysis of RGC/mm^2 (see Fig. 4 A-B) in CDR-treated retinal explants (296 ± 29 RGC/mm^2, N=4) revealed a significantly higher RGC survival rate in contrast to untreated control explants (203 ± 45 RGC/mm^2, N=4, P=0.013).

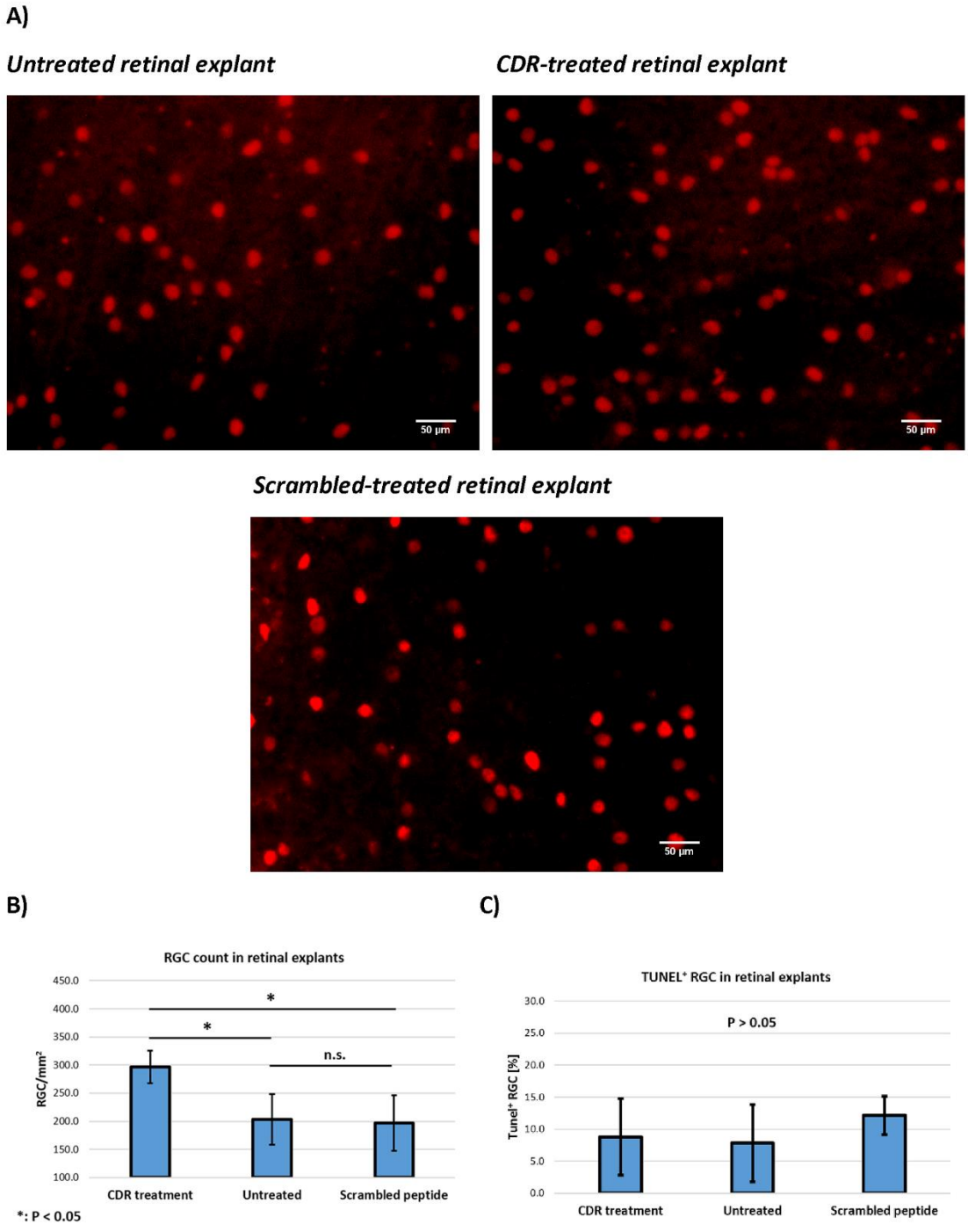

Fig. 4: Effect of the CDR peptide on the number of RGC survival by Brn3a$^+$ staining and the percentage of apoptotic RGC determined by TUNEL assay. Retinal explants (N=4 per group) were cultivated with control medium without any peptide (untreated control) or with medium with additional 25 µg/ml CDR peptide for 24 h. Furthermore, further retinal explants were also incubated in medium with 25 µg/ml scrambled peptide analog serving as proper control. **(A)** Brn3a$^+$ staining of retinal flatmounts without any treatment, treated with the CDR

peptide or treated with the scrambled peptide analog. **(B)** CDR-treated explants showed significant higher RGC survival in contrast to untreated control group and scrambled peptide group (P<0.05). **(C)** Quantitative analysis of TUNEL$^+$ RGC did not show any significant difference between the groups (P>0.05).

In addition, a scramble peptide analog (*YVWAGSTLSRTGNFY*) was used as proper control in further retinal explants (197 ± 50 RGC/mm^2, N=4, P=0.014) and verified the sequence specificity of the CDR-induced, neuroprotective effects on RGCs. However, no significant differences in the percentage distribution of Brn3a$^+$ and TUNEL$^+$ cells (see Fig. 4 C) were found between all three experimental groups (Untreated control: 8.8 ± 6.0 %, CDR: 7.9 ± 6.0 % and scrambled peptide: 12.2 ± 3.0 %, P > 0.05).

3.3 CDR-induced proteomic changes in retinal explants

To unravel the neuroprotective and anti-apoptotic effects of the CDR1 sequence motive *AS<u>GYTFTNYG</u>LSWVR* on RGCs, we performed LC-MS based quantitative proteomics of the untreated and CDR-treated retinal explants (N=3 per group, see supplementary file 2). In total 354 retinal proteins were identified in both experimental groups with an FDR < 1 %. Up to 6 % of all identified proteins showed a significant level change (P <0.05) between the CDR-treated retinas and the untreated control explants (see Fig. 5). Interestingly, representative stress response protein markers such as heat shock protein HSP-90 alpha (*HSP90AA1*), 10kDa heat shock protein mitochondrial (*HSPE1*), endoplasmic reticulum resident protein 29 (*ERP29*) or cytochrome c oxidase subunit 6C (*COX6C*) were significantly lesser expressed in CDR-treated explants in contrast to untreated controls. On the other hand, proteins with neuroprotective or anti-oxidative properties such as voltage-dependent anion-selective protein channel 2 (*VDAC2*), GTP-binding nuclear protein Ran (*RAN*) or thioredoxin (*TXN*) were significantly more abundant in CDR-treated samples in comparison to untreated controls. But also other attractive protein markers such as carbonic anhydrase 2 (*CA2*), putative elongation factor 1-alpha-like 3 (*EEF1A1P5*) or endoplasmin (*HSP90B1*) showed at least a tendency to differently expressed between both study groups (P < 0.1; see supplementary Fig. 3). However, CDR1 sequence specific epitope target *HTRA2* (see Fig. 3) was not detected by LC-MS, probably because of limit of detection. Nevertheless, functional annotation and pathway analysis confirmed a hypothetical interaction or regulation of the CDR-induced signaling pathways by *HTRA2* (see Fig. 6).

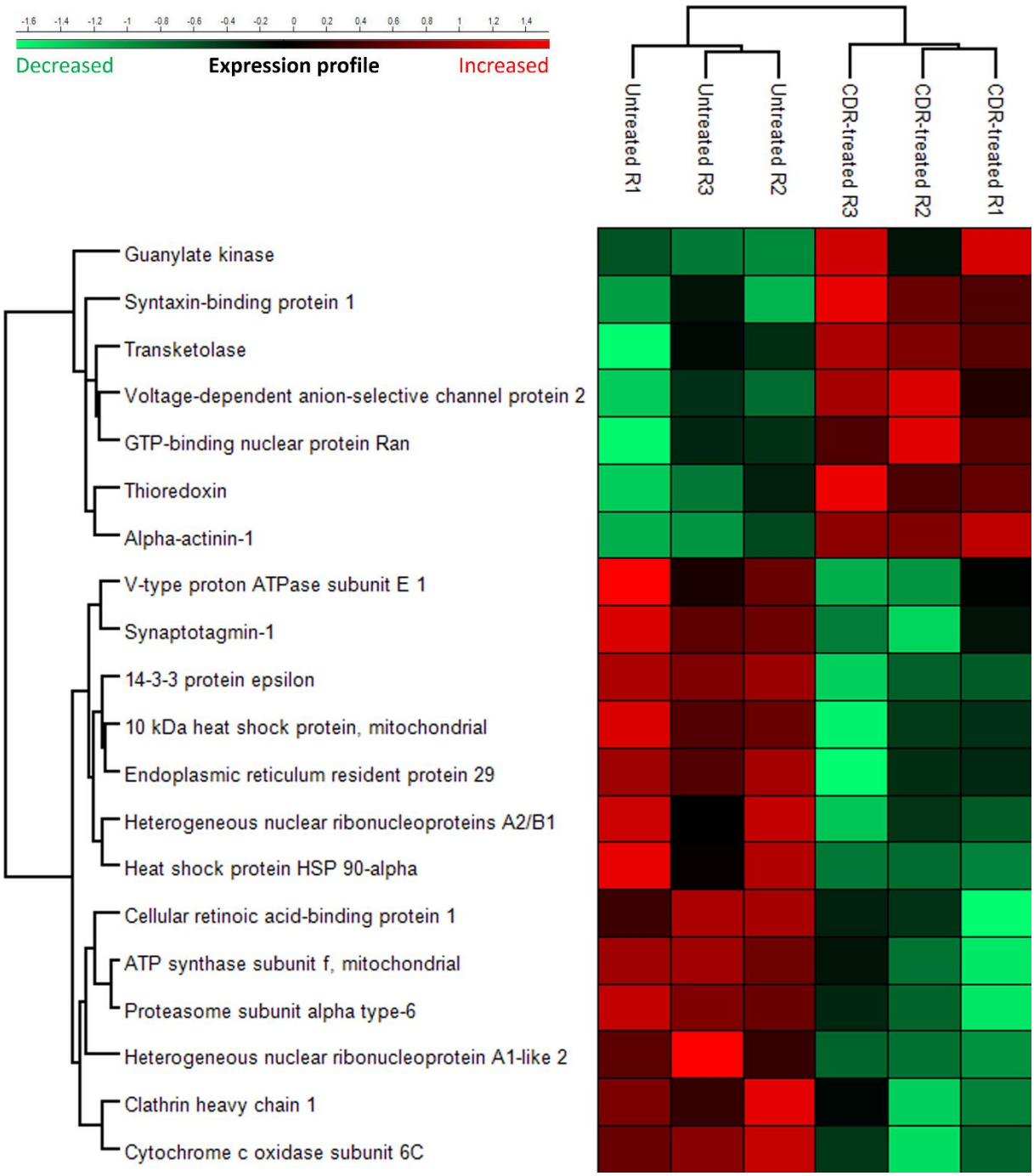

Fig. 5: Heat map showing the most significant proteomic changes (P<0.05) in retinal explants (N=3 per group) cultivated with medium without any peptide (untreated control) or with medium with 25 µg/ml CDR peptide for 24 h after optic nerve cut (ONC).

Additionally, IPA analysis revealed that the top five significant canonical pathways involved include mitochondrial dysfunction, protein ubiquitination pathway, oxidative phosphorylation, PI3K/AKT signaling and the thioredoxin pathway (see Tab. 1). Furthermore, most of the significantly differentially expressed proteins participated in various biological activities, namely post-translational modifications, protein folding, molecular transport, protein trafficking and maintenance of the cellular functions (see Tab. 2).

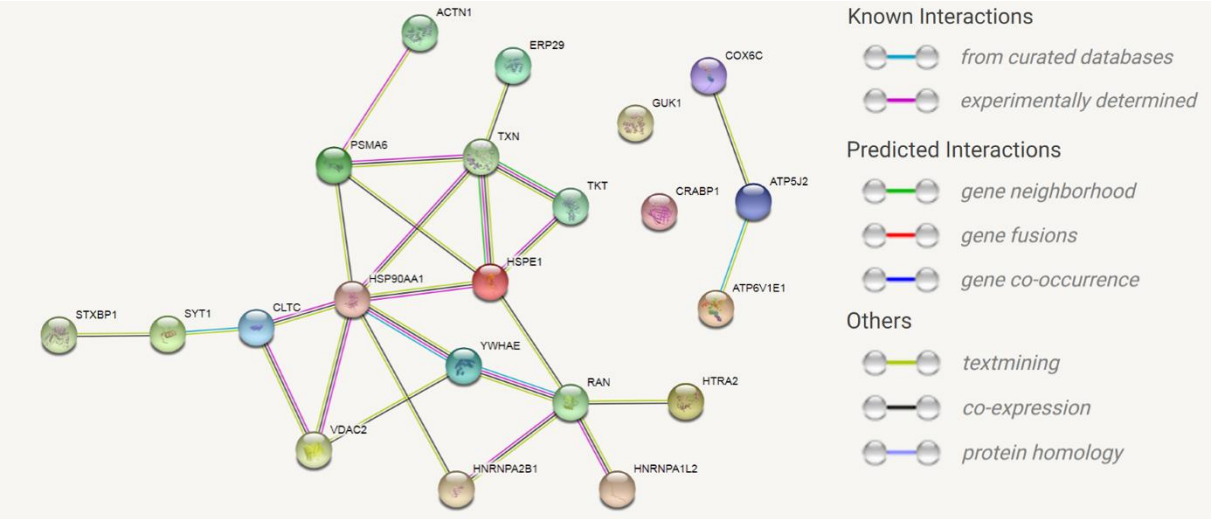

Fig. 6: Analysis of the CDR-induced signaling pathways in the retinal explants after 24h of incubation. Search Tool for the Retrieval of Interacting Genes/Proteins (STRING) shows the signaling pathways of the most significant changed proteins using medium confidence score (0.4). Epitope target *HTRA2* shows at least a textmining and co-expression to GTP-binding nuclear protein RAN.

Tab. 1: List of CDR-induced top canonical pathways revealed by Ingenuity Pathway Analysis (IPA).

Canonical Pathway	-log (P-value)	Molecules
Mitochondrial Dysfunction	3.37	*COX6C, ATP5MF, VDAC2*
Protein Ubiquitination Pathway	2.82	*PSMA6, HSPE1, HSP90AA1*
Oxidative Phosphorylation	2.39	*COX6C, ATP5MF*
PI3K/AKT Signaling	2.24	*YWHAE, HSP90AA1*
Thioredoxin Pathway	2.21	*TXN*
Pentose Phosphate Pathway (Non-oxidative)	2.21	*TKT*
Aldosterone Signaling in Epithelial Cells	2.03	*HSPE1, HSP90AA1*
Pentose Phosphate Pathway	2.02	*TKT*
NRF2-mediated Oxidative Stress Response	1.89	*ERP29, TXN*

Tab. 2: List of top molecular and cellular functions analyzed by Ingenuity Pathway Analysis (IPA).

Molecular and Cellular Functions	P-value	Number of molecules
Post-Translational Modification	$8.59 \cdot 10^{-7}$ - $8.59 \cdot 10^{-7}$	4
Protein Folding	$8.59 \cdot 10^{-7}$ - $8.59 \cdot 10^{-7}$	4
Molecular Transport	$1.31 \cdot 10^{-2}$ - $7.28 \cdot 10^{-6}$	14
Protein Trafficking	$1.25 \cdot 10^{-2}$ - $7.28 \cdot 10^{-6}$	6
Cellular Function and Maintenance	$1.48 \cdot 10^{-2}$ - $3.57 \cdot 10^{-5}$	9

4 Discussion

In recent years, immunopeptidomics is one of the fastest growing research areas with considerable progress in the field of personalized cancer immunotherapy [45]. As the term "immunopeptidomics" is generally associated with the MS-based identification of tumor-specific neoantigens serving as basis for the targeted cancer therapy [45], the present study offers completely new treatment strategies for various autoimmune-related diseases with special focus on glaucoma. Since several years short synthetic CDR peptides are commonly used as remarkably active biomolecules that trigger a wide range of effector functions such as immunomodulatory, antimicrobial, antiviral or antitumor activities [27,29–31,28]. Furthermore, synthetic CDR peptides have excellent properties as therapeutic agents mainly because of their small size, low immunogenicity, good tissue penetration characteristics as well as their ease and cost-effective manufacturing with structural modification possibilities [46]. However, all the previous studies referred to CDR peptides of already sequenced antibody molecules with known biological activity or antigen specificity and never focused on polyclonal-derived CDR sequences with unknown biological function.

In the present study, two CDR1 sequence motives (*ASGYTFTNYGLSWVR* and *ASQSVSSYLAWYQQK*), which were present in low abundance in the sera of glaucoma patients, were investigated for potential interaction partners (or epitope targets) in the retinal porcine proteome and screened for potential neuroprotective or even neurodamaging effects on RGCs in an *ex vivo* glaucoma model. The established epitope identification workflow (see Fig.1) revealed the protein serine protease *HTRA2*, mitochondrial (see Fig. 3) as a high confident interaction partner of the CDR1 sequence motive *ASGYTFTNYGLSWVR*. On one hand, *HTRA2* has drawn attention as a key player in apoptotic pathways promoting the degradation of anti-apoptotic proteins (e.g. X-linked inhibitor of apoptosis protein, *XIAP*) and the activation of caspase-dependent and –independent pathways [47–49]. Thereby, *HTRA2* is increasingly released from the mitochondria to the cytosol during cellular stress responses [47–49] and was also observed after optic nerve crush in the rat retina [50]. On the other hand, recent studies also indicated that transgenic *htra2*^{mnd2} mice deficient in *HTRA2* activity show early signs of onset neurodegeneration, multiple tissue atrophy and early lethality; thereby, strengthening the important role of *HTRA2* in neuronal cell survival and mitochondrial

homeostasis [51–54]. In accordance, dysfunction of *HTRA2* protein activity is also associated with other neurodegenerative diseases such as Parkinson's or Alzheimer's disease and represents an interesting target in cancer therapy [47,55]. Interestingly, inhibition of *HTRA2* activity, particularly the catalytic protein domain, prevented myocardial dysfunction and inflammation-mediated tissue damaging events after ischemia/reperfusion injury in rat hearts *in vivo* [56]. However, the exact role of *HTRA2* is still unknown in glaucoma and represents a very attractive target for future glaucoma-related study designs. Ding *et al.* (2009) [57] have already highlighted the importance of *HTRA2*-mediated apoptotic processes in murine RPE cells during oxidative stress conditions and proposed *HTRA2* as one of the key players in the pathogenesis of the age-related macular degeneration (AMD). Due to that reason, it is not far-fetched to speculate that *HTRA2* may also play important key functions in other eye-related disorders.

For the first time, we could demonstrate the CDR-induced, neuroprotective activities of sequence motive *AS<u>GYTFTNYG</u>LSWVR* on RGCs *ex vivo* (see Fig. 4 A-B) and verified the sequence specificity of these effects using a scrambled peptide analog as proper control. The number of RGC/mm^2 in the dorsal periphery of the porcine retina was in the range of previous publications [58,59] and confirms the reliability of the obtained results. However, no significant differences in the number of apoptotic cells were observed between all three experimental groups ($P>0.05$, see Fig. 4 C). In general, apoptotic processes are largely dependent on the cell type as well as environmental stimuli and can vary from 12 to 24 hours [60,61]. Since the TUNEL assay only indicates the last stage of apoptosis by *in situ* detection of fragmented DNA and just covers a period about 2 to 3 hours [62,63], the considered time frame could be too short to detect any significant changes in the cell death rate between the different groups. Nevertheless, considering the quantitative proteomic results (see Fig. 5), we identified an increased expression of anti-apoptotic and anti-oxidative proteins (e.g. *VDAC2* and *TXN*) in CDR-treated retinal explants in comparison to the untreated controls accompanied by decreased levels of proteins associated with the cellular stress response (e.g. *HSPE1*, *ERP29* and *HSP90AA1*). Mitochondrial *VDAC2*, for instance, plays an important role in the cell homeostasis by ROS neutralization [64] and triggers anti-apoptotic functions by direct inhibition of pro-apoptotic *BAK* [65]. In accordance, the protein *TXN* is responsible for the mitochondrial redox homeostasis and acts as important regulator of the energy metabolism in neuronal cells [66]. On the contrary, the proteins *HSP90AA1, HSPE1*, *ERP29* and are mainly

functioning as molecular chaperone complexes essential for the maintenance of the protein folding, trafficking and secretion (see Tab. 2) during cellular stress responses and are a hallmark for various neurodegenerative diseases including glaucoma [67–69]. Interestingly, mitochondrial dysfunction, protein ubiquitination pathway and oxidative phosphorylation (Tab. 1) were annotated as the three main affected canonical pathways and have already been discussed for several years as the primarily responsible pathological factors in glaucoma [70–73]. As already outlined, *HTRA2* plays an essential role in the mitochondrial homeostasis by protein quality control (PQC) [51–54] and also already showed direct inhibitory effects on E3 ubiquitin ligase activity [74,75], strengthening the hypothesis that *HTRA2* may act as master regulator of the affected canonical pathways potentially by direct interaction (inhibition) with CDR1 sequence motive *AS<u>GYTFTNYG</u>LSWVR*. In addition, the oxidative and non-oxidative pentose phosphate pathway (PPP) was also affected in the CDR-treated retinal explants and is mainly regulated by the increased expression of the protein transketolase (*TKT*) [76]. Remarkably, Kuehne *et al.* (2015) [77] postulated an important physiological role of the oxidative and non-oxidative PPP in the stabilization of the redox balance system and ROS clearance in human skin cells and was also already associated to glaucoma [78,79]. Since transgenic *htra2*^{mnd2} mice with deficient *HTRA2* activity are known to show an obvious heart enlargement with left ventricular hypertrophy accompanied by decreased mitochondrial energy supply and decreased glucose metabolism [52,51], *HTRA2* can also be assumed as an important master regulator and stabilizer for the mitochondrial energy metabolism. In addition, Ding *et al.* (2009) [57] further verified a decreased amount of mitochondria and an abnormal mitochondrial morphology in the retina of *HTRA2*-deficient mice compared to wild-type, indicating a fundamental function of *HTRA2* in the maintenance of the mitochondrial homeostasis in the eye. However, it still has to be determined if all these retinal proteomic changes are due to the direct interaction (inhibition) of *HTRA2* with the CDR1 sequence motive *AS<u>GYTFTNYG</u>LSWVR* or to other cell-mediated mechanism (e.g. receptor binding). Furthermore, it has to be proven if the CDR-induced protein markers represent the direct interaction partners of *HTRA2* or if they just develop as a consequence because of CDR-induced downstream signaling cascades.

5 Conclusion

The present study shows for the first time that short synthetic disease associated CDR peptides without any information about the native antigen specificity provide a great potential for the amelioration or treatment of glaucoma. Moreover, our results support for the first time the mitochondrial serine protease HTRA2 as important key player in the pathogenesis of glaucoma and should be particularly focused in future glaucoma research projects. However, this innovative procedural method would also offer completely new therapeutic strategies in other immune mediated inflammatory and neurodegenerative diseases. Beyond that, we want to encourage other research groups to apply the established MS-based platform for CDR peptide identification [25] in combination with the present MS based epitope identification workflow for biomarker discovery to other autoimmune related neurodegenerative diseases in future study designs.

6 Abbrevations

AAB	Autoantibodies
ABC	Ammonium bicarbonate
ACN	Acetonitrile
AGC	Automatic gain control
AMD	Age-related macular degeneration
CDR	Complementarity-determining region
CID	Collision-induced dissociation
CTRL	Control group
DE	Dynamic exclusion
DTT	Dithiothreitol
EtOH	Ethanol
FA	Formic Acid
Fab	Antigen-binding fragment
Fc	Crystallisable fragment
FDR	False discovery rate
FR	Framework region
IAA	Iodoacetamide
IOP	Intraocular pressure
IPA	Ingenuity Pathway Analysis
LC-MS	Liquid chromatography-mass spectrometry
MeOH	Methanol
MS	Mass spectrometry
ONC	Optic nerve cut
PBS	Phosphate-buffered saline
POAG	Primary open-angle glaucoma
RGC	Retinal ganglion cells
ROS	Reactive oxygen species
RPE	Retinal pigment epithelium
STRING	Search Tool for the Retrieval of Interacting Genes/Proteins
TIC	Total ion current
TFA	Trifluoroacetic acid
VH	Variable heavy chain

7 Declarations

7.1 Ethical Approval and Consent to participate

The use of animal by-products of the house swine for scientific research purposes was approved by the Kreisverwaltung Mainz-Bingen in Germany (Identification Code: DE 07 315 0006 21, approved on 13 January 2014).

7.2 Availability of supporting data

The supplementary materials consist of supplementary file 1 and supplementary file 2. Supplementary file 1 contains protein identifications of the affinity capture experiments and supplementary file 2 contains protein identifications of the CDR-treated and untreated retinal explants. MS raw data were uploaded to the ProteomeXchange Consortium via the PRIDE partner repository.

7.3 Competing interests

The authors declare no conflict of interest.

7.4 Funding

This research received no external funding.

8 References

1. Weinreb, R.N.; Aung, T.; Medeiros, F.A. The pathophysiology and treatment of glaucoma: a review. *JAMA* **2014**, *311*, 1901–1911, doi:10.1001/jama.2014.3192.
2. Grus, F.H.; Joachim, S.C.; Hoffmann, E.M.; Pfeiffer, N. Complex autoantibody repertoires in patients with glaucoma. *Mol. Vis.* **2004**, *10*, 132–137.
3. Grus, F.H.; Joachim, S.C.; Pfeiffer, N. Analysis of complex autoantibody repertoires by surface-enhanced laser desorption/ionization-time of flight mass spectrometry. *Proteomics* **2003**, *3*, 957–961, doi:10.1002/pmic.200300375.
4. Yang, J.; Tezel, G.; Patil, R.V.; Romano, C.; Wax, M.B. Serum autoantibody against glutathione S-transferase in patients with glaucoma. *Invest. Ophthalmol. Vis. Sci.* **2001**, *42*, 1273–1276.
5. Wax, M.B.; Tezel, G.; Kawase, K.; Kitazawa, Y. Serum autoantibodies to heat shock proteins in glaucoma patients from Japan and the United States. *Ophthalmology* **2001**, *108*, 296–302.
6. Zhao, W.; Yin, Z.; Li, J.; Ma, M.; Li, C. Autoantibodies associated with glaucoma. *Biomedical Research* **2017**, *28*.
7. Skonieczna, K.; Grabska-Liberek, I.; Terelak-Borys, B.; Jamrozy-Witkowska, A. Selected autoantibodies and normal-tension glaucoma. *Med. Sci. Monit.* **2014**, *20*, 1201–1209, doi:10.12659/MSM.890548.
8. Tezel, G.; Seigel, G.M.; Wax, M.B. Autoantibodies to small heat shock proteins in glaucoma. *Invest. Ophthalmol. Vis. Sci.* **1998**, *39*, 2277–2287.
9. Wax, M.B.; Tezel, G.; Saito, I.; Gupta, R.S.; Harley, J.B.; Li, Z.; Romano, C. Anti-Ro/SS-A positivity and heat shock protein antibodies in patients with normal-pressure glaucoma. *Am. J. Ophthalmol.* **1998**, *125*, 145–157.
10. Joachim, S.C.; Bruns, K.; Lackner, K.J.; Pfeiffer, N.; Grus, F.H. Antibodies to alpha B-crystallin, vimentin, and heat shock protein 70 in aqueous humor of patients with normal tension glaucoma and IgG antibody patterns against retinal antigen in aqueous humor. *Curr. Eye Res.* **2007**, *32*, 501–509, doi:10.1080/02713680701375183.
11. Tezel, G.; Edward, D.P.; Wax, M.B. Serum autoantibodies to optic nerve head glycosaminoglycans in patients with glaucoma. *Arch. Ophthalmol.* **1999**, *117*, 917–924.

12. Grus, F.H.; Joachim, S.C.; Bruns, K.; Lackner, K.J.; Pfeiffer, N.; Wax, M.B. Serum autoantibodies to alpha-fodrin are present in glaucoma patients from Germany and the United States. *Invest. Ophthalmol. Vis. Sci.* **2006**, *47*, 968–976, doi:10.1167/iovs.05-0685.
13. Joachim, S.C.; Wuenschig, D.; Pfeiffer, N.; Grus, F.H. IgG antibody patterns in aqueous humor of patients with primary open angle glaucoma and pseudoexfoliation glaucoma. *Mol. Vis.* **2007**, *13*, 1573–1579.
14. Bell, K.; Gramlich, O.W.; von Thun Und Hohenstein-Blaul, Nadine; Beck, S.; Funke, S.; Wilding, C.; Pfeiffer, N.; Grus, F.H. Does autoimmunity play a part in the pathogenesis of glaucoma? *Prog. Retin. Eye Res.* **2013**, *36*, 199–216, doi:10.1016/j.preteyeres.2013.02.003.
15. Wilding, C.; Bell, K.; Beck, S.; Funke, S.; Pfeiffer, N.; Grus, F.H. γ-Synuclein antibodies have neuroprotective potential on neuroretinal cells via proteins of the mitochondrial apoptosis pathway. *PLoS ONE* **2014**, *9*, e90737, doi:10.1371/journal.pone.0090737.
16. Wilding, C.; Bell, K.; Funke, S.; Beck, S.; Pfeiffer, N.; Grus, F.H. GFAP antibodies show protective effect on oxidatively stressed neuroretinal cells via interaction with ERP57. *J. Pharmacol. Sci.* **2015**, *127*, 298–304, doi:10.1016/j.jphs.2014.12.019.
17. Bell, K.; Wilding, C.; Funke, S.; Perumal, N.; Beck, S.; Wolters, D.; Holz-Muller, J.; Pfeiffer, N.; Grus, F.H. Neuroprotective effects of antibodies on retinal ganglion cells in an adolescent retina organ culture. *J. Neurochem.* **2016**, *139*, 256–269, doi:10.1111/jnc.13765.
18. Bell, K.; Wilding, C.; Funke, S.; Pfeiffer, N.; Grus, F.H. Protective effect of 14-3-3 antibodies on stressed neuroretinal cells via the mitochondrial apoptosis pathway. *BMC Ophthalmol.* **2015**, *15*, 64, doi:10.1186/s12886-015-0044-9.
19. Teister, J.; Anders, F.; Beck, S.; Funke, S.; Pein, H. von; Prokosch, V.; Pfeiffer, N.; Grus, F. Decelerated neurodegeneration after intravitreal injection of α-synuclein antibodies in a glaucoma animal model. *Sci. Rep.* **2017**, *7*, 6260, doi:10.1038/s41598-017-06702-1.
20. Samaranayake, H.; Wirth, T.; Schenkwein, D.; Raty, J.K.; Yla-Herttuala, S. Challenges in monoclonal antibody-based therapies. *Ann. Med.* **2009**, *41*, 322–331, doi:10.1080/07853890802698842.
21. Costa, D. de; Broodman, I.; Calame, W.; Stingl, C.; Dekker, Lennard J M; Vernhout, R.M.; de Koning, Harry J; Hoogsteden, H.C.; Sillevis Smitt, Peter A E; van Klaveren, Rob J; et al.

Peptides from the variable region of specific antibodies are shared among lung cancer patients. *PLoS ONE* **2014**, *9*, e96029, doi:10.1371/journal.pone.0096029.

22. Costa, D. de; Broodman, I.; VanDuijn, M.M.; Stingl, C.; Dekker, Lennard J M; Burgers, P.C.; Hoogsteden, H.C.; Sillevis Smitt, Peter A E; van Klaveren, Rob J; Luider, T.M. Sequencing and quantifying IgG fragments and antigen-binding regions by mass spectrometry. *J. Proteome Res.* **2010**, *9*, 2937–2945, doi:10.1021/pr901114w.
23. Singh, V.; Stoop, M.P.; Stingl, C.; Luitwieler, R.L.; Dekker, L.J.; van Duijn, M.M.; Kreft, K.L.; Luider, T.M.; Hintzen, R.Q. Cerebrospinal-fluid-derived immunoglobulin G of different multiple sclerosis patients shares mutated sequences in complementarity determining regions. *Mol. Cell. Proteomics* **2013**, *12*, 3924–3934, doi:10.1074/mcp.M113.030346.
24. Broodman, I.; Costa, D. de; Stingl, C.; Dekker, Lennard J M; VanDuijn, M.M.; Lindemans, J.; van Klaveren, Rob J; Luider, T.M. Mass spectrometry analyses of κ and λ fractions result in increased number of complementarity-determining region identifications. *Proteomics* **2012**, *12*, 183–191, doi:10.1002/pmic.201100244.
25. Schmelter, C.; Perumal, N.; Funke, S.; Bell, K.; Pfeiffer, N.; Grus, F.H. Peptides of the variable IgG domain as potential biomarker candidates in primary open-angle glaucoma (POAG). *Hum. Mol. Genet.* **2017**, *26*, 4451–4464, doi:10.1093/hmg/ddx332.
26. Sela-Culang, I.; Kunik, V.; Ofran, Y. The Structural Basis of Antibody-Antigen Recognition. *Front. Immunol.* **2013**, *4, doi:*10.3389/fimmu.2013.00302.
27. Gabrielli, E.; Pericolini, E.; Cenci, E.; Ortelli, F.; Magliani, W.; Ciociola, T.; Bistoni, F.; Conti, S.; Vecchiarelli, A.; Polonelli, L. Antibody complementarity-determining regions (CDRs): A bridge between adaptive and innate immunity. *PLoS ONE* **2009**, *4*, e8187, doi:10.1371/journal.pone.0008187.
28. Gabrielli, E.; Pericolini, E.; Cenci, E.; Monari, C.; Magliani, W.; Ciociola, T.; Conti, S.; Gatti, R.; Bistoni, F.; Polonelli, L.; et al. Antibody Constant Region Peptides Can Display Immunomodulatory Activity through Activation of the Dectin-1 Signalling Pathway. *PLoS ONE* **2012**, *7*, e43972, doi:10.1371/journal.pone.0043972.
29. Polonelli, L.; Ponton, J.; Elguezabal, N.; Moragues, M.D.; Casoli, C.; Pilotti, E.; Ronzi, P.; Dobroff, A.S.; Rodrigues, E.G.; Juliano, M.A.; et al. Antibody complementarity-determining regions (CDRs) can display differential antimicrobial, antiviral and antitumor activities. *PLoS ONE* **2008**, *3*, e2371, doi:10.1371/journal.pone.0002371.

30. Figueiredo, C.R.; Matsuo, A.L.; Massaoka, M.H.; Polonelli, L.; Travassos, L.R. Anti-tumor activities of peptides corresponding to conserved complementary determining regions from different immunoglobulins. *Peptides* **2014**, *59*, 14–19, doi:10.1016/j.peptides.2014.06.007.
31. Dobroff, A.S.; Rodrigues, E.G.; Juliano, M.A.; Friaca, D.M.; Nakayasu, E.S.; Almeida, I.C.; Mortara, R.A.; Jacysyn, J.F.; Amarante-Mendes, G.P.; Magliani, W.; et al. Differential Antitumor Effects of IgG and IgM Monoclonal Antibodies and Their Synthetic Complementarity-Determining Regions Directed to New Targets of B16F10-Nex2 Melanoma Cells. *Transl. Oncol.* **2010**, *3*, 204–217.
32. Rabaça, A.N.; Arruda, D.C.; Figueiredo, C.R.; Massaoka, M.H.; Farias, C.F.; Tada, D.B.; Maia, V.C.; Silva Junior, P.I.; Girola, N.; Real, F.; et al. AC-1001 H3 CDR peptide induces apoptosis and signs of autophagy in vitro and exhibits antimetastatic activity in a syngeneic melanoma model. *FEBS Open Bio* **2016**, *6*, 885–901, doi:10.1002/2211-5463.12080.
33. Brosh, N.; Zinger, H.; Mozes, E. Treatment of induced murine SLE with a peptide based on the CDR3 of an anti-DNA antibody reverses the pattern of pathogenic cytokines. *Autoimmunity* **2002**, *35*, 211–219.
34. Sharabi, A.; Dayan, M.; Zinger, H.; Mozes, E. A new model of induced experimental systemic lupus erythematosus (SLE) in pigs and its amelioration by treatment with a tolerogenic peptide. *J. Clin. Immunol.* **2010**, *30*, 34–44, doi:10.1007/s10875-009-9326-4.
35. Sharabi, A.; Sthoeger, Z.M.; Mahlab, K.; Lapter, S.; Zinger, H.; Mozes, E. A tolerogenic peptide that induces suppressor of cytokine signaling (SOCS)-1 restores the aberrant control of IFN-gamma signaling in lupus-affected (NZB x NZW)F1 mice. *Clin. Immunol.* **2009**, *133*, 61–68, doi:10.1016/j.clim.2009.06.010.
36. Perumal, N.; Funke, S.; Wolters, D.; Pfeiffer, N.; Grus, F.H. Characterization of human reflex tear proteome reveals high expression of lacrimal proline-rich protein 4 (PRR4). *Proteomics* **2015**, *15*, 3370–3381, doi:10.1002/pmic.201400239.
37. Manicam, C.; Perumal, N.; Wasielica-Poslednik, J.; Ngongkole, Y.C.; Tschabunin, A.; Sievers, M.; Lisch, W.; Pfeiffer, N.; Grus, F.H.; Gericke, A. Proteomics Unravels the Regulatory Mechanisms in Human Tears Following Acute Renouncement of Contact Lens Use: A Comparison between Hard and Soft Lenses. *Sci. Rep.* **2018**, *8*, 11526, doi:10.1038/s41598-018-30032-5.

38. Funke, S.; Perumal, N.; Beck, S.; Gabel-Scheurich, S.; Schmelter, C.; Teister, J.; Gerbig, C.; Gramlich, O.W.; Pfeiffer, N.; Grus, F.H. Glaucoma related Proteomic Alterations in Human Retina Samples. *Sci. Rep.* **2016**, *6*, 29759, doi:10.1038/srep29759.
39. Funke, S.; Markowitsch, S.; Schmelter, C.; Perumal, N.; Mwiiri, F.K.; Gabel-Scheurich, S.; Pfeiffer, N.; Grus, F.H. In-Depth Proteomic Analysis of the Porcine Retina by Use of a four Step Differential Extraction Bottom up LC MS Platform. *Mol. Neurobiol.* **2016, doi:**10.1007/s12035-016-0172-0.
40. Perumal, N.; Funke, S.; Pfeiffer, N.; Grus, F.H. Proteomics analysis of human tears from aqueous-deficient and evaporative dry eye patients. *Sci. Rep.* **2016**, *6*, 29629, doi:10.1038/srep29629.
41. Schmelter, C.; Funke, S.; Treml, J.; Beschnitt, A.; Perumal, N.; Manicam, C.; Pfeiffer, N.; Grus, F.H.; Grus, F. Comparison of Two Solid-Phase Extraction (SPE) Methods for the Identification and Quantification of Porcine Retinal Protein Markers by LC-MS/MS. *Int. J. Mol. Sci.* **2018**, *19*, 3847, doi:10.3390/ijms19123847.
42. Schmelter, C.; Perumal, N.; Funke, S.; Bell, K.; Pfeiffer, N.; Grus, F.H. Peptides of the variable IgG domain as potential biomarker candidates in primary open-angle glaucoma (POAG). *Hum. Mol. Genet.* **2017**, *26*, 4451–4464, doi:10.1093/hmg/ddx332.
43. Bach, M.; Lehmann, A.; Brunnert, D.; Vanselow, J.T.; Hartung, A.; Bargou, R.C.; Holzgrabe, U.; Schlosser, A.; Chatterjee, M. Ugi Reaction-Derived alpha-Acyl Aminocarboxamides Bind to Phosphatidylinositol 3-Kinase-Related Kinases, Inhibit HSF1-Dependent Heat Shock Response, and Induce Apoptosis in Multiple Myeloma Cells. *J. Med. Chem.* **2017**, *60*, 4147–4160, doi:10.1021/acs.jmedchem.6b01613.
44. Manicam, C.; Perumal, N.; Pfeiffer, N.; Grus, F.H.; Gericke, A. First insight into the proteome landscape of the porcine short posterior ciliary arteries: Key signalling pathways maintaining physiologic functions. *Sci. Rep.* **2016**, *6*, 38298, doi:10.1038/srep38298.
45. Bassani-Sternberg, M. Mass Spectrometry Based Immunopeptidomics for the Discovery of Cancer Neoantigens. *Methods Mol. Biol.* **2018**, *1719*, 209–221, doi:10.1007/978-1-4939-7537-2_14.
46. Murali, R.; Greene, M.I. Structure based antibody-like peptidomimetics. *Pharmaceuticals (Basel)* **2012**, *5*, 209–235, doi:10.3390/ph5020209.

47. Vande Walle, L.; Lamkanfi, M.; Vandenabeele, P. The mitochondrial serine protease HtrA2/Omi: an overview. *Cell Death Differ.* **2008**, *15*, 453–460, doi:10.1038/sj.cdd.4402291.
48. Goo, H.-G.; Rhim, H.; Kang, S. Pathogenic Role of Serine Protease HtrA2/Omi in Neurodegenerative Diseases. *Curr. Protein Pept. Sci.* **2017**, *18*, 746–757, doi:10.2174/1389203717666160311115750.
49. Hegde, R.; Srinivasula, S.M.; Zhang, Z.; Wassell, R.; Mukattash, R.; Cilenti, L.; DuBois, G.; Lazebnik, Y.; Zervos, A.S.; Fernandes-Alnemri, T.; et al. Identification of Omi/HtrA2 as a mitochondrial apoptotic serine protease that disrupts inhibitor of apoptosis protein-caspase interaction. *J. Biol. Chem.* **2002**, *277*, 432–438, doi:10.1074/jbc.M109721200.
50. Cui, L.; He, W.-J.; Xu, F.; Jiang, L.; Lv, M.-L.; Huang, H.; Xu, J.-P.; Wu, Y.; Zhong, H.-B.; Zhang, S.-Y.; et al. Alterations in the expression of Hs1-associated protein X-1 in the rat retina after optic nerve crush. *Mol. Med. Rep.* **2016**, *14*, 4761–4766, doi:10.3892/mmr.2016.5824.
51. Kang, S.; Fernandes-Alnemri, T.; Alnemri, E.S. A novel role for the mitochondrial HTRA2/OMI protease in aging. *Autophagy* **2013**, *9*, 420–421, doi:10.4161/auto.22920.
52. Goo, H.-G.; Jung, M.K.; Han, S.S.; Rhim, H.; Kang, S. HtrA2/Omi deficiency causes damage and mutation of mitochondrial DNA. *Biochim. Biophys. Acta* **2013**, *1833*, 1866–1875, doi:10.1016/j.bbamcr.2013.03.016.
53. Jones, J.M.; Datta, P.; Srinivasula, S.M.; Ji, W.; Gupta, S.; Zhang, Z.; Davies, E.; Hajnoczky, G.; Saunders, T.L.; van Keuren, M.L.; et al. Loss of Omi mitochondrial protease activity causes the neuromuscular disorder of mnd2 mutant mice. *Nature* **2003**, *425*, 721–727, doi:10.1038/nature02052.
54. Martins, L.M.; Morrison, A.; Klupsch, K.; Fedele, V.; Moisoi, N.; Teismann, P.; Abuin, A.; Grau, E.; Geppert, M.; Livi, G.P.; et al. Neuroprotective role of the Reaper-related serine protease HtrA2/Omi revealed by targeted deletion in mice. *Mol. Cell. Biol.* **2004**, *24*, 9848–9862, doi:10.1128/MCB.24.22.9848-9862.2004.
55. Skorko-Glonek, J.; Zurawa-Janicka, D.; Koper, T.; Jarzab, M.; Figaj, D.; Glaza, P.; Lipinska, B. HtrA protease family as therapeutic targets. *Curr. Pharm. Des.* **2013**, *19*, 977–1009.
56. Bhuiyan, M.S.; Fukunaga, K. Inhibition of HtrA2/Omi ameliorates heart dysfunction following ischemia/reperfusion injury in rat heart in vivo. *Eur. J. Pharmacol.* **2007**, *557*, 168–177, doi:10.1016/j.ejphar.2006.10.067.

57. Ding, X.; Patel, M.; Shen, D.; Herzlich, A.A.; Cao, X.; Villasmil, R.; Klupsch, K.; Tuo, J.; Downward, J.; Chan, C.-C. Enhanced HtrA2/Omi expression in oxidative injury to retinal pigment epithelial cells and murine models of neurodegeneration. *Invest. Ophthalmol. Vis. Sci.* **2009**, *50*, 4957–4966, doi:10.1167/iovs.09-3381.
58. Ruiz-Ederra, J.; García, M.; Hernández, M.; Urcola, H.; Hernández-Barbáchano, E.; Araiz, J.; Vecino, E. The pig eye as a novel model of glaucoma. *Exp. Eye Res.* **2005**, *81*, 561–569, doi:10.1016/j.exer.2005.03.014.
59. Garcá, M.; Ruiz-Ederra, J.; Hernández-Barbáchano, H.; Vecino, E. Topography of pig retinal ganglion cells. *J. Comp. Neurol.* **2005**, *486*, 361–372, doi:10.1002/cne.20516.
60. Wolbers, F.; Buijtenhuijs, P.; Haanen, C.; Vermes, I. Apoptotic cell death kinetics in vitro depend on the cell types and the inducers used. *Apoptosis* **2004**, *9*, 385–392.
61. Saraste, A. Morphologic criteria and detection of apoptosis. *Herz* **1999**, *24*, 189–195.
62. Negoescu, A.; Guillermet, C.; Lorimier, P.; Brambilla, E.; Labat-Moleur, F. Importance of DNA fragmentation in apoptosis with regard to TUNEL specificity. *Biomed. Pharmacother.* **1998**, *52*, 252–258, doi:10.1016/S0753-3322(98)80010-3.
63. Negoescu, A.; Lorimier, P.; Labat-Moleur, F.; Drouet, C.; Robert, C.; Guillermet, C.; Brambilla, C.; Brambilla, E. In situ apoptotic cell labeling by the TUNEL method: Improvement and evaluation on cell preparations. *J. Histochem. Cytochem.* **1996**, *44*, 959–968.
64. Maurya, S.R.; Mahalakshmi, R. Mitochondrial VDAC2 and cell homeostasis: Highlighting hidden structural features and unique functionalities. *Biol. Rev. Camb. Philos. Soc.* **2017**, *92*, 1843–1858, doi:10.1111/brv.12311.
65. Cheng, E.H.Y.; Sheiko, T.V.; Fisher, J.K.; Craigen, W.J.; Korsmeyer, S.J. VDAC2 inhibits BAK activation and mitochondrial apoptosis. *Science* **2003**, *301*, 513–517, doi:10.1126/science.1083995.
66. Holzerova, E.; Danhauser, K.; Haack, T.B.; Kremer, L.S.; Melcher, M.; Ingold, I.; Kobayashi, S.; Terrile, C.; Wolf, P.; Schaper, J.; et al. Human thioredoxin 2 deficiency impairs mitochondrial redox homeostasis and causes early-onset neurodegeneration. *Brain* **2016**, *139*, 346–354, doi:10.1093/brain/awv350.
67. McLaughlin, T.; Falkowski, M.; Wang, J.J.; Zhang, S.X. Molecular Chaperone ERp29: A Potential Target for Cellular Protection in Retinal and Neurodegenerative Diseases. *Adv. Exp. Med. Biol.* **2018**, *1074*, 421–427, doi:10.1007/978-3-319-75402-4_52.

68. Zuehlke, A.D.; Beebe, K.; Neckers, L.; Prince, T. Regulation and function of the human HSP90AA1 gene. *Gene* **2015**, *570*, 8–16, doi:10.1016/j.gene.2015.06.018.
69. Meng, Q.; Li, B.X.; Xiao, X. Toward Developing Chemical Modulators of Hsp60 as Potential Therapeutics. *Front. Mol. Biosci.* **2018**, *5*, 35, doi:10.3389/fmolb.2018.00035.
70. Kong, G.Y.X.; van Bergen, N.J.; Trounce, I.A.; Crowston, J.G. Mitochondrial dysfunction and glaucoma. *J. Glaucoma* **2009**, *18*, 93–100, doi:10.1097/IJG.0b013e318181284f.
71. Lee, S.; van Bergen, N.J.; Kong, G.Y.; Chrysostomou, V.; Waugh, H.S.; O'Neill, E.C.; Crowston, J.G.; Trounce, I.A. Mitochondrial dysfunction in glaucoma and emerging bioenergetic therapies. *Exp. Eye Res.* **2011**, *93*, 204–212, doi:10.1016/j.exer.2010.07.015.
72. Campello, L.; Esteve-Rudd, J.; Cuenca, N.; Martin-Nieto, J. The ubiquitin-proteasome system in retinal health and disease. *Mol. Neurobiol.* **2013**, *47*, 790–810, doi:10.1007/s12035-012-8391-5.
73. Dibas, A.; Yorio, T. Abnormalities in Ubiquitin Proteasomal System: Role in Optic NerveE Damage in Glaucoma? *Invest. Ophthalmol. Vis. Sci.* **2007**, *48*, 4176.
74. Park, H.-M.; Kim, G.-Y.; Nam, M.-K.; Seong, G.-H.; Han, C.; Chung, K.C.; Kang, S.; Rhim, H. The serine protease HtrA2/Omi cleaves Parkin and irreversibly inactivates its E3 ubiquitin ligase activity. *Biochem. Biophys. Res. Commun.* **2009**, *387*, 537–542, doi:10.1016/j.bbrc.2009.07.079.
75. Cilenti, L.; Ambivero, C.T.; Ward, N.; Alnemri, E.S.; Germain, D.; Zervos, A.S. Inactivation of Omi/HtrA2 protease leads to the deregulation of mitochondrial Mulan E3 ubiquitin ligase and increased mitophagy. *Biochim. Biophys. Acta* **2014**, *1843*, 1295–1307, doi:10.1016/j.bbamcr.2014.03.027.
76. Zhao, J.; Zhong, C.-J. A review on research progress of transketolase. *Neurosci. Bull.* **2009**, *25*, 94–99, doi:10.1007/s12264-009-1113-y.
77. Kuehne, A.; Emmert, H.; Soehle, J.; Winnefeld, M.; Fischer, F.; Wenck, H.; Gallinat, S.; Terstegen, L.; Lucius, R.; Hildebrand, J.; et al. Acute Activation of Oxidative Pentose Phosphate Pathway as First-Line Response to Oxidative Stress in Human Skin Cells. *Mol. Cell* **2015**, *59*, 359–371, doi:10.1016/j.molcel.2015.06.017.
78. Casson, R.; Chidlow, G.; Ebneter, A.; Han, G.; Gilhotra, J.; Wood, J. Glucose-induced Temporary Visual Recovery in Human Glaucoma: A Prospective, Double-blind, Randomised Study. *Invest. Ophthalmol. Vis. Sci.* **2013**, *54*, 4009.

79. Guymer, C.; Wood, J.P.M.; Chidlow, G.; Casson, R.J. Neuroprotection in glaucoma: recent advances and clinical translation. *Clinical & Experimental Ophthalmology* **2019**, *47*, 88–105, doi:10.1111/ceo.13336.

9 Supplementary Figures & Tables

A)

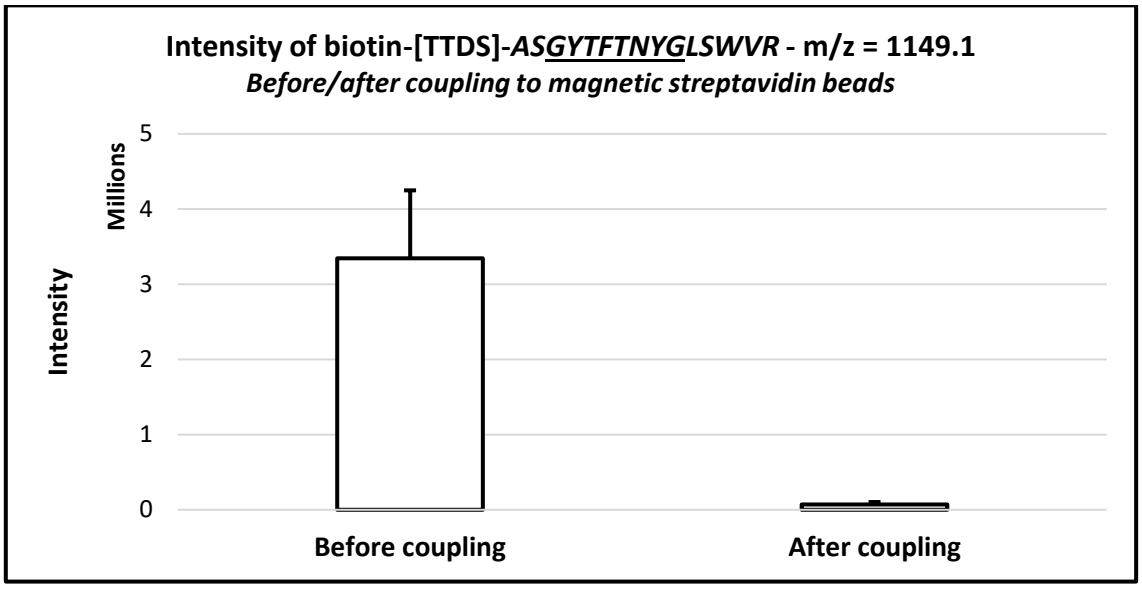

B)

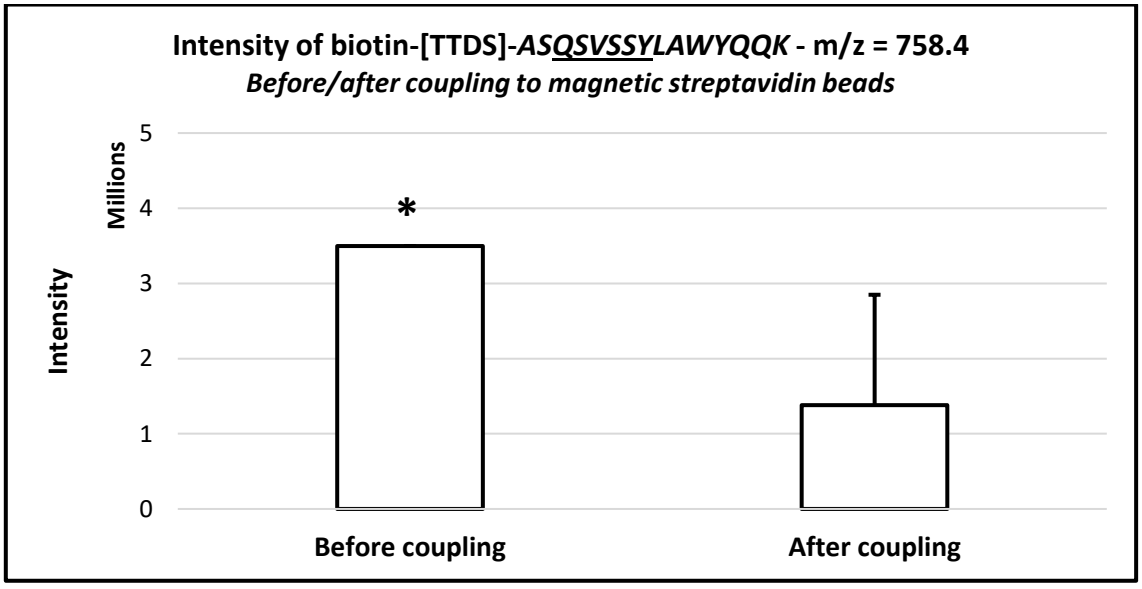

Supplementary Fig. 1: Bar plot showing the intensity of synthetic biotin-[TTDS]-*ASGYTFTNYGLSWVR* **(A)** and synthetic biotin-[TTDS]-*ASQSVSSYLAWYQQK* **(B)** before and after coupling to commercial available magnetic streptavidin beads (N=3 per group). *: Groups marked with an asterisk are presented only by one replicate.

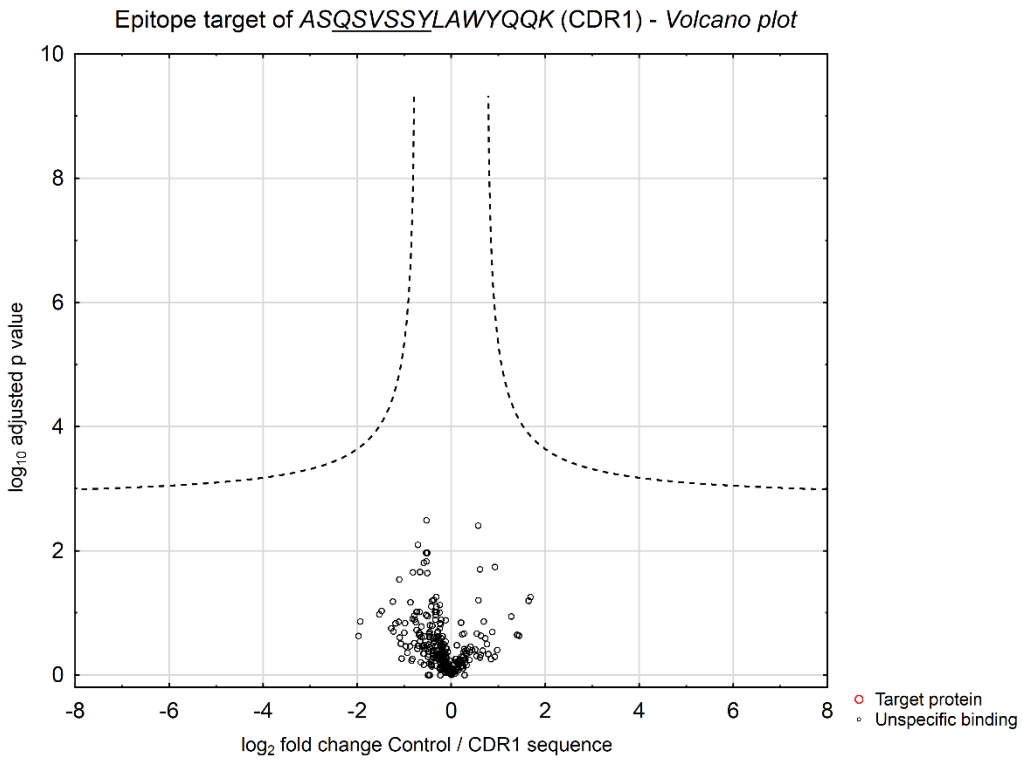

Supplementary Fig. 2: Identification of potential epitope targets of the CDR peptides by affinity based proteomic strategy with 5 mg homogenized pig retina. Volcano plot showing log2 fold change plotted against -log10 adjusted P value for samples from CDR-labeled bead group (N=3) versus samples from control bead group (N=3) ($P<0.001$; log2 fold change > 3). No significant interaction partner was identified for synthetic CDR1 peptide *ASQSVSSYLAWYQQK.*

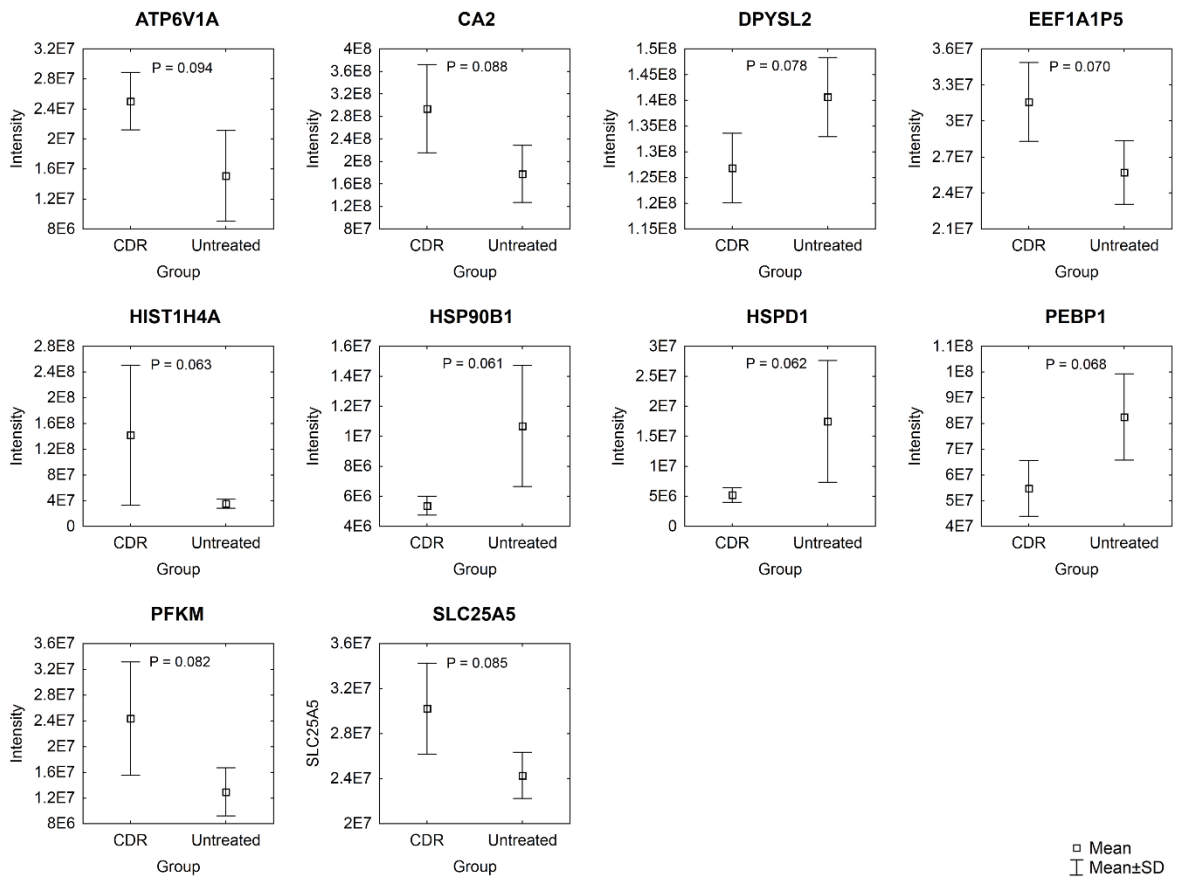

Supplementary Fig. 3: Bar plots showing proteins with at least a tendency (P < 0.1) to be differentially expressed between CDR-treated retinal explants and untreated controls (N=3 per group). Retinal explants were cultivated either with medium without any peptide (untreated control) or with medium with 25 µg/ml CDR peptide for 24 h after optic nerve cut (ONC).

2.3 Publication III

Comparison of Two Solid-Phase Extraction (SPE) Methods for the Identification and Quantification of Porcine Retinal Protein Markers by LC-MS/MS.

Schmelter C*, Funke S*, Treml J, Beschnitt A, Perumal N, Manicam C, Bell K, Pfeiffer N, Grus FH

International Journal of Molecular Sciences, 2018

PMID: 30513899, DOI: 10.3390/ijms19123847

* = authors contributed equally

International Journal of
Molecular Sciences

MDPI

Article

Comparison of Two Solid-Phase Extraction (SPE) Methods for the Identification and Quantification of Porcine Retinal Protein Markers by LC-MS/MS

Carsten Schmelter †, Sebastian Funke †, Jana Treml, Anja Beschnitt, Natarajan Perumal, Caroline Manicam, Norbert Pfeiffer and Franz H. Grus *

Department of Experimental and Translational Ophthalmology, University Medical Center, Johannes Gutenberg University, 55131 Mainz, Germany; cschmelter@eye-research.org (C.S.); sfunke@eye-research.org (S.F.); jana-treml@gmx.de (J.T.); a.beschnitt@gmx.net (A.B.); nperumal@eye-research.org (N.P.); caroline.manicam@unimedizin-mainz.de (C.M.); norbert.pfeiffer@unimedizin-mainz.de (N.P.)

* Correspondence: grus@eye-research.org; Tel.: +49-6131-173328; Fax: +49-6131-175509

† These authors contributed equally to this work.

Received: 19 September 2018; Accepted: 27 November 2018; Published: 3 December 2018

Abstract: Proper sample preparation protocols represent a critical step for liquid chromatography-mass spectrometry (LC-MS)-based proteomic study designs and influence the speed, performance and automation of high-throughput data acquisition. The main objective of this study was to compare two commercial solid-phase extraction (SPE)-based sample preparation protocols (comprising SOLAμ^{TM} HRP SPE spin plates from Thermo Fisher Scientific and ZIPTIP® C18 pipette tips from Merck Millipore) for analytical performance, reproducibility, and analysis speed. The house swine represents a promising animal model for studying human eye diseases including glaucoma and provides excellent requirements for the qualitative and quantitative MS-based comparison in terms of ocular proteomics. In total six technical replicates of two protein fractions [extracted with 0.1% dodecyl-ß-maltoside (DDM) or 1% trifluoroacetic acid (TFA)] of porcine retinal tissues were subjected to in-gel trypsin digestion and purified with both SPE-based workflows (N = 3) prior to LC-MS analysis. On average, 550 ± 70 proteins (1512 ± 199 peptides) and 305 ± 48 proteins (806 ± 144 peptides) were identified from DDM and TFA protein fractions, respectively, after ZIPTIP® C18 purification, and SOLAμ^{TM} workflow resulted in the detection of 513 ± 55 proteins (1347 ± 180 peptides) and 300 ± 33 proteins (722 ± 87 peptides), respectively (FDR < 1%). Venn diagram analysis revealed an average overlap of 65 ± 2% (DDM fraction) and 69 ± 4% (TFA fraction) in protein identifications between both SPE-based methods. Quantitative analysis of 25 glaucoma-related protein markers also showed no significant differences (P > 0.05) regarding protein recovery between both SPE methods. However, only glaucoma-associated marker *MECP2* showed a significant (P = 0.02) higher abundance in ZIPTIP®-purified replicates in comparison to SOLAμ^{TM}-treated study samples. Nevertheless, this result was not confirmed in the verification experiment using in-gel trypsin digestion of recombinant *MECP2* (P = 0.24). In conclusion, both SPE-based purification methods worked equally well in terms of analytical performance and reproducibility, whereas the analysis speed and the semi-automation of the SOLAμ^{TM} spin plates workflow is much more convenient in comparison to the ZIPTIP® C18 method.

Keywords: mass spectrometry; glaucoma animal model; biomarkers; sample clean-up; ZIPTIP® C18 pipette tips; SOLAμTM HRP SPE spin plates

1. Introduction

Solid phase extraction (SPE) is a crucial technique in liquid chromatography-mass spectrometry (LC-MS)-based protein biomarker recovery, and therefore, the choice of appropriate SPE techniques must be planned carefully. Robustness, reproducibility, sensitivity, and economic parameters encompassing time and costs have to be addressed along with the selection of proper SPE protocols. There is an increasing number of SPE sorbent materials feasible for LC-MS-based proteomics in the current market, which compromises various formats; e.g., pipette tips, cartridges, discs, multi-well-plates, magnetic beads and sorbent materials, as reviewed elsewhere [1–7]. Since the implementation of SPE in LC-MS workflows should be cost- and time-effective while enhancing analysis speed, reproducibility, and minimizing processing errors, an important feature of a SPE technique is its ability for automation in compliance with a high-throughput proteomics methodology. Moreover, the SPE technique should be also compatible with the biological material of interest; for example, the retinal tissues in the present study. There is a growing demand to study the retina in the field of glaucoma proteomics, because it represents the primary ocular site that is affected in this neurodegenerative disorder, which is indicated by aberrant proteomic alterations [8]. To study these proteomic alterations LC-MS-based proteomic workflows represent the state-of-the-art strategy that provide sensitive and semi-quantitative information of the identified protein species [9–11]. This is particularly important for electrospray ionization (ESI) LC-MS-based proteomic workflows, in which the SPE platform is recommended for desalting, ionic detergent-removal (e.g., SDS) and peptide enrichment prior to LC-MS analysis and is mandatory for proper peptide ionization. Thus far, several different types of devices and sorbents have been developed and commercialized for proper sample clean-up procedures [12]. Our current LC-MS-based workflow for discovery proteomic approaches was successfully used for in-depth proteome characterization of retina samples from various species such as rat [13,14], pig [15] and human [16]. Recently, the LC-MS-based proteomic platform was also used for the quantitative proteomic analysis of a new established porcine retinal organ culture [17], which allows to monitor the expression levels of retinal proteins during experimental glaucomatous conditions. In the former retina proteomic studies, the ZIPTIP® C18 pipette tip SPE was used as a standard operation protocol (SOP) for sample clean-up prior to LC-MS analysis. The purpose of the present work was to evaluate the suitability of a less laborious SPE method that can be implemented in the established LC-MS-based proteomic workflow and therefore, to compare the performance of SOLAμ™ HRP SPE spin plates with the former ZIPTIP® C18 pipette tips for the analysis of the porcine retinal proteome. Moreover, the main focus of the present study was on specific selected retinal protein markers, which were recently found to be associated with the pathophysiology of glaucoma [16] and represent interesting marker candidates for quantitative protein recovery. Both SPE techniques will be evaluated for specific protein/peptide recovery performance as well as for analysis speed of the porcine retinal proteome characterization and possibly considering an (semi-)automated integration of both SPE-based methods.

2. Results

2.1. 1-D SDS Page of Porcine Retinal Proteins

Both protein fractions (extracted with 0.1% DDM or 1% TFA) showed a high degree of congruency in the mass migration pattern with respect to the 1D SDS-PAGE (see Figure 1A,B). Each lane was subdivided into 17 slices labeled with the most abundant proteins per spot. Both protein fractions showed specific and reproducible protein pattern and particularly the DDM fraction contained predominantly cytoplasm-derived and membrane-associated proteins such as clathrin heavy chain 1 (≈150 kDa, highest protein score: 547, *CLTC*), retinol-binding protein 3 (≈98 kDa, highest protein score: 325, *RBP3*), glutathione S-transferase P (≈30–20 kDa, highest protein score: 1948, *GSTP1*) or reticulon-4 (≈17 kDa, highest protein score: 558, *RTN4*). In contrast, the TFA fraction exhibited mostly nucleus-derived proteins such as high mobility group protein B1 (≈28 kDa highest protein score: 818,

HMGB1), different kinds of histones (e.g., Histone H1.4 ≈ 28–17 kDa, highest protein score: 3421, *HIST1H1E*), but also many mitochondrial (e.g., ATP synthase subunit beta, mitochondrial, ≈12 kDa, highest protein score: 1352, *ATP5B*) as well as ribosomal proteins (e.g., 60S ribosomal protein L12; ≈12 kDa, highest protein score: 589, *RPL12*).

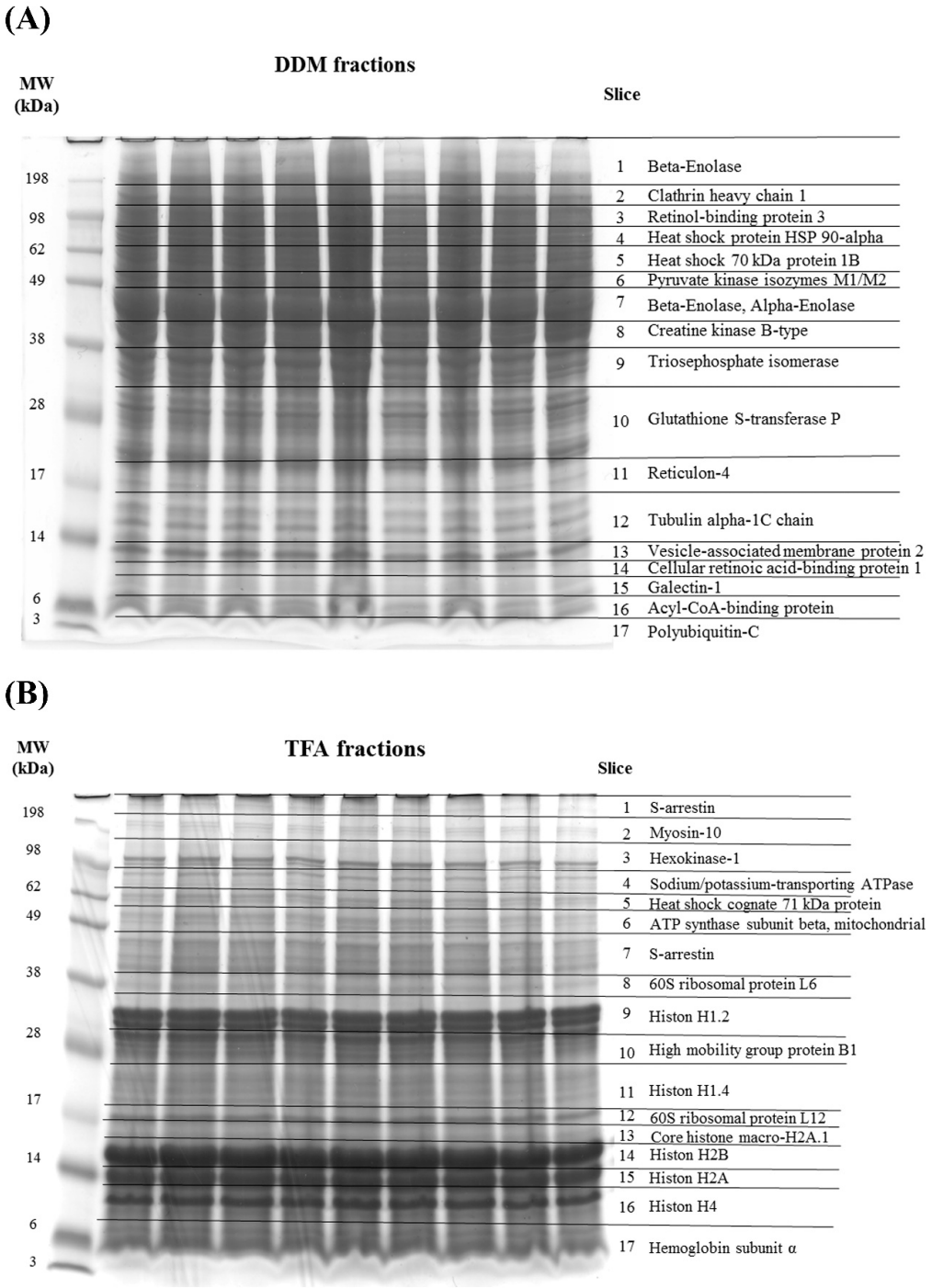

Figure 1. 1-D SDS PAGE of porcine retinal proteins after extraction with 0.1% dodecyl-ß-maltoside (DDM) or 1% trifluoroacetic acid (TFA) buffer labeled with the most abundant proteins per spot. Each sample lane contains a total protein amount of 50 µg. (**A**) Protein migration pattern of the 0.1% DDM extract mostly containing cytoplasm-derived or membrane-associated proteins. (**B**) Protein migration pattern of the 1% TFA extract predominantly consists out of nucleus-derived proteins.

2.2. Qualitative Comparison between Both SPE-Based Peptide Purification Methods

In order to evaluate qualitative differences regarding protein identifications, in total six technical replicates of two protein fractions (DDM and TFA) were purified with two different SPE-protocols (ZIPTIP® and SOLAμ™) prior to LC-MS/MS analysis (as described in detail in 2.4). On average the DDM fractions provided the identification of 550 ± 70 proteins (1512 ± 199 peptides) after ZIPTIP® C18 purification protocol, whereas SOLAμ™ purification workflow resulted in the identification of 513 ± 55 proteins (1347 ± 180 peptides) using high-confident filtering criteria (FDR < 1%). In contrast, the ZIPTIP® C18 purification technique leads to the detection of 305 ± 48 proteins (806 ± 144 peptides) in the TFA fraction, whereas SOLAμ™ purification protocol identified 300 ± 33 proteins (722 ± 87 peptides, see Supplementary Files S1 and S2). No significant differences ($P > 0.05$) regarding protein and peptide identifications were observed between both SPE-based purification methods using Student's *t*-test.

In the next step of the analysis, the identified proteins were classified according to their specific protein ion scores in order to evaluate if there are significant differences in the identification of group–specific proteins species (see Figure 2). On average, 7 ± 3 proteins of the SOLAμ™-purified DDM fraction showed a protein score of >3000. Up to 318 ± 70 proteins indicated a protein score of <3000 >70 and 186 ± 25 proteins were detected with a protein score of <70. On the other hand, the ZIPTIP® C18 procedure resulted in the detection 9 ± 3 proteins with a protein score of >3000 in the DDM fraction. On average 359 ± 78 proteins showed a protein score of <3000 >70 and up to 183 ± 48 proteins were identified with a protein score of <70. Nevertheless, no significant group-specific differences (Mann-Whitney U-test, $P > 0.05$) in terms of the protein ion score were observed between both SPE methods. The proteins of the TFA fraction showed a similar distribution pattern with respect to the protein ion score, but also no significant changes (Mann–Whitney U-test, $P > 0.05$) were observed between both methods. Furthermore, we also clustered the identified peptides according to their characteristic molecular weights (MW), in order to analyze if there are any significant differences in the detection of group-specific peptide sequences between both purification protocols (see Figure 3). On average both SPE workflows resulted in comparable peptide identification rates (SOLAμ™: 1115 ± 149 peptides; ZIPTIP®: 1254 ± 156 peptides) within the mass range of 900 to 1800 Da in the DDM fraction. With both SPE methods the number of identified peptides (SOLAμ™: 232 ± 31 peptides; ZIPTIP®: 258 ± 45 peptides) decreased at the edges of the mass range between 600-900 Da and >1800 Da. Nevertheless, none of the groups showed significant differences (Student's *t*-test, $P > 0.05$) between both purification methods in the DDM fraction. In addition, the MW-classified peptides of the TFA fraction showed a similar distribution pattern, but also no significant differences (Student's *t*-test, $P > 0.05$) were found between SOLAμ™ - and ZIPTIP®-purified study samples.

Venn diagram analysis revealed that on average 65 ± 2% of all identified proteins were detected with both SPE-based purification methods (SOLAμ™ and ZIPTIP®) in the DDM fraction (Figure 4). Also, the TFA fraction provided an average overlap of 69 ± 4% of all identified proteins between both purification methods (Figure 5). Even on the peptide level both methods resulted in an overlap of 60 ± 1% in the DDM fraction and an overlap of 62 ± 5% in the TFA fraction (Supplementary Figures S1 and S2). Furthermore, around 98% of all identified proteins in both protein fractions (DDM and TFA) could be annotated to cellular compartments according to the gene ontology (GO) analysis. Additionally, the identified proteins from the DDM and TFA fractions did not show any conspicuous differences regarding the cellular localization between both SPE-based purification methods (Figure 6).

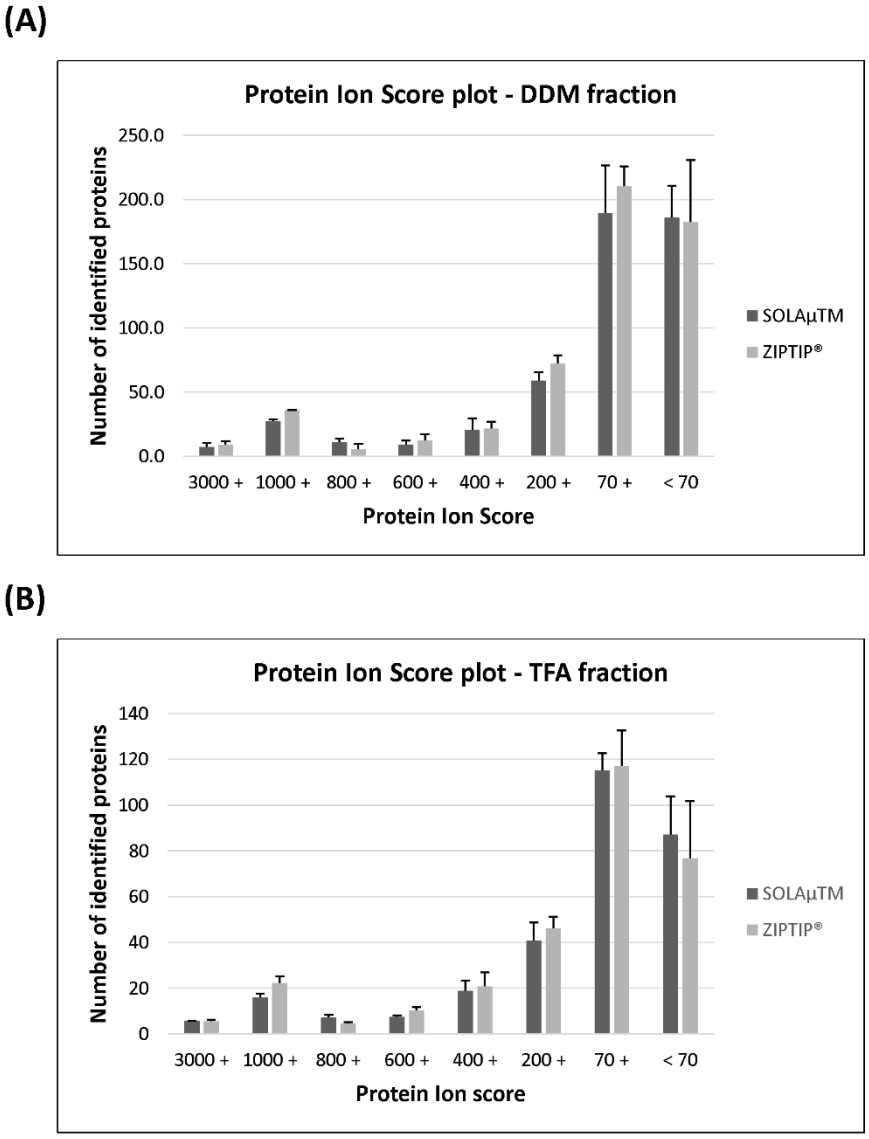

Figure 2. Distribution plot shows the classification of the identified proteins according to their specific protein ion scores. Proteins were clustered to the protein ion scores in the range of ≥3000, <3000 to ≥1000, <1000 to ≥800, <800 to ≥600, <400 to ≥200, <200 to ≥70 and <70. (**A**) Ion score distribution plot of the identified proteins in the DDM fraction after enrichment with to different solid phase extraction (SPE)-based purification methods (SOLAμ^{TM} and ZIPTIP$^{®}$). (**B**) Distribution profile of the identified proteins in the TFA fraction according to their specific ion scores after enrichment with two different SPE methods.

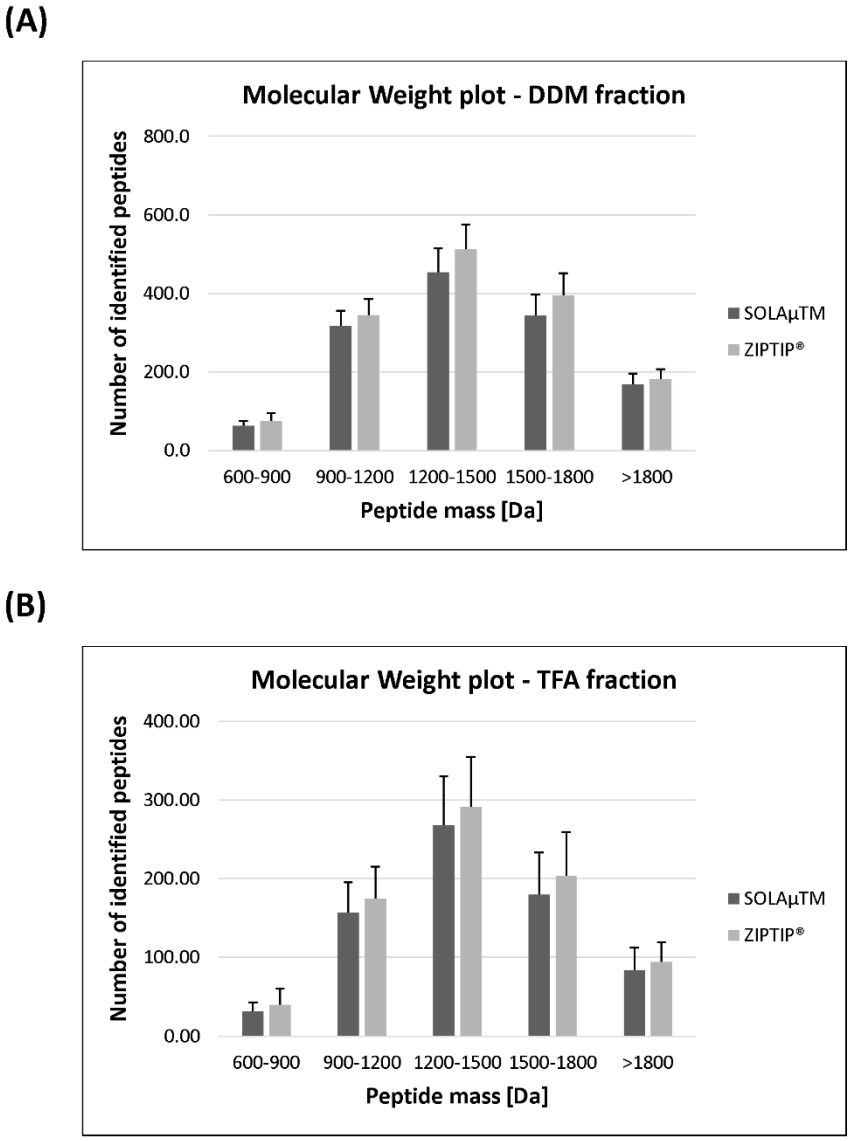

Figure 3. Distribution plot shows the classification of the identified peptides according to their characteristic molecular weight (MW). Peptides were clustered in the molecular mass range of ≥1800 Da, <1800 to ≥1500 Da, <1500 to ≥1200 Da, <1200 to ≥ 900 Da and <900 to ≥ 600 Da. (**A**) Bar plot shows the MW distribution of the identified peptides in the DDM fraction after enrichment with to different SPE-based purification methods (SOLAμ^{TM} and ZIPTIP®). (**B**) Distribution profiles of the MW of the identified peptides in the TFA fraction after enrichment with to different purification methods.

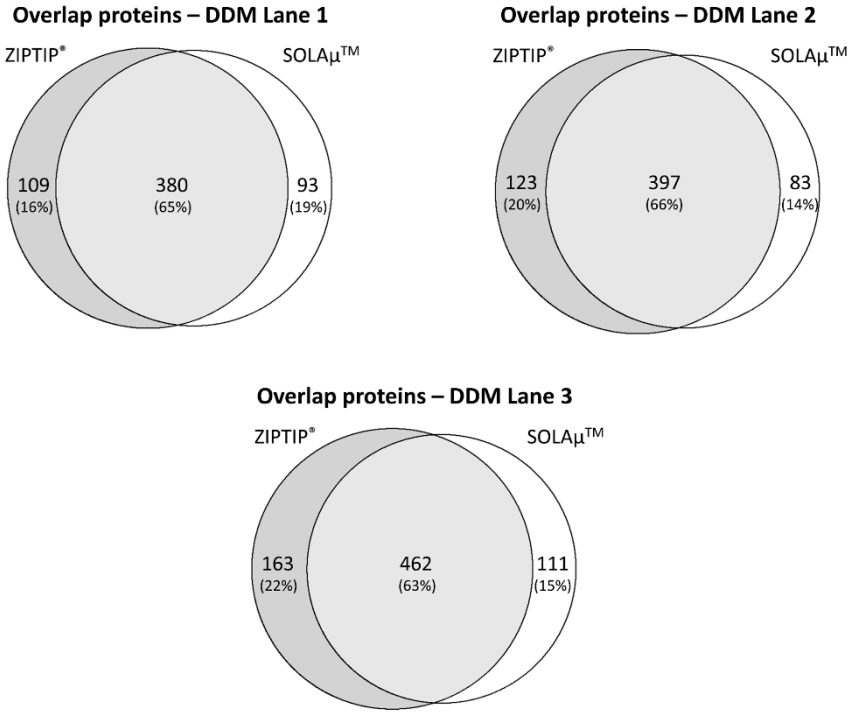

Figure 4. Venn diagram showing the overlap (percentage distribution) of identified proteins in the DDM fraction between six technical replicates. Three technical replicates were either purified by ZIPTIP® pipette tips or SOLAμ™ microtiter plates. On average 65 ± 2% of all identified proteins were detected with both SPE-based purification methods.

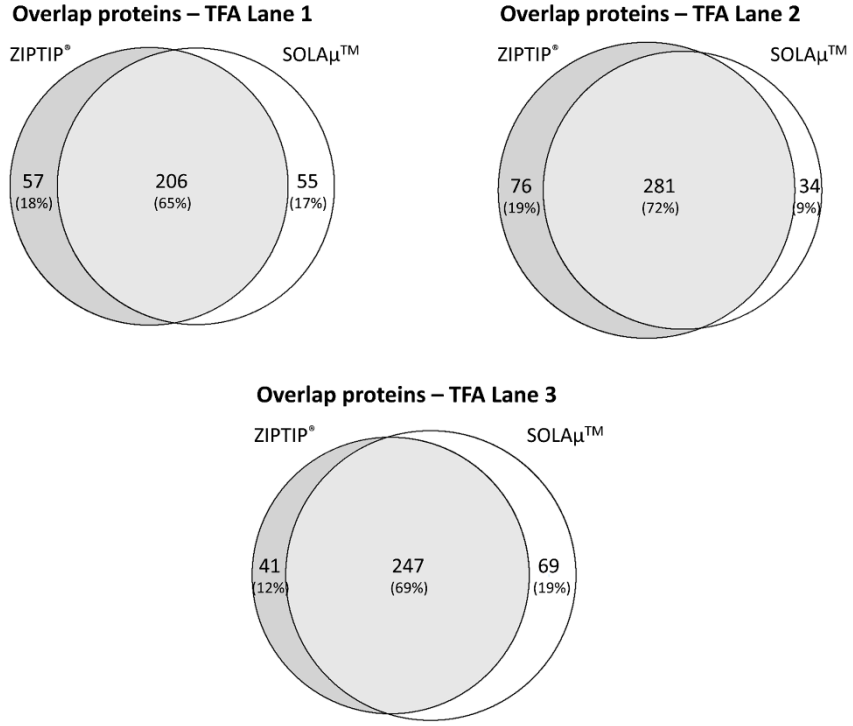

Figure 5. Venn diagram showing the overlap (percentage distribution) of identified proteins in the TFA fraction between six technical replicates. Three technical replicates were either purified by ZIPTIP® pipette tips or SOLAμ™ microtiter plates. On average 69 ± 4% of all identified proteins were detected with both SPE-based purification methods.

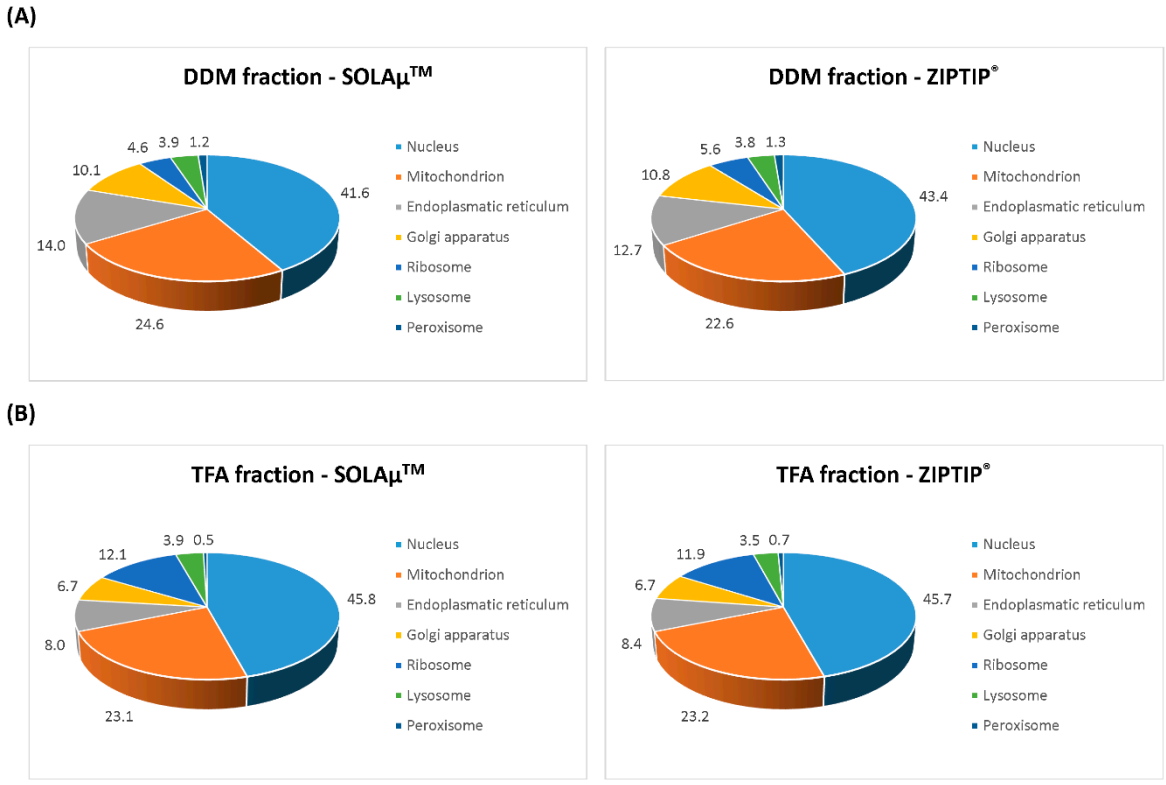

Figure 6. Gene ontology (GO) annotation analysis of all identified porcine retinal proteins. Proteins were clustered according to their cellular compartments such as nucleus, mitochondrion, endoplasmatic reticulum, golgi apparatus, ribosome, lysosome or peroxisome. DDM (**A**) as well as TFA fraction (**B**) did not show any conspicuous differences regarding the cellular localization of the identified proteins between both SPE-based purification methods (SOLAμ™ and ZIPTIP®).

2.3. Quantitative Analysis between Both SPE-Based Peptide Purification Methods

The aim of the second part of this study was to identify if there are significant differences in the label-free quantification (LFQ) of proteins between both SOLAμ™ and ZIPTIP® C18 purification methods. For the quantitative analysis, several glaucoma-associated retinal biomarker candidates were selected, which showed different expression levels ($P < 0.1$) in retinal tissues of glaucoma patients in contrast to healthy controls [16]. Up to 15 of these glaucoma-associated biomarker candidates were identified in the DDM fraction, whereas the TFA fraction contained up to 10 retinal biomarker candidates (Figure 7 and Supplementary Table S1). The three most abundant marker candidates of the DDM fraction were elongation factor 1-alpha 1 (*EEF1A1*), ADP/ATP translocase 3 (*SLC25A6*) and ras-related protein Rab-11B (*RAB11B*). In contrast, the TFA fraction provided the three most abundant biomarker candidates histone H1.0 (*H1F0*), α-crystallin B chain (*CRYAB*) and methyl-CpG-binding protein 2 (*MECP2*). Approximately 96% of the identified biomarker candidates did not show any significant differences (Student's t-test, $P > 0.05$) in the LFQ analysis between both SPE purification methods. Only protein marker *MECP2* showed a significant higher abundance (Student's *t*-test, $P = 0.02$) in ZIPTIP®-purified replicates in contrast to SOLAμ™-purified study samples. Verification experiment with tryptic in-gel digestion of recombinant protein *MECP2* (see Supplementary Figure S3) resulted in a slightly higher abundance in the ZIPTIP®-purified study samples (LFQ intensity=$11.5 \times 10^7 \pm 2.7 \times 10^7$, $N = 9$) compared to SOLAμ™-purified replicates (LFQ intensity=$10.1 \times 10^7 \pm 2.2 \times 10^7$, $N = 9$), however no significant difference (Student's *t*-test, $P = 0.24$) was found.

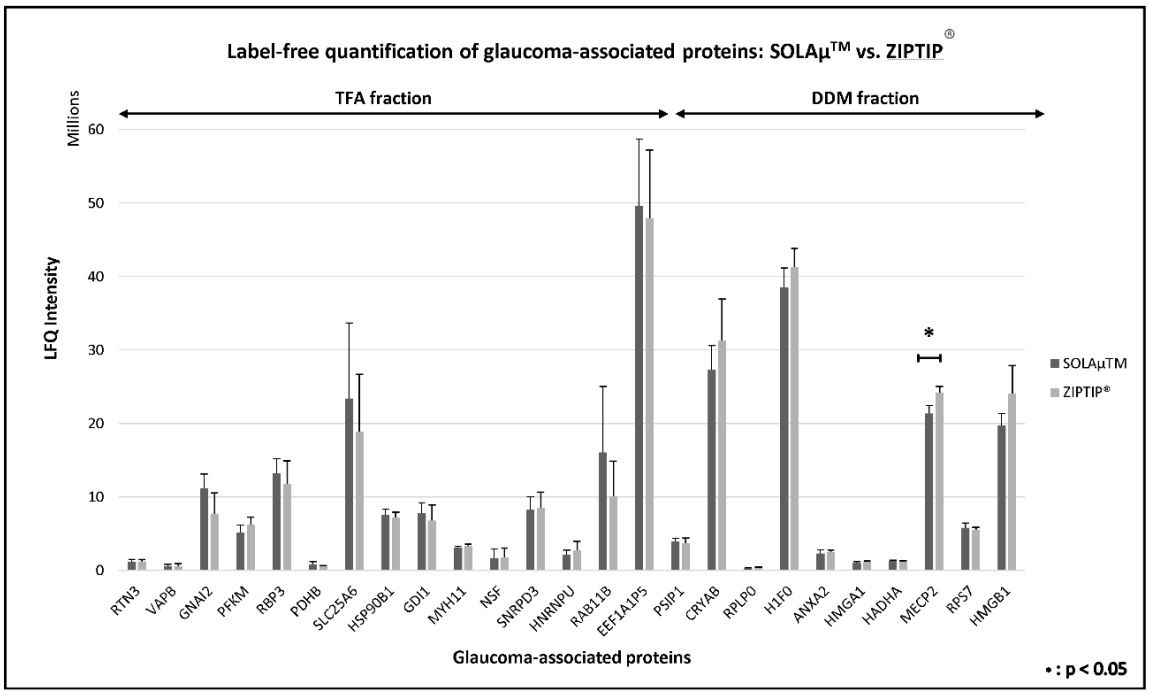

Figure 7. Bar plot shows the label-free quantification results of 25 glaucoma-associated biomarker candidates after enrichment with two different SPE purification methods (SOLAμ^{TM} and ZIPTIP®). Marker candidates on the left were identified in the DDM fraction, whereas proteins on the right were detected in the TFA fraction (FDR < 1%). Only protein *MECP2* showed a significant ($p < 0.05$) higher abundance in ZIPTIP®-purified replicates in comparison to SOLAμ^{TM}-purified study samples.

3. Discussion

The LC-MS-based proteomic analysis of the porcine retinal tissue samples provided a sensitive view into the complex porcine retina proteome and is in confidence with recent protein catalogues of the pig retina [15,18–20]. The present study contributes to a better characterization of the pig eye proteome and promotes the house swine (*Sus scrofa*) as a suitable candidate for ocular disease model systems [21–24]. However, the "core proteome" of the pig retina was congruently characterized with both SPE methods via ZIPTIP® C18 pipette tips or SOLAμ^{TM} HRP spin plates (see Supplementary Files S1 and S2), facilitating the LC-MS-based detection of high abundant proteins such as clathrin heavy chain 1 (*CLTC*), pyruvate kinase isozymes M1/M2 (*PKM*), creatine kinase B-type (*CKB*), glyceraldehyde-3-phosphate dehydrogenase (*GAPDH*), rhodopsin (*RHO*), various tubulin chains as well as 14-3-3 proteins. Moreover, subcellular compartments were comparably distinguished with both purification techniques, highlighting nucleus and mitochondria as the main annotated organelles (see Figure 6). Also, both systems worked equally well concerning the identification of retinal proteins from two different protein fractions: DDM- and TFA-containing solvents provided a high overlap regarding protein and peptides identifications between both purification techniques (see Figures 4 and 5; see Supplementary Figures S1 and S2). Tabb et al. (2010) [25] observed that peptide lists from several technical replicates overlapped from 35 to 60% and is in accordance with the results of the present study. The loss of repeatability in such LC-MS-based proteomic study designs is caused due to the complexity of the sample, ion suppression effects, precursor fragmentation efficiency or several others factors as described in detail elsewhere [25–28]. Nevertheless, both SPE protocols also showed a certain degree of contrary indicated by ZIPTIP® C18- and SOLAμ^{TM}-HRP exclusive protein species (e.g., ZIPTIP®: *VAMP2* and SOLAμ^{TM}: *HSP90AB1*, see Supplementary File S1). In accordance, the ZIPTIP® C18 method showed a slightly increased detection rate of proteins not included in the "core proteome" accompanied by slight tendencies of higher peptide ion scores and a higher sensitivity over the inspected mass range (see Figures 3 and 4). However, since none of these effects was supported

by statistical significance ($P > 0.05$), an almost equal analytical performance and reproducibility of both SPE workflows can be concluded.

In terms of quantitative recovery of the glaucoma-associated retinal target proteins, there were also no distinctive statistical differences ($P > 0.05$) between both SPE methods (see Figure 7). However, for some focused retinal proteins, e.g., ADP/ATP translocase 3 (*SLC25A6*), guanine nucleotide-binding protein G(i) subunit α-2 (*GNAI2*) or Ras-related protein Rab-11B (*Rab11B*), the SOLAμ™ SPE method showed tendencies of quantitatively higher protein recovery, whereas for other target proteins, e.g., high mobility group protein B1 (*HMGB1*) or α-crystallin B chain (*CRYAB*), the ZIPTIP® C18 technique achieved a slightly trend to quantitatively higher protein abundances. Nevertheless, since all of these findings were not supported by statistical significance ($P > 0.05$) an approximately comparable protein/peptide recovery performance of the two tested SPE methods can be assumed. Exceptions are the results regarding *MECP2* extraction, since *MECP2* was significantly ($P = 0.02$) recovered in higher quantities from retinal samples purified by the use of ZIPTIP® C18 pipette tips. However, this effect could not be reproduced by verification experiment ($P = 0.24$) considering the peptide enrichment of tryptic, recombinant MECP2 with both SPE devices. The different performance in *MECP2* extraction may emphasize the special retention behavior of this protein. As a member of intrinsically disordered proteins (IDPs), *MECP2* lacks higher structural organization [29–31] providing high plasticity for molecular interactions [32], which is reflected by its amino acid sequence. This may have also influenced the retention behavior of *MECP2*-derived peptides on SPE sorbents; e.g., on HRP representing a polymeric sorbent with polar and non-polar retention properties [33].

The SOLAμ™ HRP spin plate workflow is clearly a superior method compared to the manual ZIPTIP® C18 protocol with respect to the effort, costs, and analysis time factors. Although the ZIPTIP® C18 method can be automated on robotic stations [34], the speed and robustness of such a fully automated SPE pipette tip system is hampered by the lack of resistance towards errors such as trapped air-bubbles in the resin tips or pipette tips blocked by sample debris. This error-prone procedure can be avoided by using the SOLAμ™ HRP spin plates due to the macro-porous structure of the solid phase material, which provides continuous solvent flow-through without any sample loss [35]. Furthermore, the time factor is crucial in fully automated SPE pipette tip platforms in regard to solvent diffusion, alterations in solvent composition, robot movement distances and robot working cycles. In accordance, the constant need for trouble shooting in such SPE pipette tip automation systems is an important limitation compared to the centrifugal-based SPE spin plates. Indeed, the execution of the SOLAμ™ HRP spin plate workflow still requires a certain degree of operator handling and represents only a semi-automatic platform, nevertheless, it provides a higher degree of standardization and reproducibility than the manual ZIPTIP® C18 pipette tip workflow. However, due to the semi-automatic system properties and the consequent compatibility with LC-MS-based high-throughput screening strategies, centrifugal SPE spin plates have recently been "expected to become the mainstream method of sample processing in the future" [36] and were successfully used in various proteomic study designs focusing on human cerebrospinal fluid [37], human serum [38], human lung tissues [39] and HeLa cells [40].

In conclusion, the SOLAμ™ HRP spin plate approach represents an attractive alternative to the manual ZIPTIP® C18 pipette tip workflow and is particularly recommended for high-throughput discovery proteomic platforms to enhance cost-, labor- and time-effectiveness purposes. Nevertheless, considering the sensitive performance of the manually applied ZIPTIP® C18 tips, a targeted use of these pipette tips for the analysis of specific marker proteins such as *SLC25A6*, *GNAI2*, *Rab11B* or *MECP2* should be considered. In addition, the development of a mixed-mode spin plate, benefiting from the properties of both stationary materials (HRP and C18), could be a future innovation for improved recovery of retinal proteins. Beyond that, fine-tuning adjustments of the SOLAμ™ HRP spin plate workflow such as centrifugal speed, time, temperature, elution volume, elution buffer and number of repeat cycles could significantly improve the sensitivity and accuracy of the current proteomic measurements.

4. Materials and Methods

4.1. Sample Preparation and Protein Extraction Protocols

Retinal tissues were prepared from freshly enucleated eye bulbs (N = 45) from house swine *Sus scrofa domestica* Linnaeus, 1758 individuals (sacrificed at 3–6 month, female:male = 3:2) provided by local slaughterhouses (Landmetzgerei Harth, Stadecken-Elsheim, Germany; Metzgerei Köppel, Mainz, Germany). Eye bulbs were equatorially opened with a scalpel to remove lens, vitreous body, iris and ciliary body. Retinal tissues were carefully removed from the pigment epithelium with a phosphate-buffered saline (PBS)-coated paintbrush. After this, the whole retina was cut off from the optic nerve head and stored at −80 °C until further protein extraction protocols. For the first protein extraction protocol 30 isolated retina tissues were pooled and homogenized with an Ultra-Turrax T25 sonicator (Janke & Kunkel IKA Labortechnik, Staufen im Breisgau, Germany) as described in detail in an earlier study [15]. After homogenization, 0.1% dodecyl-ß-maltoside (DDM) was added to the aliquots and sonicated for 10 min on ice. Then, the samples were gently mixed and incubated for 30 min at RT followed by centrifugation at 10,000× g for 12 min at 4 °C. The supernatant was collected and stored at −20 °C. For the second protein extraction protocol 15 isolated retina tissues were pooled and subjected to further homogenization using a Precellys® 24 homogenizer (VWR International GmbH, Darmstadt, Germany) combined with a 1.4/2.8 mm Precellys® Ceramic kit (VWR International GmbH, Darmstadt, Germany). Prior to homogenization, frozen retina tissues were added to the tubes containing the 1.4/2.8 mm ceramic balls and filled with 1.5 mL PBS. Retina samples were homogenized three times for 45 s at 5000 rpm and centrifuged afterwards at 10,000× g for 12 min at 4 °C. The supernatant containing mostly cytoplasm-derived proteins was stored at −20 °C and the remaining pellet was resuspended in 500 µL of 1% trifluoroacetic acid (TFA). Funke et al. (2016) [15] have previously shown that 1% TFA is a suitable buffer for the extraction of many nucleus-derived retinal proteins. Retina samples were homogenized three times for 45 s at 5000 rpm followed by centrifugation at 10,000× g for 12 min at 4 °C. The supernatant containing mostly nucleus-derived proteins was stored at −20 °C. Protein measurements of both protein fractions were performed using BCA protein assay kit (Thermo Fisher Scientific, Rockford, IL, USA) according to manufacturer's instructions and measured three times with a Multiscan Ascent photometer (Thermo Fisher Scientific, Rockford, IL, USA) at a wavelength of 570 nm. Human Recombinant protein *MECP2* (Methyl-CpG-binding protein 2, cat. no. 14-1067) was purchased from Merck Millipore (Billerica, MA, USA) and used for the validation experiment.

4.2. 1-D SDS Page

Both protein fractions (50 µg per lane) were separated on 10-well NuPAGE 12% Bis-Tris minigels (Thermo Fisher Scientific, Rockford, IL, USA) under reducing conditions. Gels were incorporated in the XCell SureLock™ Mini-Cell Electrophoresis System (Invitrogen, Carlsbad, CA, USA) and prepared with NuPAGE™ MOPS SDS Running Buffer 20× (Thermo Fisher Scientific, Rockford, IL, USA) according to the supplier's protocol. In addition, 10 µL of the SeabluePlus 2 Pre-Stained Protein Standard (Thermo Fisher Scientific, Rockford, IL, USA) was used as molecular weight reference and separated at 150 V for 1.5 h at 4 °C. After separation, gels were fixed and stained using Novex Colloidal Blue Staining Kit (Thermo Fisher Scientific, Rockford, IL, USA) according to the manufacturer's instructions. Gels were destained for at least 16 h and scanned using an Epson Perfection V600 Photo Scanner (Seiko Epson Corporation, Suma, Nagano, Japan) at 700 dpi. Protein migration patterns were manually inspected and subjected to further in-gel trypsin digestion.

4.3. In-gel Trypsin Digestion

In total six lanes of both protein fractions were subjected to further in-gel trypsin digestion according to a modified protocol from a previous study [41]. At first, each protein lane was subdivided into 17 slices according to their characteristic protein migration profile and cut into small pieces. The gel

pieces were destained with 100 mM ammonium bicarbonate (ABC) in 50% acetonitrile (ACN) and dehydrated with pure ACN before reduction and alkylation processes. Then, the samples were evaporated in the SpeedVac (Eppendorf, Darmstadt, Germany) for 10 min at 30 °C to dryness. Afterwards the gel pieces were resolved with 10 mM dithiothreitol (DTT) in 100 mM ABC and incubated for 30 min at 56 °C followed by incubation with 55 mM iodoacetamide (IAA) in 100 mM ABC for 30 min at RT in the dark. Then the samples were dehydrated one more time with pure ACN and dried for 10 min in the SpeedVac at 30 °C to dryness. The reduced and alkylated proteins were further digested with 10 µg/mL sequencing grade trypsin (Promega, Madison, WI, USA) in 10 mM ABC 10% ACN and incubated overnight for at least 16 h at 37 °C. On the next day, the supernatant was collected and the tryptic peptides were extracted with 10% formic acid (FA) 70% ACN for 30 min at 350 rpm. Both supernatant fractions were pooled and evaporated in the SpeedVac at 30 °C to dryness.

4.4. SPE-Based Peptide Purification

The extracted peptides were dissolved in 20 µL 0.1% TFA. In order to reduce technical variability during execution of the sample preparation protocols, the slices (N = 17) of two lanes (DDM or TFA protein fractions) were pooled to a total volume of 40 µL 0.1% TFA. Then, the peptide pools were subsequently split into two equal amounts (each 20 µL) and subjected for further SPE purification via SOLAµ™ SPE HRP plates (Thermo Fisher Scientific, Rockford, IL, USA) or via C18 SPE pipette tips (Merck Millipore, Billerica, MA, USA). In total three technical replicates of each protein fraction (DDM or TFA) were purified with both SPE methods. Purification via ZIPTIP® C18 SPE pipette tips represents the SOP in our lab and was performed according to previous publications [9–11]. In brief, the ZIPTIP® C18 SPE pipette tips were conditioned and equilibrated by pipetting 10 µL ACN three times followed by 10 µL 0.1% TFA three times. Then the sample was loaded on the stationary C18 phase by aspirate and dispense 20 times, washed three times with 0.1% TFA and finally eluted two times in 10 µL 50% ACN 0.1% TFA. This procedure was repeated, the pooled eluate fractions (40 µL) were evaporated in the SpeedVac at 30 °C to dryness and stored at −20 °C. The SPE-based peptide purification via SOLAµ™ SPE HRP plates was performed according to the manufacturer's instructions. Activation and elution of the SOLAµ^{TM} SPE membranes was performed with 100 µL methanol (MeOH), whereas the washing step was performed with 100 µL 5% MeOH. After each step of the sample preparation protocol the SOLAµ^{TM} SPE plate was centrifuged at 4000× g for 3 min and the flow-through/eluate fractions were collected in 96-well microtiter microplates (Costar Corning Incorporated, Corning, NY, USA). Eluates were transferred into new reaction tubes, evaporated in the SpeedVac at 30 °C to dryness and stored at −20 °C prior to further LC-MS/MS analysis.

4.5. LC-MS/MS Analysis

LC-MS measurements were performed by a Rheos Allegro pump (Thermo Fisher Scientific, Rockford, IL, USA) downscaled to a capillary HPLC system (flow rate: 6.7 ± 0.3 µL/min) online coupled to a hybrid linear ion trap - Orbitrap MS (LTQ Orbitrap XL; Thermo Fisher Scientific, Rockford, IL, USA). Purified tryptic peptides were resolved in 10 µL 0.1 TFA and 6 µL were injected into a BioBasic® C18 column system (30 × 0.5 mm pre-column + 150 × 0.5 mm analytical column; Thermo Fisher Scientific, Rockford, IL, USA). Solvent A consists of 1.94% ACN, 0.06% MeOH, and 0.05% FA in water and solvent B consists of 95% ACN, 3% MeOH and 0.05% FA in water. Peptides were eluted within 50 min using following gradient program: 15–20% B (0–2 min), 20–60% B (2–35 min), 60–100% B (35–40 min), 100–0% B (40–45 min), and 0% B (45–50 min). The LTQ Orbitrap operated in positive ionization mode and data-dependent acquisition (DDA) mode: High-resolution survey full scan (from m/z 300 to 2000) was performed in the Orbitrap with a resolution of 30.000 at 400 m/z and the target automatic gain control was set to 1×10^6 ions. For internal calibration the lock mass was set to 445.120025 m/z (polydimethylcyclosiloxane). Dynamic exclusion mode was enabled with the following settings: repeat count = 1, repeat duration = 30 s, exclusion list size = 100, exclusion duration = 90 s and exclusion mass width= ± 20 ppm. Based on the high-resolution MS scan the five most

intense precursor ions were selected for further collision-induced dissociation (CID) fragmentation in the ion trap employing normalized collision energy of 35%. Manual inspection of the total ion current (TIC) chromatogram was performed using Qual Browser v. 2.0.7 SP1 (Thermo Fisher Scientific, Rockford, IL, USA). LC-MS raw data were uploaded to the ProteomeXchange Consortium via the PRIDE [42] partner repository with the dataset identifier PXD011755.

4.6. Peptide Identification and Quantification

For protein identification acquired LC-MS profiles were analyzed with software package Proteome Discoverer (Version 1.1; Thermo Fisher Scientific, Rockford, IL, USA) using the mascot search engine (version 2.2.07) to obtain peptide scoring information. Tandem MS spectra were searched against SwissProt database (SwissProt_150301) with a combination of *Homo sapiens* and *Sus scrofa* as taxonomies with following settings: peptide mass tolerance of $\pm$ 30 ppm in the range of 150–2000 Da, fragment mass tolerance of $\pm$ 0.5 Da, tryptic cleavage, a maximum of one missed cleavages, carbamidomethylation as fixed modification, acetylation (Protein N-terminal) and oxidation as variable modification. Output data were filtered considering a false discovery rate (FDR) < 1%. Given the fact that there is a limited access to proper public proteomic databases of the house swine (*Sus scrofa*) [43,44], we included the species-related proteomic database of *Homo sapiens* for protein search in order to maximize the protein identification results. Label-free quantification (LFQ) of the proteins was performed with MaxQuant computational proteomics platform version 1.5.2.8 (Max Planck Institute of Biochemistry, Martinsried, Germany). Tandem MS spectra were searched against a user-defined database, containing glaucoma-associated proteins (SwissProt_170531), with the previously described database search settings. In addition, MaxQuant specific feature "match between run" was enabled and proteins were identified considering FDR < 1%. Glaucoma-associated human protein database contains a selection of retinal protein sequences which showed at least a tendency ($P < 0.1$) to be differentially expressed between glaucoma patients and healthy controls according to a recent publication [16].

4.7. Data Analysis

Graphical presentation and *t*-test statistics for the qualitative analysis of the MS output data was performed with software package Statistica version 13 (Statsoft, Tulsa, OK, USA). Normal distribution of the data-sets was verified by the Shapiro–Wilk test. Student's *t*-test was applied for parametric data and Mann–Whitney U-test for non-parametric data. Venn diagram analysis was performed with statistics program R version 3.2.0 with VennDiagram package version 1.6.17 (Available online: https://www.r-project.org/). Combined protein lists from the SOLAμ™- and ZIPTIP®-purified protein fractions were subjected to gene ontology (GO) analysis using software program Cytoscape version 2.8.3 with BINGO 2.44 plugin ((Available online: www.cytoscape.org). Thereby, the GO category "cellular component" was screened for potential annotations. Statistical analysis of the MaxQuant generated output data was performed using software package Perseus version 1.5.5.0 (Max Planck Institute of Biochemistry, Martinsried, Germany). At first, LFQ intensities of the detected proteins were $\log_2$ transformed for further analysis [45]. Prior to statistical analysis the output data were filtered for contaminants, reversed hits, "only identified by site" and for a minimum number of three valid values in at least in one group. Finally, two-sided *t*-test statistics with *P* values <0.05 was applied in order to identify significant level changes in protein abundances between both SPE-based purification methods (SOLAμ™ and ZIPTIP®).

Supplementary Materials: Supplementary materials can be found at http://www.mdpi.com/1422-0067/19/12/3847/s1. A list of all identified proteins and peptides is provided in Supplementary Files S1 and S2. The mass spectrometry proteomics data have been deposited to the ProteomeXchange Consortium via the PRIDE [42] partner repository with the dataset identifier PXD011755.

Author Contributions: C.S. and S.F. developed the study design, organized the experimental set-up and wrote the manuscript. J.T. performed the experimental work as well as the mass spectrometric measurements and assisted in the data analysis. A.B., N.P. (Natarajan Perumal) and C.M. participated in study design, proofread the manuscript and contributed important intellectual content. N.P. (Norbert Pfeiffer) critically reviewed the

manuscript and provided important intellectual input. F.H.G. performed study coordination and study design, participated in review and approval of the manuscript.

Conflicts of Interest: The authors declare no conflict of interest.

References

1. Hennion, M.C. Solid-phase extraction: Method development, sorbents, and coupling with liquid chromatography. *J. Chromatogr. A* **1999**, *856*, 3–54. [CrossRef]
2. Poole, C.F. New trends in solid-phase extraction. *TrAC Trends Anal. Chem.* **2003**, *22*, 362–373. [CrossRef]
3. Tamayo, F.G.; Turiel, E.; Martin-Esteban, A. Molecularly imprinted polymers for solid-phase extraction and solid-phase microextraction: Recent developments and future trends. *J. Chromatogr. A* **2007**, *1152*, 32–40. [CrossRef] [PubMed]
4. Augusto, F.; Hantao, L.W.; Mogollon, N.G.S.; Braga, S.C.G.N. New materials and trends in sorbents for solid-phase extraction. *TrAC Trends Anal. Chem.* **2013**, *43*, 14–23. [CrossRef]
5. Bladergroen, M.R.; van der Burgt, Y.E.M. Solid-phase extraction strategies to surmount body fluid sample complexity in high-throughput mass spectrometry-based proteomics. *J. Anal. Methods Chem.* **2015**, *2015*, 250131. [CrossRef] [PubMed]
6. Plotka-Wasylka, J.; Szczepanska, N.; de la Guardia, M.; Namiesnik, J. Modern trends in solid phase extraction: New sorbent media. *TrAC Trends Anal. Chem.* **2016**, *77*, 23–43. [CrossRef]
7. Zwir-Ferenc, A.; Biziuk, M. Solid phase extraction technique—Trends, opportunities and applications. *Pol. J. Environ. Stud.* **2006**, *15*, 677–690.
8. Funke, S.; Perumal, N.; Bell, K.; Pfeiffer, N.; Grus, F.H. The potential impact of recent insights into proteomic changes associated with glaucoma. *Expert Rev. Proteom.* **2017**, *14*, 311–334. [CrossRef] [PubMed]
9. Schmelter, C.; Perumal, N.; Funke, S.; Bell, K.; Pfeiffer, N.; Grus, F.H. Peptides of the variable igg domain as potential biomarker candidates in primary open-angle glaucoma (poag). *Hum. Mol. Genet.* **2017**, *26*, 4451–4464. [CrossRef] [PubMed]
10. Perumal, N.; Funke, S.; Pfeiffer, N.; Grus, F.H. Characterization of lacrimal proline-rich protein 4 (prr4) in human tear proteome. *Proteomics* **2014**, *14*, 1698–1709. [CrossRef]
11. Perumal, N.; Funke, S.; Wolters, D.; Pfeiffer, N.; Grus, F.H. Characterization of human reflex tear proteome reveals high expression of lacrimal proline-rich protein 4 (prr4). *Proteomics* **2015**, *15*, 3370–3381. [CrossRef] [PubMed]
12. Tubaon, R.M.; Haddad, P.R.; Quirino, J.P. Sample clean-up strategies for ESI mass spectrometry applications in bottom-up proteomics: Trends from 2012 to 2016. *Proteomics* **2017**, *17*, 1700011. [CrossRef] [PubMed]
13. Anders, F.; Teister, J.; Funke, S.; Pfeiffer, N.; Grus, F.; Thanos, S.; Prokosch, V. Proteomic profiling reveals crucial retinal protein alterations in the early phase of an experimental glaucoma model. *Graefes Arch. Clin. Exp. Ophthalmol.* **2017**, *255*, 1395–1407. [CrossRef] [PubMed]
14. Anders, F.; Teister, J.; Liu, A.H.; Funke, S.; Grus, F.H.; Thanos, S.; von Pein, H.D.; Pfeiffer, N.; Prokosch, V. Intravitreal injection of ß-crystallin b2 improves retinal ganglion cell survival in an experimental animal model of glaucoma. *PLoS ONE* **2017**, *12*, e0175451. [CrossRef] [PubMed]
15. Funke, S.; Markowitsch, S.; Schmelter, C.; Perumal, N.; Mwiiri, F.K.; Gabel-Scheurich, S.; Pfeiffer, N.; Grus, F.H. In-depth proteomic analysis of the porcine retina by use of a four step differential extraction bottom up LC MS platform. *Mol. Neurobiol.* **2016**, *54*, 7262–7275. [CrossRef]
16. Funke, S.; Perumal, N.; Beck, S.; Gabel-Scheurich, S.; Schmelter, C.; Teister, J.; Gerbig, C.; Gramlich, O.W.; Pfeiffer, N.; Grus, F.H. Glaucoma related proteomic alterations in human retina samples. *Sci. Rep.* **2016**, *6*, 29759. [CrossRef] [PubMed]
17. Bell, K.; Wilding, C.; Funke, S.; Perumal, N.; Beck, S.; Wolters, D.; Holz-Muller, J.; Pfeiffer, N.; Grus, F.H. Neuroprotective effects of antibodies on retinal ganglion cells in an adolescent retina organ culture. *J. Neurochem.* **2016**, *139*, 256–269. [CrossRef]
18. McKay, G.J.; Campbell, L.; Oliver, M.; Brockbank, S.; Simpson, D.A.C.; Curry, W.J. Preparation of planar retinal specimens: Verification by histology, mrna profiling, and proteome analysis. *Mol. Vis.* **2004**, *10*, 240–247.

19. Cehofski, L.J.; Kruse, A.; Kjaergaard, B.; Stensballe, A.; Honore, B.; Vorum, H. Dye-free porcine model of experimental branch retinal vein occlusion: A suitable approach for retinal proteomics. *J. Ophthalmol.* **2015**, *2015*, 839137.
20. Hauck, S.M. Proteomic analysis of the porcine interphotoreceptor matrix. *Proteomics* **2005**, *5*, 4637. [CrossRef]
21. Verma, N.; Rettenmeier, A.W.; Schmitz-Spanke, S. Recent advances in the use of sus scrofa (pig) as a model system for proteomic studies. *Proteomics* **2011**, *11*, 776–793. [CrossRef] [PubMed]
22. Bassols, A.; Costa, C.; Eckersall, P.D.; Osada, J.; Sabria, J.; Tibau, J. The pig as an animal model for human pathologies: A proteomics perspective. *Proteom. Clin. Appl.* **2014**, *8*, 715–731. [CrossRef] [PubMed]
23. Bendixen, E.; Danielsen, M.; Larsen, K.; Bendixen, C. Advances in porcine genomics and proteomics-a toolbox for developing the pig as a model organism for molecular biomedical research. *Brief Funct. Genom.* **2010**, *9*, 208–219. [CrossRef] [PubMed]
24. Hesselager, M.O.; Codrea, M.C.; Sun, Z.; Deutsch, E.W.; Bennike, T.B.; Stensballe, A.; Bundgaard, L.; Moritz, R.L.; Bendixen, E. The pigpeptideatlas: A recource for systems biology in animal production and biomedicine. *Proteomics* **2016**, *16*, 634–644. [CrossRef] [PubMed]
25. Tabb, D.L.; Vega-Montoto, L.; Rudnick, P.A.; Variyath, A.M.; Ham, A.J.; Bunk, D.M.; Kilpatrick, L.E.; Billheimer, D.D.; Blackman, R.K.; Cardasis, H.L.; et al. Repeatability and reproducibility in proteomic identifications by liquid chromatography-tandem mass spectrometry. *J. Proteome Res.* **2010**, *9*, 761–776. [CrossRef] [PubMed]
26. Berg, M.; Parbel, A.; Pettersen, H.; Fenyo, D.; Bjorkesten, L. Reproducibility of LC-MS-Based protein identification. *J. Exp. Bot.* **2006**, *57*, 1509–1514. [CrossRef] [PubMed]
27. Liu, H.; Sadygov, R.G.; Yates, J.R., 3rd. A model for random sampling and estimation of relative protein abundance in shotgun proteomics. *Anal. Chem.* **2004**, *76*, 4193–4201. [CrossRef] [PubMed]
28. Delmotte, N.; Lasaosa, M.; Tholey, A.; Heinzle, E.; van Dorsselaer, A.; Huber, C.G. Repeatability of peptide identifications in shotgun proteome analysis employing off-line two-dimensional chromatographic separations and ion-trap ms. *J. Sep. Sci.* **2009**, *32*, 1156–1164. [CrossRef]
29. Awile, O.; Krisko, A.; Sbalzarini, I.F.; Zagrovic, B. Intrinsically disordered regions may lower the hydration free energy in proteins: A case study of nudix hydrolase in the bacterium deinococcus radiodurans. *PLoS Comput. Biol.* **2010**, *6*, e1000854. [CrossRef]
30. Adams, V.H.; McBryant, S.J.; Wade, P.A.; Woodcock, C.L.; Hansen, J.C. Intrinsic disorder and autonomous domain function in the multifunctional nuclear protein, MECP2. *J. Biol. Chem.* **2007**, *282*, 15057–15064. [CrossRef]
31. Hansen, J.C.; Wexler, B.B.; Rogers, D.J.; Hite, K.C.; Panchenko, T.; Ajith, S.; Black, B.E. DNA binding restricts the intrinsic conformational flexibility of methyl CPG binding protein 2 (mecp2). *J. Biol. Chem.* **2011**, *286*, 18938–18948. [CrossRef]
32. Ausio, J.; de Paz, A.M.; Esteller, M. Mecp2: The long trip from a chromatin protein to neurological disorders. *Trends Mol. Med.* **2014**, *20*, 487–498.
33. Bardsley, J.; Jones, J.; Barratini, V.; Humphryes, P.C.; Liddicoat, T. *Improvement in Speed and Reproducibility of Protein Digestion Utilizing Novel Sample Preparation Technology in a Full Solution Workflow*; PN21209-EN 0515S; Thermo Fisher Scientific: Waltham, MA, USA, 2015.
34. Harris, C.M. Finding the right robot for MALDI. *Anal. Chem.* **2001**, *73*, 447a–451a. [CrossRef] [PubMed]
35. Scientific, T.F. *Solaμ Spe Plates Technical Guide*; Technical Guide, TG20947_E 04/14S; Thermo Fisher Scientific: Waltham, MA, USA, 2014.
36. Namera, A.; Saito, T. Spin column extraction as a new sample preparation method in bioanalysis. *Bioanalysis* **2015**, *7*, 2171–2176. [CrossRef]
37. Waldera-Lupa, D.M.; Etemad-Parishanzadeh, O.; Brocksieper, M.; Kirchgaessler, N.; Seidel, S.; Kowalski, T.; Montesinos-Rongen, M.; Deckert, M.; Schlegel, U.; Stuhler, K. Proteomic changes in cerebrospinal fluid from primary central nervous system lymphoma patients are associated with protein ectodomain shedding. *Oncotarget* **2017**, *8*, 110118–110132. [CrossRef] [PubMed]
38. Sandvik, T.A.; Husa, A.; Buchmann, M.; Ludanes, E. Routine supercritical fluid chromatography tandem mass spectrometry method for determination of vitamin k1 extracted from serum with a 96-well solid-phase extraction method. *J. Appl. Lab. Med.* **2017**, *1*, jalm-2016. [CrossRef]

39. Rosmark, O.; Ahrman, E.; Muller, C.; Elowsson Rendin, L.; Eriksson, L.; Malmstrom, A.; Hallgren, O.; Larsson-Callerfelt, A.K.; Westergren-Thorsson, G.; Malmstrom, J. Quantifying extracellular matrix turnover in human lung scaffold cultures. *Sci. Rep.* **2018**, *8*, 5409. [CrossRef] [PubMed]
40. Grassetti, A.V.; Hards, R.; Gerber, S.A. Offline pentafluorophenyl (PFP)-rp prefractionation as an alternative to high-PH RP for comprehensive LC-MS/MS proteomics and phosphoproteomics. *Anal. Bioanal. Chem.* **2017**, *409*, 4615–4625. [CrossRef] [PubMed]
41. Shevchenko, A.; Tomas, H.; Havlis, J.; Olsen, J.V.; Mann, M. In-gel digestion for mass spectrometric characterization of proteins and proteomes. *Nat. Protocols* **2006**, *1*, 2856–2860. [CrossRef]
42. Vizcaino, J.A.; Csordas, A.; Del-Toro, N.; Dianes, J.A.; Griss, J.; Lavidas, I.; Mayer, G.; Perez-Riverol, Y.; Reisinger, F.; Ternent, T.; et al. 2016 update of the pride database and its related tools. *Nucleic Acids Res.* **2016**, *44*, 11033. [CrossRef]
43. Dawson, H.D.; Chen, C.; Gaynor, B.; Shao, J.; Urban, J.F., Jr. The porcine translational research database: A manually curated, genomics and proteomics-based research resource. *BMC Genom.* **2017**, *18*, 643. [CrossRef] [PubMed]
44. de Almeida, A.M.; Bendixen, E. Pig proteomics: A review of a species in the crossroad between biomedical and food sciences. *J. Proteom.* **2012**, *75*, 4296–4314. [CrossRef] [PubMed]
45. Cox, J.; Mann, M. 1d and 2d annotation enrichment: A statistical method integrating quantitative proteomics with complementary high-throughput data. *BMC Bioinform.* **2012**, *13* (Suppl. 16), S12. [CrossRef]

3 Summary of the results and discussion

Glaucoma is a multifactorial disease and the exact pathophysiology of this neurodegenerative eye disorder is still poorly understood. Elevated IOP remains the major risk factor for the development and progression of glaucoma, even if up to 30 % of all patients never showed this clinical symptom [12]. Moreover, up to 7 % of the population over the age of 40 show a prevalence for ocular hypertension (IOP > 21 mmHg), but lesser then 1 % of this group develop glaucoma per year [13]. Nowadays, IOP-lowering drugs still represent the gold standard in glaucoma therapy and also show beneficial effects in patients without IOP elevation. However, this treatment option just slows down the course of the disease and the threatening blindness of the patients but does not cure or prevent the pathological processes. Due to these reasons, it is of great importance to develop new sensitive screening and treatment strategies in glaucoma therapy to provide an appropriate and personalized medical management of each patient.

Biomarker discovery represents a very challenging and time-consuming task in many clinical study designs and depends on the availability, amount and quality of the biological samples. With respect to glaucoma research, most of the collected biological fluids in clinical trials are restricted to blood serum or tear samples from the different patient cohorts. Collection of more interesting tissue samples such as retinae from human donor eyes, close to the side of damage, are limited to *post mortem* analyses and are much rarer. The sampling of aqueous humor, in contrast, is only accomplishable during cataract surgery or other intraocular surgeries and is strictly forbidden during clinical routine diagnostics in Germany. Furthermore, the complexity and structure of the biological material greatly influences the selection of proper sample preparation protocols and the application of appropriate analytical instruments. LC-MS-based proteomics has become the instrument of choice for the quantitative protein profiling in various diseases and provides excellent requirements for the identification of new potential biomarker candidates. The present doctoral thesis compromises a LC-MS-based *de novo* profiling strategy for the identification of highly specific immune-related biomarker candidates (manuscript I), which also might represent interesting target molecules for future diagnostic or therapeutic purposes. Based on these results, we investigated the neuroprotective potential of two immunoproteomic marker candidates on RGCs *ex vivo* to evaluate their potential effectiveness as future therapeutic agents in glaucoma therapy (manuscript II). Finally, we evaluated the performance of two SPE methods for sample

clean-up prior to proteomic analyses in order to increase the speed, robustness and sensitivity of the current LC-MS based analytical platform (manuscript III). In addition, the optimized and improved performance of the proteomic workflow will also be beneficial for the previous parts of the doctoral thesis, because it's accelerates the high-throughput MS analysis of larger study populations and will significantly increase the statistical robustness of study results or validation experiments in future.

3.1 Proteomic profiling of *de novo* immune-related biomarker candidates in primary-open angle glaucoma (POAG)

Main ability of the immune system is to differentiate between self and foreign antigens and to provoke immune responses against bacterial pathogens or helminths. However, during the last decades it was extensively proven that each individual exhibits a natural panel of self-reactivity comprising autoantibodies (AAB), which seem to be important for the maintenance of the immunological homeostasis. However, the exact role of the natural AAB repertoire is still unclear, but it is assumed that they have regulatory functions and might play a protective role in the cellular homeostasis [59,69]. Furthermore, it is hypothesized that any disruption of the immunological equilibrium state may result in proinflammatory or autoaggressive conditions favoring the formation of autoimmune-related neurodegenerative diseases. Due to that reason, represents the humoral immune response system, particularly AABs, an early and sensitive indicator for pathological conditions and may be used as reliable marker for early diagnostic purposes.

The pathogenesis of glaucoma is also accompanied by significant changes in the natural autoimmune response indicated by decreased as well as increased systemic AAB titers against various retinal proteins, e.g. *HSP27* and *MBP*. So far, AAB profiling studies were mainly performed by conventional immunoproteomic techniques such as microarray or western blot analysis and are dependent on predefined protein panels providing the basis for the detection of specific antigen-antibody interactions. Major drawback of these approaches are the missing structural information about the active binding sites (paratopes) of the AAB molecules and the sequence variation of the paratopes along the different individuals. Recent studies have already demonstrated the high structural convergence and sequence coverage of disease-specific AABs in unrelated HIV as well as leukemia patients [70,71]. Furthermore, active immunization of individual rats with specific antigens led to the development of

congruent paratope sequence motives [72] and highlighted the humoral immune response as sensitive indicator for pathological or immunostimulating conditions. All these findings underline the importance of antigenic pressures during humoral immune responses and may explain the convergent development of (auto-)antibodies in different individuals. Based on this fundamental knowledge, de Costa and colleagues (2010) [73] established an LC-MS-based proteomic platform for the reproducible sequencing and quantification of constant IgG fragments and the antigen-binding fragments (Fab) of antibodies. This analytical approach does not require any previous information about the targeted (auto-)antigens and resulted in the identification of highly specific immune-related biomarker candidates in lung cancer [74] and multiple sclerosis patients [75]. In addition, it was possible to develop a 12-antibody-peptide model for the discrimination of lung cancer patients from healthy controls with a sensitivity of 84 % and specificity of 90 % and achieved much higher identification rates than conventional CT screening technologies [74].

Within the scope of the present thesis, the established LC-MS-based analytical platform was applied for the first time for the *de novo* screening of immune-related biomarker candidates in sera of POAG patients in comparison to healthy controls. In brief, all sera-derived IgG molecules were purified from each subject and prepared as described in detail in manuscript I: chapter 2.1; IgG Fab was subjected for further in-solution trypsin digestion and subsequently measured by LC-MS-based quantitative proteomics. Statistical analysis revealed in total 75 peptides of the variable IgG domain, which were significantly differentially distributed between POAG patients and healthy controls and provided a group-specific clustering of all subjects by the principal component analysis (PCA). Sequence annotation analysis identified 9 CDR1, 7 CDR2 and 6 CDR3 sequences, whereas most of the peptides were assigned to the framework regions (18 FR1, 10 FR2, 22 FR3 and 3 FR4) of the antibodies. CDRs are hypervariable regions determining the antigen specificity of the antibodies surrounded by moderately mutated sequence motives termed as FRs [76]. This also explains the preferred identification of FR regions by MS, because lesser mutated parts of the antibodies are more likely to be shared between several B cell clones and therefore easier to detect compared to highly diverse CDR sequences. Remarkably, up to 90 % of these marker peptides were much lesser expressed in the IgG Fab structure of POAG patients in comparison to healthy controls. If the systemic low abundance of most of the signature peptides result from either increased protein deposits or increased antibody clearance rates in POAG patients remains to be

determined. However, our group already demonstrated increased IgG accumulations in glaucomatous retinal tissues of human donor eyes [77] followed by increased infiltration of IgG-secreting B cells. Moreover, we were able to verify IgG deposits in an experimental glaucoma animal model which were strongly associated by increased numbers of $Iba1^+$ microglia cells and increased caspase 3 activity in RGCs indicating apoptotic processes [58,78]. In addition, Kuehne *et al.* (2006) [79] also showed increased expression levels of specific complement system molecules (C1q and C3) in the retina of a chronic glaucomatous rat model and proved the potential occurrence of (auto-)antibody-induced cell death of RGCs *in vivo*.

Besides the identification of specific signature peptides of the variable IgG domain, the present study also evaluated the overall expression profiles of specific VH or VL (κ or λ) family gene segments in the systemic immune response. As final result, the gene segment VH3 was on average significantly higher expressed in the IgG Fab structure of POAG patients in contrast to healthy controls, whereas the gene segment VH2 was significantly lesser presented in the POAG group. Interestingly, also other studies demonstrated the increased expression of VH3 and VH4 gene segments in the CSF of multiple sclerosis patients [75] and decreased VH3 family expression in patients with late stage HIV-1 disease [80]. Particularly in HIV research it is supposed that the VH3 deficiency in the late stage of the disease may contribute to impaired immune responses to infections and vaccines [80–82]. With respect to glaucoma, our group could induce glaucomatous-like damage in the retina of rats by active systemic immunization with a mixture of optic nerve antigens [83] or with recombinant *HSP60* [84]. These findings clearly indicate that specific (auto-)antigenic pressures can promote or even initiate the development of glaucomatous-like damages *in vivo* and are consistent with the disturbed VH gene family distribution in the humoral immune response of glaucoma patients.

3.2 Neuroprotective effects of polyclonal-derived CDR sequence motives on RGCs in an *ex vivo* glaucoma model

In recent years, short synthetic CDR peptides became known as highly active molecules triggering different kinds of biological functions, which are independent of the antigen specificity of the native antibodies. The CDR-induced effects vary from protective functions such as antimicrobial, antifungal or antitumor activities [85–88] to more regulatory functions such as immuno-modulatory, -suppressive or -stimulatory properties [89–92]. In terms of glaucoma, our group recently demonstrated neuroprotective effects of disease-associated

AABs (e.g. against *GFAP*, 14-3-3, α- and γ-synuclein) on RGCs in different cell culture experiments [60–63] and in an IOP-dependent glaucoma animal model [64]. However, major disadvantages of antibodies for therapeutic purposes are the high-manufacturing costs, inadequate pharmacokinetic properties or poor tissue accessibility hampering their application in daily clinical routine [93]. Moreover, all therapeutic antibodies have to be humanized for the medical applications by means of laborious procedures such as CDR grafting or phage-display technologies in order to reduce the immunogenic properties of the antibody molecules [94,95]. To overcome these limitations, synthetic CDR peptides provide an attractive alternative to antibody-based immunotherapy, because of their small size, ease and cost-effective production, low immunogenicity and their good tissue penetration characteristics [96]. Promisingly, many studies already highlighted the beneficial effects of a synthetic tolerogenic CDR1 peptide in different Systemic Lupus Erythematosus (SLE) animal models by triggering the immunosuppressive cytokine production in B and T cells [90,91,97]. Based on this knowledge, synthetic CDR peptides provide a great therapeutic potential for the treatment of various autoimmune-related neurodegenerative diseases with special focus on glaucoma.

Main objective of the second part of this doctoral thesis was to evaluate if polyclonal-derived IgG V domain sequence motives (revealed from manuscript I: chapter 2.1) show neuroprotective or even neurotoxic effects on RGCs in an *ex vivo* glaucoma model. Due to that, we selected two disease-associated CDR1 sequence motives (*AS<u>GYTFTNYG</u>LSWVR* homologous to IGHV1-18*02 and *AS<u>QSVSSY</u>LAWYQQK* homologous to IGKV3-11*01), which were significantly lesser expressed in the IgG Fab structure of POAG patients in contrast to healthy controls. In comparison to previous study designs [85–93], the present synthetic CDR peptides show a polyclonal origin shared between several B cell clones and are not derived from native antibody molecules with known antigen specificity and biofunction. However, to investigate the CDR-induced effects on RGCs we applied the adolescent retina organ culture from the house swine (*Sus scrofa domesticus*) for the experimental analyses. This *ex vivo* glaucoma model is based on the production of retina–retinal pigment epithelium (RPE) explants of freshly removed eye bulbs from local slaughterhouses and the cultivation of these explants for 24 h as described in detail in manuscript II: chapter 2.2. Stress factor for the RGCs in this model represents the optic nerve cut (ONC) by the slaughterer and was already used to confirm the neuroprotective effects of specific AABs against *GFAP* and γ-synuclein [63].

Interestingly, incubation of the stressed retinal explants with CDR1 sequence motive *ASGYTFTNYGLSWVR* (25 µg/ml) resulted in about 30 % higher RGC survival rates in comparison to untreated controls. Sequence specificity of these effects were verified by use of a scrambled peptide analog (*YVWAGSTLSRTGNFY*) as further control, which did not show any effects on RGCs *ex vivo* compared to the untreated retinal explants.

State-of-the-art LC-MS-based affinity capture experiments identified the mitochondrial serine protease *HTRA2* as significant interaction partner (epitope target) of CDR1 sequence motive *ASGYTFTNYGLSWVR* in the retinal porcine proteome. The specificity and uniqueness of this peptide-protein interaction was further verified by spike-in experiment of recombinant *HTRA2*, even if the scrambled peptide analog (*YVWAGSTLSRTGNFY*) also showed some low affinity for the target molecule. Interestingly, Fellouse *et al.* (2004) [98] and Koide and colleagues (2009) [99] demonstrated the dominant role of tyrosine (*abbr. Y*) residues in antigen recognition processes and the importance for the formation of proper protein-protein complexes. Particularly, both highlighted the specific physicochemical properties of tyrosine (e.g. amphipathic characteristics) as important requirements for the formation of nonpolar, hydrogen-bonding and cation-π interactions to other molecules. Due to these facts, it can be assumed that especially tyrosine residues *Y(4)* and *Y(9)* of the CDR1 sequence motive, in the respective distance to each other, are primarily responsible for the proper binding of *HTRA2*. However, despite the loss of this important binding motive in the scrambled peptide analog, it still seems to have some low affinity for the target protein, probably because of single tyrosine residues *Y(1)* or *Y(15)*. In accordance, several studies already provided evidence for the significance of single tyrosine residues in the maintenance and stability of entire protein-protein interaction complexes [100–102]. In addition, affinity capture experiments revealed no significant retinal interaction partner of CDR1 sequence motive *ASQSVSSYLAWYQQK* and therefore it was not tested in the *ex vivo* glaucoma model.

Epitope target *HTRA2* represents a very promising biomarker candidate in glaucoma research, because of its contradictory functions as either pro-apoptotic molecule [103–105] or as important regulator of the mitochondrial homeostasis and neuronal cell survival (see Figure 3) [106–109]. On the one hand, *HTRA2* is increasingly released from the mitochondria to the cytosol during cellular stress responses and promotes the degradation of anti-apoptotic proteins and the activation of caspase-dependent apoptotic pathways [103–105]. On the other hand, *HtrA2/Omi* knockout mice deficient in *HTRA2* protein activity are characterized by

a lethal neurodegenerative phenotype [106–109] accompanied by an increased accumulation of misfolded proteins in the mitochondria [110]. However, to unravel the complex CDR-induced, neuroprotective effects on RGCs in the *ex vivo* glaucoma model, we performed LC-MS based quantitative proteomic analyses of the CDR-treated and untreated retinal explants.

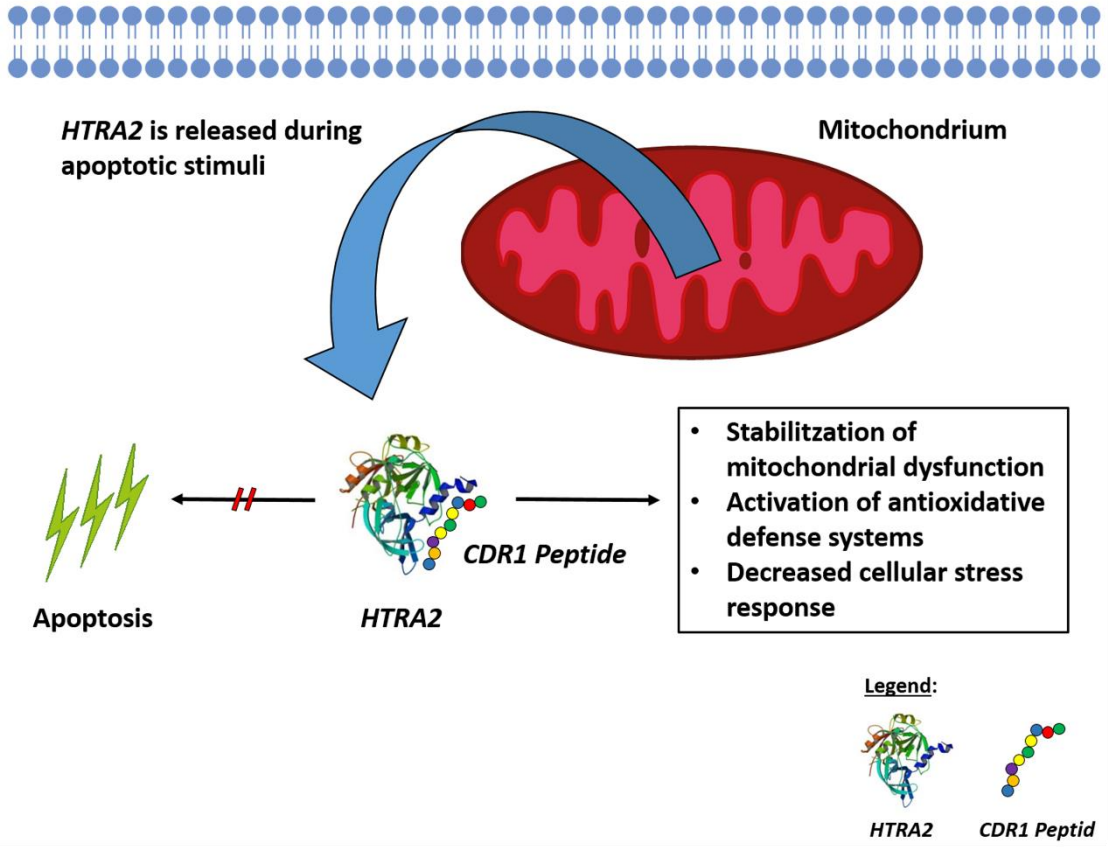

Figure 3: Potential mechanism of action of CDR1 sequence motive *ASGYTFTNYGLSWVR* in the stressed retinal explants. Serine protease *HTRA2* is increasingly released from mitochondria to cytosol during apoptotic stimuli. The CDR-induced inhibition or modulation of the protein activity of *HTRA2* results in decreased apoptotic cell death rates. The specific peptide-protein interaction promotes the stabilization of the mitochondrial dysfunction, the activation of antioxidative defense systems and a decreased cellular stress response.

Overall, we identified a decreased expression of proteins involved in the cellular stress response (e.g. endoplasmic reticulum resident protein 29, *ERP29* and 14-3-3 protein epsilon, *YWHAE*) in CDR-treated retinal explants in comparison to untreated controls accompanied by increased levels of proteins associated with antioxidative and neuroprotective functions (e.g. thioredoxin, *TXN* and GTP-binding nuclear protein RAN, *RAN*). Stress marker protein *ERP29*, for instance, has important functions in protein trafficking, ER homeostasis, cell survival as well as apoptosis [111] and was also found to be upregulated in glaucomatous RGCs in rats [112]. In accordance with that, stress-associated *YWHAE* was significantly increased in

cerebrospinal fluid (CSF) of Alzheimer's disease (AD) patients [113] and seems to play a key role in autophagic processes [114,115]. On the contrary, the CDR-induced expression of protein *TXN* represents an important regulator of the mitochondrial redox homeostasis as well as the ROS neutralization system [116] and significantly increased the life-span of transgenic mice overexpressing human *TXN1* [117]. In addition, CDR-induced upregulation of protein *RAN* serves as important master regulator of the classical import/export cycle in the nucleus [118] and also seems to show a co-expression behavior to *HTRA*2 indicated by pathway analysis. Moreover, transgenic *Grn*-KO mice, which are also deficient in proper *RAN* expression, showed early signs of retinal neurodegeneration processes [118] indicating the important function of *RAN* in eye-related diseases.

In summary, it can be concluded that the synthetic CDR1 peptide *ASGYTFTNYGLSWVR* has neuroprotective effects on RGCs during glaucomatous-like stress conditions by triggering various antiapoptotic signaling pathways and interaction networks. Nevertheless, it still has to be determined if all quantitative proteomic changes may be caused by direct interaction (inhibition) of *HTRA2* with CDR1 sequence motive *ASGYTFTNYGLSWVR* or may result from other CDR-induced downstream signaling pathways.

3.3 Comparison of two solid-phase extraction (SPE) methods for the LC-MS-based characterization of the retinal porcine proteome

The selection of proper sample preparation protocols represents a crucial step prior to LC-MS-based proteomic study designs and greatly influences the quality, sensitivity and robustness of the proteomic data acquisition. Since the trend in MS is nowadays towards the integration of more cost-effective and faster instrumentations without any loss in sensitivity, the aim of the third part of the present thesis was to evaluate two commercial solid-phase extraction (SPE) methods with respect to analytical performance, reproducibility and analysis speed. The ZIPTIP® C18 pipette tips from Merck Millipore represent the current standard operation protocol (SOP) for sample cleanup and peptide enrichment prior to LC-MS analysis in our laboratory and was already used in several proteomic study designs [119–123]. Nevertheless, the present SOP is a time-consuming manual task with many repeat cycles per operator and also requires a certain degree of handling experience. In addition, pipette tip-based SPE platforms can only be automated to a very limited degree. Due to that reason, we compared the current SOP for sample clean-up with the less labor-intensive SOLAμ™ HRP

SPE spin plates from Thermo Fisher Scientific in consideration of effort, cost and analysis time factors (see Figure 4). In order to evaluate these properties of both SPE-based sample preparation protocols, protein fractions from retinal tissues of the house swine (*Sus scrofa domesticus*) [63] were used for the qualitative and quantitative LC-MS-based comparison. The house swine represents a promising model organism for studying human eye diseases including neurodegenerative retinal disorders and was already used as *ex vivo* glaucoma model in a former study design [63].

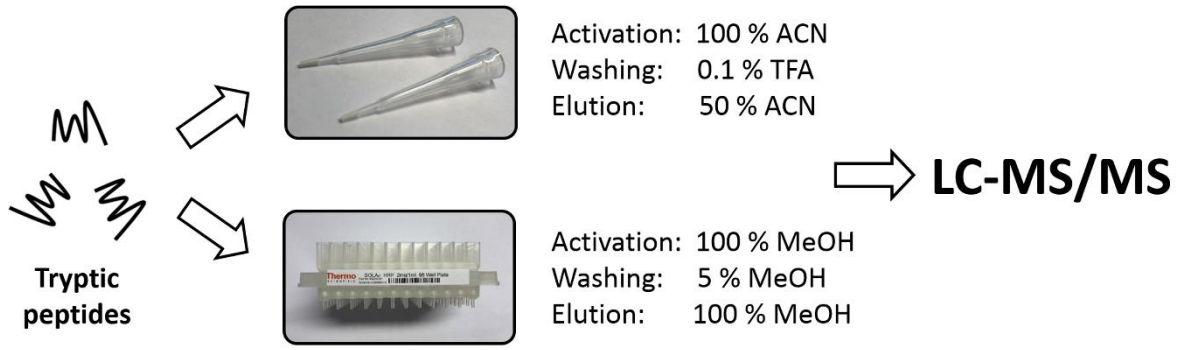

Figure 4*:* Schematic workflow of the two solid-phase extraction (SPE) methods. Purification and enrichment of the tryptic peptides was performed either with ZIPTIP® C18 pipette tips (Merck Millipore) or SOLAμ™ HRP SPE spin plates (Thermo Fisher Scientific) prior to LC-MS/MS analysis. The ZIPTIP® C18 pipette tips were activated with 100 % acetonitrile (ACN), washed with 0.1 % trifluoroacetic acid (TFA) and peptides were eluted with 50 % ACN. The membranes of the SOLAμ™ HRP SPE spin plates were activated with 100 % methanol (MeOH), washed with 5 % MeOH and peptides were eluted with 100 % MeOH.

Both SPE-based sample preparation protocols provided a comprehensive characterization of the complex retinal pig proteome and was in accordance with previous protein catalogues of the pig retina [120,124–126]. The major proportion of the retinal proteins were adequately detected with both SPE-based purification techniques including high abundant proteins such as fructose-bisphosphate aldolase C (*ALDOC*), glial fibrillary acidic protein (*GFAP*) or alpha-enolase (*ENO1*). Differences in the detection profile were more presented by low abundant protein species indicated by low protein ions scores such as 60S ribosomal protein L13 (*RPL13*, protein ion score: 43) exclusively identified by ZIPTIP® C18 method or E3-ubiquitin-protein ligase RBX1 (*RBX1*, protein ion score: 46) exclusively detected by SOLAμ™ HRP spin plates. Indeed, the ZIPTIP® C18 pipette tip method indicated a slightly higher sensitivity regarding peptide/protein identifications over the inspected mass range but was not supported by statistical significance ($P > 0.05$). Also, in terms of quantitative biomarker recovery of specific glaucoma-associated marker candidates, both SPE methods showed an almost equal analytical performance. However, the ease applicability and the convenient

execution protocol of the SOLAμ™ HRP spin plates clearly benefits compared to the time-consuming and labor-intensive ZIPTIP® C18 pipette tip workflow. Due to the high compatibility of the SOLAμ™ HRP spin plates to centrifugal devices or vacuum pump technologies, the present SPE-based workflow is easy to establish in any common research laboratory and allows much more standardization and reproducibility than the manual ZIPTIP® C18 pipette tip protocol. Particularly, clinical research facilities with main focus on LC-MS-based biomarker identification are recommended to use the SOLAμ™ HRP technology for high-throughput discovery proteomic approaches. In addition, the faster sample preparation protocol is also of special interest for the LC-MS-based characterization of the highly diverse antibody repertoire, since it will facilitate the sequencing of larger study cohorts in a shorter timeframe and will accordingly increase the statistical power of the proteomic data.

3.4 Critical discussion

The present doctoral thesis comprises a state-of-the-art LC-MS-based *de novo* profiling strategy for the identification of new biomarker candidates in sera of glaucoma patients. Serum is a complex biological body fluid containing various proteins, vitamins, hormones, carbohydrates, lipids, amino acids and electrolytes and was previously termed as the most diverse and complex human proteome [127,128]. Due to its circular flow through the body and the permanent contact to several tissues or organs, serum represents an attractive source for biomarker discovery in various diseases [129]. Nevertheless, the presence of high abundant proteins still interferes with the proper LC-MS-based identification and quantification of low abundant and disease-specific biomarker candidates. Particularly albumin contributes with up to 50 % to total serum proteome and hampers the LC-MS analysis by masking effects without previously performed prefractionation steps or depletion techniques [130].

However, the present thesis focused on the LC-MS-based analytical characterization of highly diverse IgG molecules, which represent a high abundant protein family in the human serum proteome. With a proportion of 25 % Ig molecules are the second major protein constituent of the serum and especially the IgG isotype represents with a bulk of 80 % the most abundant antibody class [130,131]. In addition, the collection of serum samples can be easily performed during routine clinical trials and counts as a minimally invasive procedure. Due to these reasons, represents the IgG antibody class a highly attractive target for LC-MS-based study

designs focusing the human serum proteome. The hypothesis that the theoretical diversity of antibodies ranging from 10^{11} to 10^{50} completely exceeds the real number of existent antibody molecules per individual (about 10^{12}) has been around for many years and negates the concept of similar antibody structure motives (paratopes) along different individuals [38]. Nevertheless, current studies confirmed the occurrence of identical or similar Ig-derived signature peptides, particularly CDRs, in various diseases and are possibly traced back to common (auto-)antigenic pressures during disease progression or even before onset [70,71,132]. Dekker *et al.* (2011) [133] demonstrated the sensitive and accurate LC-MS-based detection of specific CDR peptides at relatively low concentration levels (in the range of 10^{-15}-10^{-18} mol) and proved the general identification of clinically relevant CDR peptides in patient samples. Several studies also verified relative high concentrations of specific AABs in the blood serum ranging from 1 till 100 µg/ml [134,135] facilitating the potential detection of these immune-related biomarker candidates by LC-MS. In contrast, tumor-specific proteins secreted by the respective tumor cells occur in much lower concentrations in the blood serum (e.g. PSA from 2.6 to 4 ng/ml) due to a lower expression levels, increased degradation rates and specific clearance [73,136]. Based on this knowledge, antibodies provide much more potential as diagnostic or prognostic marker candidates than the respective antigens and are much easier to detect in terms of natural bioavailability. The present study (manuscript I: chapter 2.1) resulted in the LC-MS-based identification of several sera-derived IgG V domain peptide motives which may be consistent with the pathogenesis of glaucoma. Nevertheless, various other factors such as advanced age [32], gender-specific differences [33], genetic susceptibility [30] and even primary diseases or infections [31,137] are known to influence the complex natural AAB repertoire and hamper the identification of specific and unique immune-related biomarker candidates. To overcome this problem, the definition of strict selection criteria for the study participants are essential for the reliability and robustness of the respective study results.

Furthermore, in the second part of this doctoral thesis (manuscript II: chapter 2.2) we could confirm that specific synthetic CDR peptides show a close connection to the pathophysiology of glaucoma and also have a great potential as therapeutic agents in future glaucoma therapy. Saying this, we have to note that the adolescent retina organ culture used as model to prove the CDR-induced effects on RGCs *ex vivo* also shows several limitations and disadvantages compared to the complex pathomechanism found in glaucoma patients. The optic nerve cut

(ONC) during slaughtering serves as stress factor for the RGCs in the *ex vivo* glaucoma model and leads to a significant loss of RGCs after 24 h of incubation. Kalesnykas *et al.* (2012) [138] demonstrated that the optic nerve crush in mice leads too much higher RGC loss and decreased neurite outgrowth compared to a IOP-dependent experimental glaucoma animal model. This highlights the importance of different stress factors on the degree of neurological damage in both glaucoma model systems. Nowadays, the general applicability of cell cultures experiments in glaucoma research is clearly restricted due to the controversial origin of the immortalized cell line such as RGC-5 [139] and impairs the selection of proper glaucoma model systems *in vitro*. Indeed, various *in vivo* glaucoma animal models are characterized by constant and moderate IOP elevations accompanied by glaucoma-like damages (as reviewed in [140]), but there is still no ideal model system which mirrors all main characteristics of glaucoma. Considering the trend to reduce or replace the need for animal experiments, *in vitro* designed experimental set-ups represent excellent alternatives to provide first valuable hints about the applicability and effectiveness of potential drug candidates. In conclusion, the present thesis provided important new insights into the complex autoimmune processes in glaucoma and emphasized synthetic CDR peptides as innovative new strategy in glaucoma therapy.

4 Conclusion and outlook

The main objective of the present doctoral thesis was to unravel the complex biological function and activity of AABs and to evaluate their potential role in the development or progression of glaucoma. To answer these questions, the present work comprises a state-of-the-art LC-MS-based *de novo* screening technology to characterize highly diverse systemic IgG antibody molecules and to identify new immune-related biomarker candidates (manuscript I). Beyond that, the present project offers a completely new therapeutic strategy for the treatment of glaucoma based on synthetic polyclonal-derived CDR peptides. (manuscript II). As final part of the thesis, we compared the performance of two commercial SPE technologies for sample preparation and peptide enrichment to increase the speed, robustness and sensitivity of the current LC-MS-based proteomic platform (manuscript III).

As first part of the doctoral thesis, the LC-MS-based discovery proteomic platform provided the identification of 75 peptides of the variable IgG domain serving as potential biomarker candidates in POAG patients. Up to 28 of these marker candidates were further validated by targeted MS and proved for the first time that glaucoma is accompanied by significant changes in the structural arrangement of the variable antibody domain. Sequence annotation revealed 5 CDR1, 2 CDR2 and 1 CDR3 peptides serving as active binding sites of probably glaucoma-associated AABs. Furthermore, we observed significant shifts in the variable heavy chain family distribution (VH2: ↓ and VH3: ↑ in POAG) and disturbed κ/λ ratios in glaucoma patients providing strong evidence that the disease pattern goes along with systemic effects on the antibody production and B cell maturation. As future prospective, it would be of interest to apply the established LC-MS-based analytical platform to other glaucoma subgroups (NTG and PEXG) and risk groups (OHT) in order to identify new subgroup-specific IgG V domain peptides which may be suitable for group classification. Beyond that, the expression of the specific signature peptides could be also screened in longitudinal study designs to evaluate the prognostic potential of these immunopeptides as sensitive indicator for disease progression. The Gutenberg Health Study (GHS) at the University Medical Center in Mainz represents a prospective and population-based study center for various diseases including glaucoma and would offer optimal conditions for these long-term observations [141]. Furthermore, the application of additional endopeptidases (e.g. Asp-N) for the enzymatic digest could also significantly increase the identification rates of highly diverse CDR peptides. At the beginning of most CDR3 regions, for instance, is a lysine or arginine

residue determining the cleavage site for trypsin [73]. Particular the VH CDR3 plays a key role in antigen recognition processes and is highly important for the formation of proper antigen-antibody complexes [142]. Tryptic CDR3 peptides without N-terminal parts of the flanking sequence are difficult to sequence by LC-MS and could be avoided by multiple enzyme digests providing important additional sequence information.

Based on the previous results, in the second part of the doctoral thesis we could demonstrate that specific glaucoma-associated CDR1 peptides show a neuroprotective effect on RGCs *ex vivo* by stabilization of the mitochondrial homeostasis and the activation of antioxidative defense systems. These study results confirm the immense potential of synthetic CDR peptides in future glaucoma therapy and emphasize their versatile functions as neuroprotective compounds. Particularly, CDR1 sequence motive *AS<u>GYTFTNYG</u>LSWVR* seems to inhibit or modulate the molecular function of retinal protein *HTRA2* (mitochondrial) resulting in lesser cellular stress levels and higher RGC survival rates *in vitro*. However, if this specific CDR peptide-protein interaction may block important binding sites or leads to specific conformational changes of *HTRA2* has still to be determined. Nevertheless, previous studies already confirmed that the specific inhibition of the catalytic domain significantly decreases the proteolytic activity of *HTRA2* and leads to much lesser apoptotic cell death rates *in vivo* and *ex vivo* [143,144]. In future studies it should be focused, if further synthetic CDR peptides may also show neuroprotective properties on RGCs and could provide the basis for a synergistic combination therapy in glaucoma treatment by different mode of actions.

As final part of the present doctoral thesis, we compared our current pipette tip-based SPE workflow (ZIPTIP® C18 SPE from Merck Millipore) for sample clean-up and peptide enrichment prior to LC-MS analysis with the centrifugal-based SPE spin plates (SOLAμ™ HRP SPE from Thermo Fisher Scientific). Both SPE purification platforms worked equally well regarding the analytical performance and protein/peptides recovery properties, whereas the execution of the SPE spin plate workflow provides much more standardizations and time saving aspects compared to the pipette tip-based SPE method. In future it would be of interest to develop a new mixed-mode spin plate which benefits from the characteristics of both SPE materials (C18 and HRP). This may lead to a more sensitive and accurate MS-based detection of retinal proteins and would present a clear improvement for quantitative proteomic study designs. Moreover, the faster and semi-automatic characteristics of the new sample preparation protocol are also beneficial for the previous parts of the doctoral thesis, since it will facilitate

the high-throughput analysis of larger study cohorts and will significantly increase the statistical robustness and reliability of study results in future.

5 References

1. Weinreb, R.N.; Aung, T.; Medeiros, F.A. The pathophysiology and treatment of glaucoma: a review. *JAMA* **2014**, *311*, 1901–1911.
2. Tham, Y.-C.; Li, X.; Wong, T.Y.; Quigley, H.A.; Aung, T.; Cheng, C.-Y. Global prevalence of glaucoma and projections of glaucoma burden through 2040: A systematic review and meta-analysis. *Ophthalmology* **2014**, *121*, 2081–2090.
3. Guedes, G.; Tsai, J.C.; Loewen, N.A. Glaucoma and aging. *Curr. Aging Sci.* **2011**, *4*, 110–117.
4. Flammer, J.; Orgul, S.; Costa, V.P.; Orzalesi, N.; Krieglstein, G.K.; Serra, L.M.; Renard, J.-P.; Stefansson, E. The impact of ocular blood flow in glaucoma. *Prog. Retin. Eye Res.* **2002**, *21*, 359–393.
5. Garcia-Valenzuela, E.; Shareef, S.; Walsh, J.; Sharma, S.C. Programmed cell death of retinal ganglion cells during experimental glaucoma. *Exp. Eye Res.* **1995**, *61*, 33–44.
6. Kong, G.Y.X.; van Bergen, N.J.; Trounce, I.A.; Crowston, J.G. Mitochondrial dysfunction and glaucoma. *J. Glaucoma* **2009**, *18*, 93–100.
7. Tikunova, E.V.; Churnosov, M.I. Genetic studies of primary open-angle glaucoma. *Vestn. Oftalmol.* **2014**, *130*, 96–99.
8. Bell, K.; Gramlich, O.W.; von Thun Und Hohenstein-Blaul, Nadine; Beck, S.; Funke, S.; Wilding, C.; Pfeiffer, N.; Grus, F.H. Does autoimmunity play a part in the pathogenesis of glaucoma? *Prog. Retin. Eye Res.* **2013**, *36*, 199–216.
9. Wax, M.B. The case for autoimmunity in glaucoma. *Exp. Eye Res.* **2011**, *93*, 187–190.
10. Weinreb, R.N.; Khaw, P.T. Primary open-angle glaucoma. *Lancet (London, England)* **2004**, *363*, 1711–1720.
11. Fea, A.M.; Bertaina, L.; Consol, G.; i; Damato, D.; Lorenzi, U.; Grignolo, F.M. Angle Closure Glaucoma: Pathogenesis and Evaluation. A Review. *Journal of Clinical & Experimental Ophthalmology* **2012**, *3*, 1–17.
12. Gutteridge, I.F. Normal tension glaucoma: diagnostic features and comparisons with primary open angle glaucoma. *Clin. Exp. Optom.* **2000**, *83*, 161–172.
13. Gordon, M.O.; Beiser, J.A.; Brandt, J.D.; Heuer, D.K.; Higginbotham, E.J.; Johnson, C.A.; Keltner, J.L.; Miller, J.P.; Parrish, R.K.; Wilson, M.R.*; et al.* The Ocular Hypertension Treatment Study: Baseline factors that predict the onset of primary open-angle glaucoma. *Arch. Ophthalmol.* **2002**, *120*, 714-20; discussion 829-30.
14. Vazquez, L.E.; Lee, R.K. Genomic and Proteomic Pathophysiology of Pseudoexfoliation Glaucoma. *International ophthalmology clinics* **2014**, *54*, 1–13.
15. Conlon, R.; Saheb, H.; Ahmed, I.I.K. Glaucoma treatment trends: A review. *Canadian journal of ophthalmology. Journal canadien d'ophtalmologie* **2017**, *52*, 114–124.
16. Hoxha, G.; Spahiu, K.; Kaçaniku, G.; Ismajli-Hoxha, F.; Ismaili, M. Comparison of prostaglandin analogue, beta-blockers and prostaglandin analogue/beta-blockers fixed combination in patients with primary open-angle glaucoma. *Spektrum der Augenheilkunde* **2013**, *27*, 239–244.

17. Webers, C.A.B.; Beckers, H.J.M.; Zeegers, M.P.; Nuijts, R.M.M.A.; Hendrikse, F.; Schouten, J.S.A.G. The intraocular pressure-lowering effect of prostaglandin analogs combined with topical beta-blocker therapy: A systematic review and meta-analysis. *Ophthalmology* **2010**, *117*, 2067-74.e1-6.

18. Inoue, K. Managing adverse effects of glaucoma medications. *Clinical Ophthalmology (Auckland, N.Z.)* **2014**, *8*, 903–913.

19. Nagar, M.; Ogunyomade, A.; O'Brart, D.P.S.; Howes, F.; Marshall, J. A randomised, prospective study comparing selective laser trabeculoplasty with latanoprost for the control of intraocular pressure in ocular hypertension and open angle glaucoma. *Br. J. Ophthalmol.* **2005**, *89*, 1413–1417.

20. Damji, K.F.; Shah, K.C.; Rock, W.J.; Bains, H.S.; Hodge, W.G. Selective laser trabeculoplasty v argon laser trabeculoplasty: A prospective randomised clinical trial. *The British journal of ophthalmology* **1999**, *83*, 718–722.

21. Bovell, A.M.; Damji, K.F.; Hodge, W.G.; Rock, W.J.; Buhrmann, R.R.; Pan, Y.I. Long term effects on the lowering of intraocular pressure: Selective laser or argon laser trabeculoplasty? *Canadian journal of ophthalmology. Journal canadien d'ophtalmologie* **2011**, *46*, 408–413.

22. Kerrigan-Baumrind, L.A.; Quigley, H.A.; Pease, M.E.; Kerrigan, D.F.; Mitchell, R.S. Number of ganglion cells in glaucoma eyes compared with threshold visual field tests in the same persons. *Investigative ophthalmology & visual science* **2000**, *41*, 741–748.

23. Zhang, C.; Tatham, A.J.; Weinreb, R.N.; Zangwill, L.M.; Yang, Z.; Zhang, J.Z.; Medeiros, F.A. Relationship between ganglion cell layer thickness and estimated retinal ganglion cell counts in the glaucomatous macula. *Ophthalmology* **2014**, *121*, 2371–2379.

24. Nayak, B.K.; Maskati, Q.B.; Parikh, R. The unique problem of glaucoma: Under-diagnosis and over-treatment. *Indian Journal of Ophthalmology* **2011**, *59*, S1-2.

25. Abbas, A.K.; Lichtman, A.H.; Pillai, S. *Cellular and molecular immunology*, 7th ed; Saunders Elsevier: Philadelphia, Pa., 2011.

26. Kawai, T.; Akira, S. The role of pattern-recognition receptors in innate immunity: update on Toll-like receptors. *Nature immunology* **2010**, *11*, 373–384.

27. Miller, J.F. Immune self-tolerance mechanisms. *Transplantation* **2001**, *72*, S5-9.

28. Kohler, H.; Bayry, J.; Nicoletti, A.; Kaveri, S.V. Natural autoantibodies as tools to predict the outcome of immune response? *Scandinavian journal of immunology* **2003**, *58*, 285–289.

29. Oppezzo, P.; Dighiero, G. Autoantibodies, tolerance and autoimmunity. *Pathologie-biologie* **2003**, *51*, 297–304.

30. Gutierrez-Roelens, I.; Lauwerys, B.R. Genetic susceptibility to autoimmune disorders: clues from gene association and gene expression studies. *Current molecular medicine* **2008**, *8*, 551–561.

31. Rosenblum, M.D.; Remedios, K.A.; Abbas, A.K. Mechanisms of human autoimmunity. *The Journal of clinical investigation* **2015**, *125*, 2228–2233.

32. Goronzy, J.J.; Weyand, C.M. Immune aging and autoimmunity. *Cellular and molecular life sciences : CMLS* **2012**, *69*, 1615–1623.

33. Ngo, S.T.; Steyn, F.J.; McCombe, P.A. Gender differences in autoimmune disease. *Frontiers in Neuroendocrinology* **2014**, *35*, 347–369.

34. Kaplan, H.J.; Niederkorn, J.Y. *Regional Immunity and Immune Privilege*; Karger Publishers, 2007.

35. Streilein, J.W. Immunoregulatory mechanisms of the eye. *Progress in retinal and eye research* **1999**, *18*, 357–370.

36. Zhou, R.; Caspi, R.R. Ocular immune privilege. *F1000 Biology Reports* **2010**, *2*.

37. Schroeder, H.W., JR; Cavacini, L. Structure and function of immunoglobulins. *J. Allergy Clin. Immunol.* **2010**, *125*, 52.

38. Li, Z.; Woo, C.J.; Iglesias-Ussel, M.D.; Ronai, D.; Scharff, M.D. The generation of antibody diversity through somatic hypermutation and class switch recombination. *Genes Dev.* **2004**, *18*, 1–11.

39. Arnold, J.N.; Wormald, M.R.; Sim, R.B.; Rudd, P.M.; Dwek, R.A. The impact of glycosylation on the biological function and structure of human immunoglobulins. *Annual review of immunology* **2007**, *25*, 21–50.

40. Wax, M.B.; Barrett, D.A.; Pestronk, A. Increased incidence of paraproteinemia and autoantibodies in patients with normal-pressure glaucoma. *Am. J. Ophthalmol.* **1994**, *117*, 561–568.

41. Joachim, S.C.; Wuenschig, D.; Pfeiffer, N.; Grus, F.H. IgG antibody patterns in aqueous humor of patients with primary open angle glaucoma and pseudoexfoliation glaucoma. *Mol. Vis.* **2007**, *13*, 1573–1579.

42. Joachim, S.C.; Bruns, K.; Lackner, K.J.; Pfeiffer, N.; Grus, F.H. Antibodies to alpha B-crystallin, vimentin, and heat shock protein 70 in aqueous humor of patients with normal tension glaucoma and IgG antibody patterns against retinal antigen in aqueous humor. *Current eye research* **2007**, *32*, 501–509.

43. Latalska, M.; Gerkowicz, M.; Kosior-Jarecka, E.; Koziol-Montewka, M.; Pietras-Trzpiel, M. Serum and aqueous humor antibodies to beta-2 glycoprotein I in patients with glaucoma and cataract. *Klinika oczna* **2004**, *106*, 162–163.

44. Wax, M.B.; Tezel, G.; Kawase, K.; Kitazawa, Y. Serum autoantibodies to heat shock proteins in glaucoma patients from Japan and the United States. *Ophthalmology* **2001**, *108*, 296–302.

45. Wax, M.B.; Tezel, G.; Saito, I.; Gupta, R.S.; Harley, J.B.; Li, Z.; Romano, C. Anti-Ro/SS-A positivity and heat shock protein antibodies in patients with normal-pressure glaucoma. *Am. J. Ophthalmol.* **1998**, *125*, 145–157.

46. Joachim, S.C.; Reichelt, J.; Berneiser, S.; Pfeiffer, N.; Grus, F.H. Sera of glaucoma patients show autoantibodies against myelin basic protein and complex autoantibody profiles against human optic nerve antigens. *Graefes Arch. Clin. Exp. Ophthalmol.* **2008**, *246*, 573–580.

47. Grus, F.H.; Joachim, S.C.; Bruns, K.; Lackner, K.J.; Pfeiffer, N.; Wax, M.B. Serum autoantibodies to alpha-fodrin are present in glaucoma patients from Germany and the United States. *Invest. Ophthalmol. Vis. Sci.* **2006**, *47*, 968–976.

48. Tezel, G.; Edward, D.P.; Wax, M.B. Serum autoantibodies to optic nerve head glycosaminoglycans in patients with glaucoma. *Arch. Ophthalmol.* **1999**, *117*, 917–924.

49. Maruyama, I.; Ohguro, H.; Ikeda, Y. Retinal ganglion cells recognized by serum autoantibody against gamma-enolase found in glaucoma patients. *Invest. Ophthalmol. Vis. Sci.* **2000**, *41*, 1657–1665.

50. Maruyama, I.; Ikeda, Y.; Nakazawa, M.; Ohguro, H. Clinical roles of serum autoantibody against neuron-specific enolase in glaucoma patients. *Tohoku J. Exp. Med.* **2002**, *197*, 125–132.

51. Yang, J.; Tezel, G.; Patil, R.V.; Romano, C.; Wax, M.B. Serum autoantibody against glutathione S-transferase in patients with glaucoma. *Invest. Ophthalmol. Vis. Sci.* **2001**, *42*, 1273–1276.

52. Grus, F.H.; Joachim, S.C.; Sandmann, S.; Thiel, U.; Bruns, K.; Lackner, K.J.; Pfeiffer, N. Transthyretin and complex protein pattern in aqueous humor of patients with primary open-angle glaucoma. *Mol. Vis.* **2008**, *14*, 1437–1445.

53. Joachim, S.C.; Pfeiffer, N.; Grus, F.H. Autoantibodies in patients with glaucoma: a comparison of IgG serum antibodies against retinal, optic nerve, and optic nerve head antigens. *Graefes Arch. Clin. Exp. Ophthalmol.* **2005**, *243*, 817–823.

54. Reindl, M.; Linington, C.; Brehm, U.; Egg, R.; Dilitz, E.; Deisenhammer, F.; Poewe, W.; Berger, T. Antibodies against the myelin oligodendrocyte glycoprotein and the myelin basic protein in multiple sclerosis and other neurological diseases: A comparative study. *Brain : a journal of neurology* **1999**, *122 (Pt 11)*, 2047–2056.

55. Mario Gonzalez-Gronow1, 2*, Salvatore V. Pizzo2 1Department of Biological Sciences, Laboratory of Environmental Neurotoxicology, Faculty of Medicine, Universidad Católica del Norte, Coquimbo, Chile 2Department of Pathology, Duke University Medical Center, Durham, NC, USA. *Relevance of Catalytic Autoantibodies to Myelin Basic Protein (MBP) in Autoimmune Disorders*; SciAccess Publishers, 2018.

56. Oakley, A. Glutathione transferases: A structural perspective. *Drug metabolism reviews* **2011**, *43*, 138–151.

57. Tezel, G.; Wax, M.B. The mechanisms of hsp27 antibody-mediated apoptosis in retinal neuronal cells. *J. Neurosci.* **2000**, *20*, 3552–3562.

58. Joachim, S.C.; Gramlich, O.W.; Laspas, P.; Schmid, H.; Beck, S.; Pein, H.D. von; Dick, H.B.; Pfeiffer, N.; Grus, F.H. Retinal ganglion cell loss is accompanied by antibody depositions and increased levels of microglia after immunization with retinal antigens. *PLoS ONE* **2012**, *7*, e40616.

59. Shoenfeld, Y.; Toubi, E. Protective autoantibodies: Role in homeostasis, clinical importance, and therapeutic potential. *Arthritis & Rheumatism* **2005**, *52*, 2599–2606.

60. Wilding, C.; Bell, K.; Beck, S.; Funke, S.; Pfeiffer, N.; Grus, F.H. γ-Synuclein antibodies have neuroprotective potential on neuroretinal cells via proteins of the mitochondrial apoptosis pathway. *PLoS ONE* **2014**, *9*, e90737.

61. Bell, K.; Wilding, C.; Funke, S.; Pfeiffer, N.; Grus, F.H. Protective effect of 14-3-3 antibodies on stressed neuroretinal cells via the mitochondrial apoptosis pathway. *BMC Ophthalmol.* **2015**, *15*, 64.

62. Wilding, C.; Bell, K.; Funke, S.; Beck, S.; Pfeiffer, N.; Grus, F.H. GFAP antibodies show protective effect on oxidatively stressed neuroretinal cells via interaction with ERP57. *Journal of pharmacological sciences* **2015**, *127*, 298–304.

63. Bell, K.; Wilding, C.; Funke, S.; Perumal, N.; Beck, S.; Wolters, D.; Holz-Muller, J.; Pfeiffer, N.; Grus, F.H. Neuroprotective effects of antibodies on retinal ganglion cells in an adolescent retina organ culture. *J. Neurochem.* **2016**, *139*, 256–269.

64. Teister, J.; Anders, F.; Beck, S.; Funke, S.; Pein, H. von; Prokosch, V.; Pfeiffer, N.; Grus, F. Decelerated neurodegeneration after intravitreal injection of α-synuclein antibodies in a glaucoma animal model. *Sci. Rep.* **2017**, *7*, 6260.

65. Kraj, A.; Silberring, J., Eds. *Introduction to Proteomics*, 1st ed; Wiley, J: New York, NY, 2008.

66. Zhao, J.; Patwa, T.H.; Pal, M.; Qiu, W.; Lubman, D.M. Analysis of Protein Glycosylation and Phosphorylation Using Liquid Phase Separation, Protein Microarray Technology, and Mass Spectrometry. *Methods in molecular biology (Clifton, N.J.)* **2009**, *492*, 321–351.

67. Resing, K.A.; Ahn, N.G. Proteomics strategies for protein identification. *FEBS Letters* **2005**, *579*, 885–889.

68. Chiou, S.-H.; Wu, C.-Y. Clinical proteomics: current status, challenges, and future perspectives. *The Kaohsiung journal of medical sciences* **2011**, *27*, 1–14.

69. Poletaev, A.; Boura, P. The immune system, natural autoantibodies and general homeostasis in health and disease. *Hippokratia* **2011**, *15*, 295–298.

70. Hoogeboom, R.; van Kessel, Kok P M; Hochstenbach, F.; Wormhoudt, T.A.; Reinten, R.J.A.; Wagner, K.; Kater, A.P.; Guikema, J.E.J.; Bende, R.J.; van Noesel, Carel J M. A mutated B cell chronic lymphocytic leukemia subset that recognizes and responds to fungi. *J. Exp. Med.* **2013**, *210*, 59–70.

71. Scheid, J.F.; Mouquet, H.; Ueberheide, B.; Diskin, R.; Klein, F.; Oliveira, T.Y.K.; Pietzsch, J.; Fenyo, D.; Abadir, A.; Velinzon, K.*; et al.* Sequence and structural convergence of broad and potent HIV antibodies that mimic CD4 binding. *Science* **2011**, *333*, 1633–1637.

72. VanDuijn, M.M.; Dekker, Lennard J M; Zeneyedpour, L.; Smitt, Peter A E Sillevis; Luider, T.M. Immune responses are characterized by specific shared immunoglobulin peptides that can be detected by proteomic techniques. *J. Biol. Chem.* **2010**, *285*, 29247–29253.

73. Costa, D. de; Broodman, I.; VanDuijn, M.M.; Stingl, C.; Dekker, Lennard J M; Burgers, P.C.; Hoogsteden, H.C.; Sillevis Smitt, Peter A E; van Klaveren, Rob J; Luider, T.M. Sequencing and quantifying IgG fragments and antigen-binding regions by mass spectrometry. *J. Proteome Res.* **2010**, *9*, 2937–2945.

74. Costa, D. de; Broodman, I.; Calame, W.; Stingl, C.; Dekker, Lennard J M; Vernhout, R.M.; de Koning, Harry J; Hoogsteden, H.C.; Sillevis Smitt, Peter A E; van Klaveren, Rob J*; et al.* Peptides from the variable region of specific antibodies are shared among lung cancer patients. *PLoS ONE* **2014**, *9*, e96029.

75. Singh, V.; Stoop, M.P.; Stingl, C.; Luitwieler, R.L.; Dekker, L.J.; van Duijn, M.M.; Kreft, K.L.; Luider, T.M.; Hintzen, R.Q. Cerebrospinal-fluid-derived immunoglobulin G of different multiple sclerosis patients shares mutated sequences in complementarity determining regions. *Mol. Cell. Proteomics* **2013**, *12*, 3924–3934.

76. Sela-Culang, I.; Kunik, V.; Ofran, Y. The Structural Basis of Antibody-Antigen Recognition. *Frontiers in Immunology* **2013**, *4*.

77. Gramlich, O.W.; Beck, S.; von Thun Und Hohenstein-Blaul, Nadine; Boehm, N.; Ziegler, A.; Vetter, J.M.; Pfeiffer, N.; Grus, F.H. Enhanced insight into the autoimmune component of glaucoma: IgG autoantibody accumulation and pro-inflammatory conditions in human glaucomatous retina. *PLoS ONE* **2013**, *8*, e57557.

78. Joachim, S.C.; Mondon, C.; Gramlich, O.W.; Grus, F.H.; Dick, H.B. Apoptotic retinal ganglion cell death in an autoimmune glaucoma model is accompanied by antibody depositions. *J. Mol. Neurosci.* **2014**, *52*, 216–224.

79. Kuehn, M.H.; Kim, C.Y.; Ostojic, J.; Bellin, M.; Alward, W.L.M.; Stone, E.M.; Sakaguchi, D.S.; Grozdanic, S.D.; Kwon, Y.H. Retinal synthesis and deposition of complement components induced by ocular hypertension. *Experimental eye research* **2006**, *83*, 620–628.

80. Scamurra, R.W.; Miller, D.J.; Dahl, L.; Abrahamsen, M.; Kapur, V.; Wahl, S.M.; Milner, E.C.; Janoff, E.N. Impact of HIV-1 infection on VH3 gene repertoire of naive human B cells. *Journal of immunology (Baltimore, Md. : 1950)* **2000**, *164*, 5482–5491.

81. Berberian, L.; Shukla, J.; Jefferis, R.; Braun, J. Effects of HIV infection on VH3 (D12 idiotope) B cells in vivo. *Journal of acquired immune deficiency syndromes* **1994**, *7*, 641–646.

82. Berberian, L.; Valles-Ayoub, Y.; Sun, N.; Martinez-Maza, O.; Braun, J. A VH clonal deficit in human immunodeficiency virus-positive individuals reflects a B-cell maturational arrest. *Blood* **1991**, *78*, 175–179.

83. Joachim, S.C.; Reinehr, S.; Kuehn, S.; Laspas, P.; Gramlich, O.W.; Kuehn, M.; Tischoff, I.; Pein, H.D. von; Dick, H.B.; Grus, F.H. Immune response against ocular tissues after immunization with optic nerve antigens in a model of autoimmune glaucoma. *Molecular Vision* **2013**, *19*, 1804–1814.

84. Joachim, S.C.; Wax, M.B.; Seidel, P.; Pfeiffer, N.; Grus, F.H. Enhanced characterization of serum autoantibody reactivity following HSP 60 immunization in a rat model of experimental autoimmune glaucoma. *Current eye research* **2010**, *35*, 900–908.

85. Figueiredo, C.R.; Matsuo, A.L.; Massaoka, M.H.; Polonelli, L.; Travassos, L.R. Anti-tumor activities of peptides corresponding to conserved complementary determining regions from different immunoglobulins. *Peptides* **2014**, *59*, 14–19.

86. Dobroff, A.S.; Rodrigues, E.G.; Juliano, M.A.; Friaca, D.M.; Nakayasu, E.S.; Almeida, I.C.; Mortara, R.A.; Jacysyn, J.F.; Amarante-Mendes, G.P.; Magliani, W.*; et al.* Differential Antitumor Effects of IgG and IgM Monoclonal Antibodies and Their Synthetic Complementarity-Determining Regions Directed to New Targets of B16F10-Nex2 Melanoma Cells. *Transl. Oncol.* **2010**, *3*, 204–217.

87. Polonelli, L.; Ciociola, T.; Sperindè, M.; Giovati, L.; D'Adda, T.; Galati, S.; Travassos, L.R.; Magliani, W.; Conti, S. Fungicidal activity of peptides encoded by immunoglobulin genes. *Sci. Rep.* **2017**, *7*, 10896.

88. Polonelli, L.; Ponton, J.; Elguezabal, N.; Moragues, M.D.; Casoli, C.; Pilotti, E.; Ronzi, P.; Dobroff, A.S.; Rodrigues, E.G.; Juliano, M.A.*; et al.* Antibody complementarity-determining regions (CDRs) can display differential antimicrobial, antiviral and antitumor activities. *PLoS ONE* **2008**, *3*, e2371.

89. Gabrielli, E.; Pericolini, E.; Cenci, E.; Ortelli, F.; Magliani, W.; Ciociola, T.; Bistoni, F.; Conti, S.; Vecchiarelli, A.; Polonelli, L. Antibody complementarity-determining regions (CDRs): A bridge between adaptive and innate immunity. *PLoS ONE* **2009**, *4*, e8187.

90. Sharabi, A.; Sthoeger, Z.M.; Mahlab, K.; Lapter, S.; Zinger, H.; Mozes, E. A tolerogenic peptide that induces suppressor of cytokine signaling (SOCS)-1 restores the aberrant control of IFN-gamma signaling in lupus-affected (NZB x NZW)F1 mice. *Clinical immunology (Orlando, Fla.)* **2009**, *133*, 61–68.

91. Sharabi, A.; Dayan, M.; Zinger, H.; Mozes, E. A new model of induced experimental systemic lupus erythematosus (SLE) in pigs and its amelioration by treatment with a tolerogenic peptide. *J. Clin. Immunol.* **2010**, *30*, 34–44.

92. Gabrielli, E.; Pericolini, E.; Cenci, E.; Monari, C.; Magliani, W.; Ciociola, T.; Conti, S.; Gatti, R.; Bistoni, F.; Polonelli, L.*; et al.* Antibody Constant Region Peptides Can Display Immunomodulatory Activity through Activation of the Dectin-1 Signalling Pathway. *PLoS ONE* **2012**, *7*, e43972.

93. Samaranayake, H.; Wirth, T.; Schenkwein, D.; Raty, J.K.; Yla-Herttuala, S. Challenges in monoclonal antibody-based therapies. *Annals of medicine* **2009**, *41*, 322–331.

94. Frenzel, A.; Kügler, J.; Helmsing, S.; Meier, D.; Schirrmann, T.; Hust, M.; Dübel, S. Designing Human Antibodies by Phage Display. *Transfusion Medicine and Hemotherapy* **2017**, *44*, 312–318.

95. Kim, J.H.; Hong, H.J. Humanization by CDR grafting and specificity-determining residue grafting. *Methods in molecular biology (Clifton, N.J.)* **2012**, *907*, 237–245.

96. Murali, R.; Greene, M.I. Structure based antibody-like peptidomimetics. *Pharmaceuticals (Basel, Switzerland)* **2012**, *5*, 209–235.

97. Brosh, N.; Zinger, H.; Mozes, E. Treatment of induced murine SLE with a peptide based on the CDR3 of an anti-DNA antibody reverses the pattern of pathogenic cytokines. *Autoimmunity* **2002**, *35*, 211–219.

98. Fellouse, F.A.; Wiesmann, C.; Sidhu, S.S. Synthetic antibodies from a four-amino-acid code: a dominant role for tyrosine in antigen recognition. *Proceedings of the National Academy of Sciences of the United States of America* **2004**, *101*, 12467–12472.

99. Koide, S.; Sidhu, S.S. The Importance of Being Tyrosine: Lessons in Molecular Recognition from Minimalist Synthetic Binding Proteins. *ACS chemical biology* **2009**, *4*, 325–334.

100. Beckingham, J.A.; Housden, N.G.; Muir, N.M.; Bottomley, S.P.; Gore, M.G. Studies on a single immunoglobulin-binding domain of protein L from Peptostreptococcus magnus: the role of tyrosine-53 in the reaction with human IgG. *The Biochemical journal* **2001**, *353*, 395–401.

101. Masin, J.; Roderova, J.; Osickova, A.; Novak, P.; Bumba, L.; Fiser, R.; Sebo, P.; Osicka, R. The conserved tyrosine residue 940 plays a key structural role in membrane interaction of Bordetella adenylate cyclase toxin. *Scientific reports*, *7*, 9330.

102. Wu, L.; Fu, J.; Shen, S.-H. SKAP55 coupled with CD45 positively regulates T-cell receptor-mediated gene transcription. *Molecular and cellular biology* **2002**, *22*, 2673–2686.

103. Vande Walle, L.; Lamkanfi, M.; Vandenabeele, P. The mitochondrial serine protease HtrA2/Omi: an overview. *Cell death and differentiation* **2008**, *15*, 453–460.

104. Goo, H.-G.; Rhim, H.; Kang, S. Pathogenic Role of Serine Protease HtrA2/Omi in Neurodegenerative Diseases. *Current protein & peptide science* **2017**, *18*, 746–757.

105. Hegde, R.; Srinivasula, S.M.; Zhang, Z.; Wassell, R.; Mukattash, R.; Cilenti, L.; DuBois, G.; Lazebnik, Y.; Zervos, A.S.; Fernandes-Alnemri, T.*; et al.* Identification of Omi/HtrA2 as a mitochondrial apoptotic serine protease that disrupts inhibitor of apoptosis protein-caspase interaction. *The Journal of biological chemistry* **2002**, *277*, 432–438.

106. Kang, S.; Fernandes-Alnemri, T.; Alnemri, E.S. A novel role for the mitochondrial HTRA2/OMI protease in aging. *Autophagy* **2013**, *9*, 420–421.

107. Goo, H.-G.; Jung, M.K.; Han, S.S.; Rhim, H.; Kang, S. HtrA2/Omi deficiency causes damage and mutation of mitochondrial DNA. *Biochimica et biophysica acta* **2013**, *1833*, 1866–1875.

108. Jones, J.M.; Datta, P.; Srinivasula, S.M.; Ji, W.; Gupta, S.; Zhang, Z.; Davies, E.; Hajnoczky, G.; Saunders, T.L.; van Keuren, M.L.*; et al.* Loss of Omi mitochondrial protease activity causes the neuromuscular disorder of mnd2 mutant mice. *Nature* **2003**, *425*, 721–727.

109. Martins, L.M.; Morrison, A.; Klupsch, K.; Fedele, V.; Moisoi, N.; Teismann, P.; Abuin, A.; Grau, E.; Geppert, M.; Livi, G.P.*; et al.* Neuroprotective role of the Reaper-related serine protease HtrA2/Omi revealed by targeted deletion in mice. *Molecular and cellular biology* **2004**, *24*, 9848–9862.

110. Moisoi, N.; Klupsch, K.; Fedele, V.; East, P.; Sharma, S.; Renton, A.; Plun-Favreau, H.; Edwards, R.E.; Teismann, P.; Esposti, M.D.*; et al.* Mitochondrial dysfunction triggered by loss of HtrA2 results in the activation of a brain-specific transcriptional stress response. *Cell death and differentiation* **2009**, *16*, 449–464.

111. McLaughlin, T.; Falkowski, M.; Wang, J.J.; Zhang, S.X. Molecular Chaperone ERp29: A Potential Target for Cellular Protection in Retinal and Neurodegenerative Diseases. *Advances in experimental medicine and biology* **2018**, *1074*, 421–427.

112. Crabb, J.W.; Yuan, X.; Dvoriantchikova, G.; Ivanov, D.; Crabb, J.S.; Shestopalov, V.I. Preliminary Quantitative Proteomic Characterization of Glaucomatous in vivo Rat Retinal Ganglion Cells. *Experimental eye research* **2010**, *91*, 107–110.

113. Skanda, J.; Angela, K.; David, B. Rapidly progressive Alzheimer's disease and elevated 14-3-3 proteins in cerebrospinal fluid **2008**.

114. Jia, H.; Liang, Z.; Zhang, X.; Wang, J.; Xu, W.; Qian, H. 14-3-3 proteins: an important regulator of autophagy in diseases. *American Journal of Translational Research* **2017**, *9*, 4738–4746.

115. Pozuelo-Rubio, M. 14-3-3 Proteins are Regulators of Autophagy. *Cells* **2012**, *1*, 754–773.

116. Holzerova, E.; Danhauser, K.; Haack, T.B.; Kremer, L.S.; Melcher, M.; Ingold, I.; Kobayashi, S.; Terrile, C.; Wolf, P.; Schaper, J.*; et al.* Human thioredoxin 2 deficiency impairs mitochondrial redox homeostasis and causes early-onset neurodegeneration. *Brain* **2016**, *139*, 346–354.

117. Mitsui, A.; Hamuro, J.; Nakamura, H.; Kondo, N.; Hirabayashi, Y.; Ishizaki-Koizumi, S.; Hirakawa, T.; Inoue, T.; Yodoi, J. Overexpression of human thioredoxin in transgenic mice controls oxidative stress and life span. *Antioxidants & redox signaling* **2002**, *4*, 693–696.

118. Ward, M.E.; Taubes, A.; Chen, R.; Miller, B.L.; Sephton, C.F.; Gelfand, J.M.; Minami, S.; Boscardin, J.; Martens, L.H.; Seeley, W.W.*; et al.* Early retinal neurodegeneration and impaired Ran-mediated nuclear import of TDP-43 in progranulin-deficient FTLD. *The Journal of experimental medicine* **2014**, *211*, 1937–1945.

119. Funke, S.; Perumal, N.; Beck, S.; Gabel-Scheurich, S.; Schmelter, C.; Teister, J.; Gerbig, C.; Gramlich, O.W.; Pfeiffer, N.; Grus, F.H. Glaucoma related Proteomic Alterations in Human Retina Samples. *Sci. Rep.* **2016**, *6*, 29759.

120. Funke, S.; Markowitsch, S.; Schmelter, C.; Perumal, N.; Mwiiri, F.K.; Gabel-Scheurich, S.; Pfeiffer, N.; Grus, F.H. In-Depth Proteomic Analysis of the Porcine Retina by Use of a four Step Differential Extraction Bottom up LC MS Platform. *Mol. Neurobiol.* **2016**.

121. Perumal, N.; Funke, S.; Wolters, D.; Pfeiffer, N.; Grus, F.H. Characterization of human reflex tear proteome reveals high expression of lacrimal proline-rich protein 4 (PRR4). *Proteomics* **2015**, *15*, 3370–3381.

122. Perumal, N.; Funke, S.; Pfeiffer, N.; Grus, F.H. Proteomics analysis of human tears from aqueous-deficient and evaporative dry eye patients. *Sci. Rep.* **2016**, *6*, 29629.

123. Manicam, C.; Perumal, N.; Wasielica-Poslednik, J.; Ngongkole, Y.C.; Tschabunin, A.; Sievers, M.; Lisch, W.; Pfeiffer, N.; Grus, F.H.; Gericke, A. Proteomics Unravels the Regulatory Mechanisms in Human Tears Following Acute Renouncement of Contact Lens Use: A Comparison between Hard and Soft Lenses. *Scientific reports* **2018**, *8*, 11526.

124. Cehofski, L.J.; Kruse, A.; Kjaergaard, B.; Stensballe, A.; Honore, B.; Vorum, H. Dye-Free Porcine Model of Experimental Branch Retinal Vein Occlusion: A Suitable Approach for Retinal Proteomics. *Journal of ophthalmology* **2015**, *2015*, 839137.

125. Hauck, S.M.; Schoeffmann, S.; Deeg, C.A.; Gloeckner, C.J.; Swiatek-de Lange, M.; Ueffing, M. Proteomic analysis of the porcine interphotoreceptor matrix. *Proteomics* **2005**, *5*, 3623–3636.

126. McKay, G.J.; Campbell, L.; Oliver, M.; Brockbank, S.; Simpson, D.A.C.; Curry, W.J. Preparation of planar retinal specimens: verification by histology, mRNA profiling, and proteome analysis. *Molecular Vision* **2004**, *10*, 240–247.

127. Chandramouli, K.; Qian, P.-Y. Proteomics: Challenges, Techniques and Possibilities to Overcome Biological Sample Complexity. *Human Genomics and Proteomics : HGP* **2009**, *2009*.

128. Thadikkaran, L.; Siegenthaler, M.A.; Crettaz, D.; Queloz, P.-A.; Schneider, P.; Tissot, J.-D. Recent advances in blood-related proteomics. *Proteomics* **2005**, *5*, 3019–3034.

129. Bhosale, S.D.; Moulder, R.; Kouvonen, P.; Lahesmaa, R.; Goodlett, D.R. Mass Spectrometry-Based Serum Proteomics for Biomarker Discovery and Validation. *Methods in molecular biology (Clifton, N.J.)* **2017**, *1619*, 451–466.

130. Jaros, J.A.J.; Guest, P.C.; Bahn, S.; Martins-de-Souza, D. Affinity depletion of plasma and serum for mass spectrometry-based proteome analysis. *Methods in molecular biology (Clifton, N.J.)* **2013**, *1002*, 1–11.

131. Cassidy, J.T.; Nordby, G.L. Human serum immunoglobulin concentrations: prevalence of immunoglobulin deficiencies. *J. Allergy Clin. Immunol.* **1975**, *55*, 35–48.

132. Obermeier, B.; Mentele, R.; Malotka, J.; Kellermann, J.; Kumpfel, T.; Wekerle, H.; Lottspeich, F.; Hohlfeld, R.; Dornmair, K. Matching of oligoclonal immunoglobulin transcriptomes and proteomes of cerebrospinal fluid in multiple sclerosis. *Nat. Med.* **2008**, *14*, 688–693.

133. Dekker, L.J.M.; Zeneyedpour, L.; Brouwer, E.; van Duijn, M.M.; Sillevis Smitt, Peter A E; Luider, T.M. An antibody-based biomarker discovery method by mass spectrometry sequencing of complementarity determining regions. *Analytical and bioanalytical chemistry* **2011**, *399*, 1081–1091.

134. Willemze, A.; Shi, J.; Mulder, M.; Stoeken-Rijsbergen, G.; Drijfhout, J.W.; Huizinga, T.W.J.; Trouw, L.A.; Toes, R.E.M. The concentration of anticitrullinated protein antibodies in serum and synovial fluid in relation to total immunoglobulin concentrations. *Annals of the rheumatic diseases* **2013**, *72*, 1059–1063.

135. Storace, D.; Cammarata, S.; Borghi, R.; Sanguineti, R.; Giliberto, L.; Piccini, A.; Pollero, V.; Novello, C.; Caltagirone, C.; Smith, M.A.*; et al.* Elevation of β-Amyloid 1-42 Autoantibodies in the Blood of Amnestic Patients With Mild Cognitive Impairment. *Arch Neurol* **2010**, *67*, 867–872.

136. Catalona, W.J.; Smith, D.S.; Ornstein, D.K. Prostate cancer detection in men with serum PSA concentrations of 2.6 to 4.0 ng/mL and benign prostate examination. Enhancement of specificity with free PSA measurements. *JAMA* **1997**, *277*, 1452–1455.

137. Wilson, J.C.; Furlano, R.I.; Jick, S.S.; Meier, C.R. Inflammatory Bowel Disease and the Risk of Autoimmune Diseases. *J Crohns Colitis* **2016**, *10*, 186–193.

138. Kalesnykas, G.; Oglesby, E.N.; Zack, D.J.; Cone, F.E.; Steinhart, M.R.; Tian, J.; Pease, M.E.; Quigley, H.A. Retinal Ganglion Cell Morphology after Optic Nerve Crush and Experimental Glaucoma. *Investigative ophthalmology & visual science* **2012**, *53*, 3847–3857.

139. Sippl, C.; Tamm, E.R. What is the nature of the RGC-5 cell line? *Advances in experimental medicine and biology* **2014**, *801*, 145–154.

140. Almasieh, M.; Levin, L.A. Neuroprotection in Glaucoma: Animal Models and Clinical Trials. *Annual review of vision science* **2017**, *3*, 91–120.

141. Wild, P.S.; Zeller, T.; Beutel, M.; Blettner, M.; Dugi, K.A.; Lackner, K.J.; Pfeiffer, N.; Munzel, T.; Blankenberg, S. The Gutenberg Health Study. *Bundesgesundheitsblatt, Gesundheitsforschung, Gesundheitsschutz* **2012**, *55*, 824–829.

142. Xu, J.L.; Davis, M.M. Diversity in the CDR3 region of V(H) is sufficient for most antibody specificities. *Immunity* **2000**, *13*, 37–45.

143. Bhuiyan, M.S.; Fukunaga, K. Inhibition of HtrA2/Omi ameliorates heart dysfunction following ischemia/reperfusion injury in rat heart in vivo. *European journal of pharmacology* **2007**, *557*, 168–177.

144. Cilenti, L.; Lee, Y.; Hess, S.; Srinivasula, S.; Park, K.M.; Junqueira, D.; Davis, H.; Bonventre, J.V.; Alnemri, E.S.; Zervos, A.S. Characterization of a Novel and Specific Inhibitor for the Pro-apoptotic Protease Omi/HtrA2. *J. Biol. Chem.* **2003**, *278*, 11489–11494.

6 Appendix

6.1 Contributions to the manuscripts

Publication I:

C.S. developed the study design, organized and performed the experimental experiments and wrote the manuscript. N.P. and S.F. participated in the study design, assisted with the mass spectrometric measurements, proofread the manuscript and contributed important intellectual content. K.B. participated in sample recruitment and management, reviewed the manuscript and contributed important intellectual information. N.Pf. critically reviewed the manuscript and provided important intellectual input. F.H.G performed the study coordination as well as the study design and participated in review and approval of the manuscript.

Publication II:

C.S. developed the study design and experimental set-up, wrote the manuscript and performed the MS-based affinity capture experiments as well as data analysis. K.N.F. performed the cell culture experiments and assisted in the mass spectrometric measurements as well as data analysis. N.P. and C.M. aided in the study coordination, reviewed the manuscript and provided important intellectual knowledge. K.B. assisted in cell culture experiments and reviewed the manuscript. N.Pf. reviewed the manuscript and provided important intellectual content. F.H.G. performed the study coordination and reviewed as well as approved the manuscript.

Publication III:

C.S participated to write the manuscript, developed the study design and assisted in the mass spectrometric measurements as well as data analysis. S.F. contributed to write the manuscript and assisted in the study coordination. J.T. performed the experiments as well as the mass spectrometric measurements and participated in the data analysis. A.B., N.P. and C.M. assisted in the development of the study design, proofread the manuscript and contributed important intellectual information. N.Pf. reviewed the manuscript and provided important intellectual knowledge. F.H.G. participated in the study coordination as well as study design and critically reviewed the manuscript.

6.2 List of abbreviations

AAB Autoantibodies

ADCC Antibody-dependent cellular cytotoxicity

ACG Acute-closure glaucoma

ACN Acetonitrile

AD Alzheimer's disease

BBB Blood-brain barrier

BBR Blood-retina barrier

CDR Complementarity-determining region

CH Constant heavy chain

CL Constant light chain

CNS Central nerve system

CSF Cerebrospinal fluid

CT Computer tomography

CTRL Control group

Fab Antigen-binding fragment

Fc Crystallizable fragment

FR Framework region

HC Heavy chain

HIV Human immunodeficiency virus

IOP Intraocular pressure

LC Light chain

LC-MS Liquid chromatography-mass spectrometry

MS Multiple Sclerosis

MeOH Methanol

NTG Normal-tension glaucoma

OCT Optical coherence tomography

OHT Ocular hypertension

ONC Optic nerve cut

PAMP Pathogen-associated molecular pattern

PD Parkinson disease

PCA Principal Component Analysis

PEXG Pseudoexfoliation glaucoma

POAG Primary open-angle glaucoma

RNFL Retinal nerve fiber layer

RGC Retinal ganglion cells

RPE Retinal pigment epithelium

SOP Standard operation protocol

SPE Solid-phase extraction

SLE Selective laser trabeculoplasty

TFA Trifluoroacetic acid

VH Variable heavy chain

VL Variable light chain

6.3 List of figures